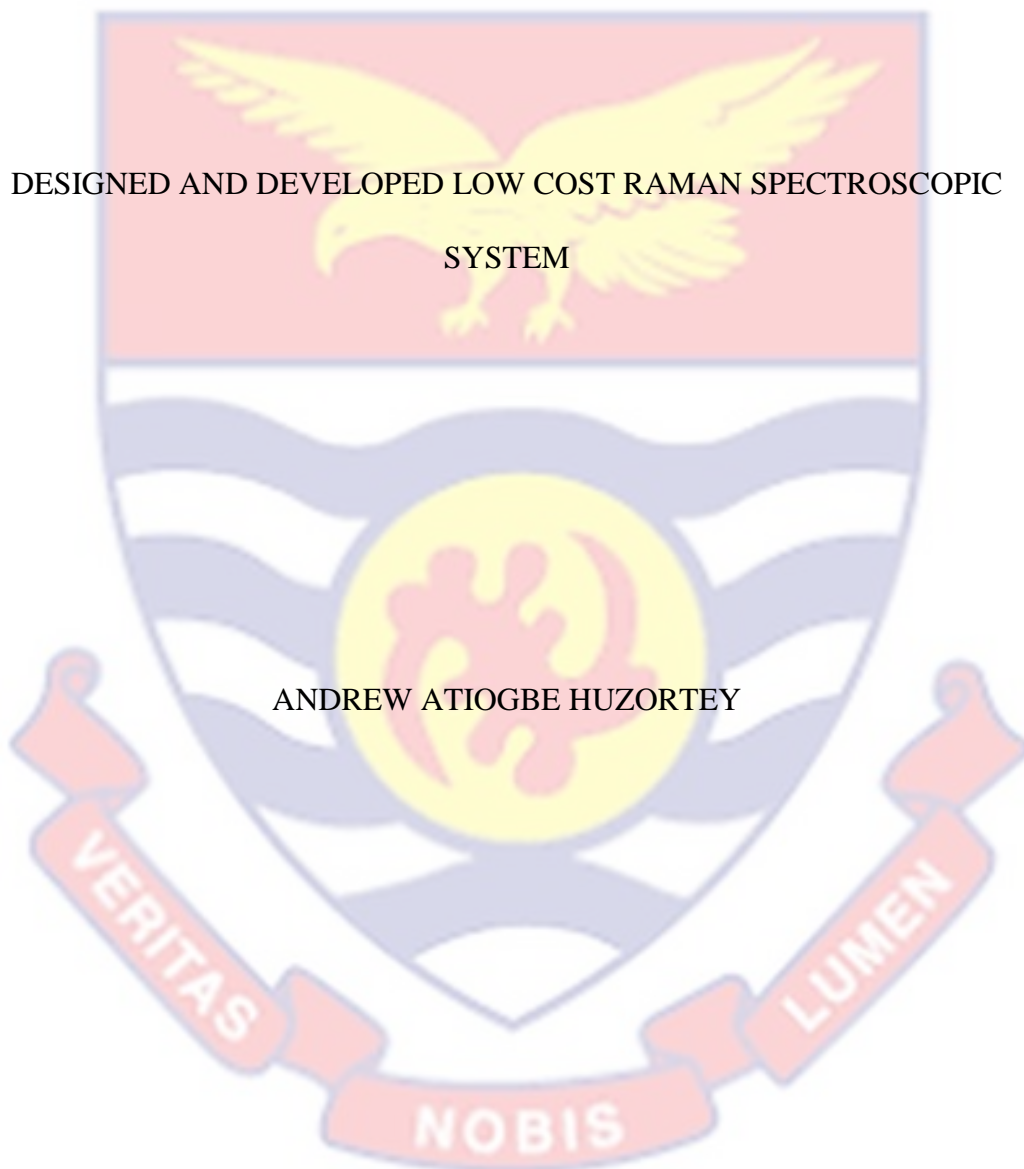


UNIVERSITY OF CAPE COAST



DESIGNED AND DEVELOPED LOW COST RAMAN SPECTROSCOPIC
SYSTEM

ANDREW ATIOTGBE HUZORTEY

2016

UNIVERSITY OF CAPE COAST

DESIGNED AND DEVELOPED LOW COST RAMAN SPECTROSCOPIC
SYSTEM

BY
ANDREW ATIIOGBE HUZORTEY

Thesis submitted to the Department of Physics, School of Physical Sciences of the
College of Agriculture and Natural Sciences, University of Cape Coast, in partial
fulfillment of the requirements for the award of Master of Philosophy Degree in
Physics

APRIL, 2016

DECLARATION

Candidate's Declaration

I hereby declare that this thesis is the result of my own original research and that no part of it has been presented for another degree in this university or elsewhere.

Candidates' Signature Date

Name: Andrew Atiogbe Huzortey

Supervisors' Declaration

We hereby declare that the preparation and presentation of the thesis were supervised in accordance with the guidelines on supervision of thesis laid down by the University of Cape Coast.

Principal Supervisor's Signature Date

Name: Dr Benjamin Anderson

Co-Supervisor's Signature Date

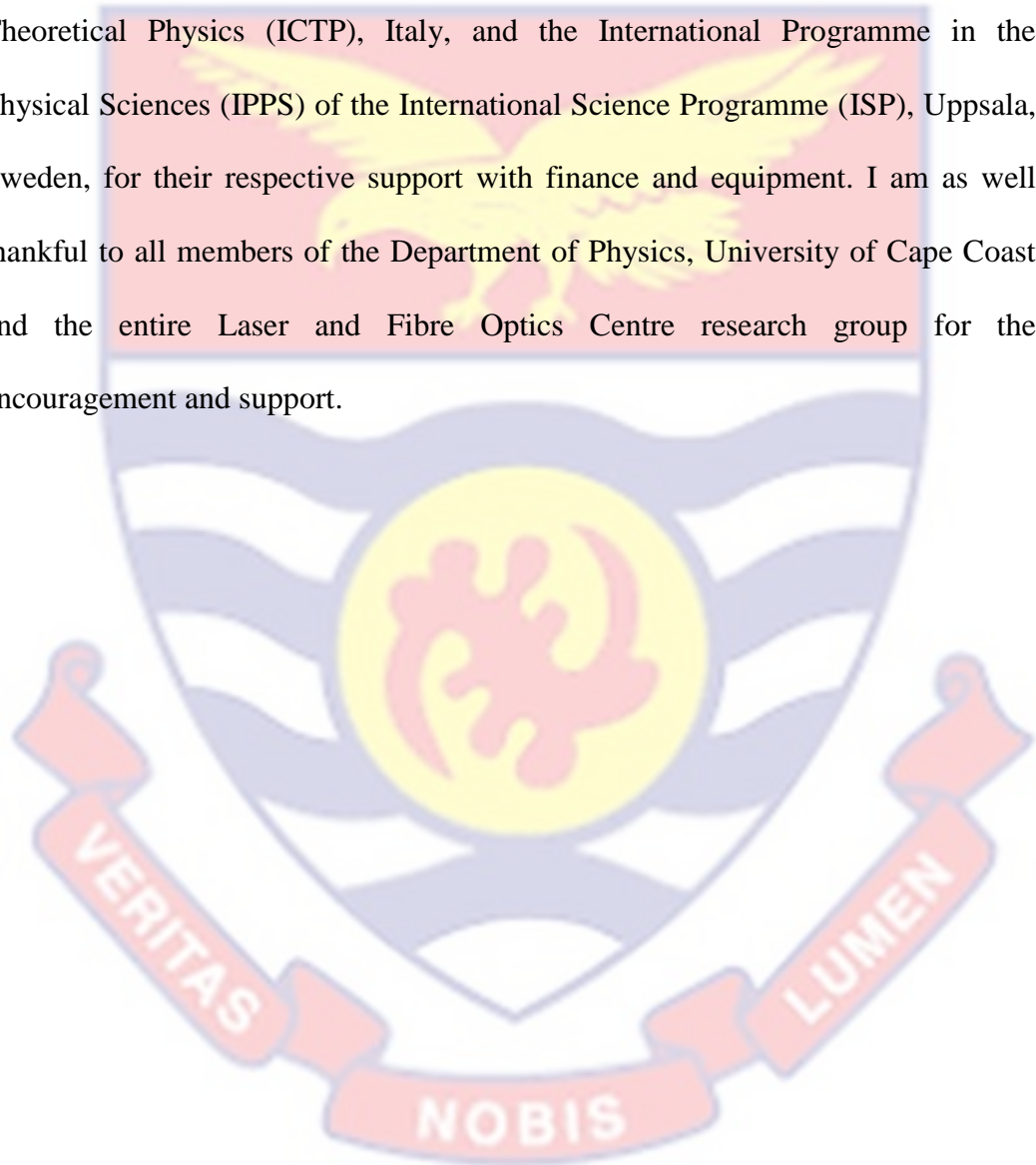
Name: Dr Alfred Owusu

ABSTRACT

Raman spectroscopy (RS) is a well-known optical technique for the study of molecular constituents of samples. However, many RS systems designed are usually immobile, quite cumbersome, and/or relatively expensive limiting the extensive use of this technique. In this study, we report a simple low-cost RS system designed with a 445 nm diode laser source, an absorptive edge filter, a USB2000 spectrometer and other relatively affordable auxiliary optical components. This makes our system suitably cost efficient for non-invasive, non-destructive objective evaluation of a sample matrix to determine its molecular constituents. Additionally, a computational procedure known as the Second Derivative Method for Raman Peak Recognition and Range Independent background subtraction Algorithm (SDM-RPR-RIA) was included for the recovery of Raman Signals from the fluorescence contaminated signals observed with the system. The low-cost RS system was employed to determine the Raman spectra of several known chemical samples. Identified functional groups including Amide (NH), organic acid (COOH), alcohol (ROH), hydroxyl (OH), methyl (CH₃) and methylene (CH₂) have all been established, based on their peak parameters, which is consistent with known results in literature. Measurements from our developed system, besides molecular identification, indicate that the developed low cost RS system setup is equally useful for polarisation and calibration studies. It is expected that the developed low cost RS system setup will become a suitable cost effective alternative to commercial Raman systems for use in academic, industrial settings, and for other novel applications among developing countries.

ACKNOWLEDGEMENTS

I am sincerely grateful to Dr Benjamin Anderson and Dr Alfred Owusu for supervising this work. My sincere appreciation equally goes to the Office of External Activities (OEA) of the Abdus Salam International Centre for Theoretical Physics (ICTP), Italy, and the International Programme in the Physical Sciences (IPPS) of the International Science Programme (ISP), Uppsala, Sweden, for their respective support with finance and equipment. I am as well thankful to all members of the Department of Physics, University of Cape Coast and the entire Laser and Fibre Optics Centre research group for the encouragement and support.



DEDICATION

To all members of my family

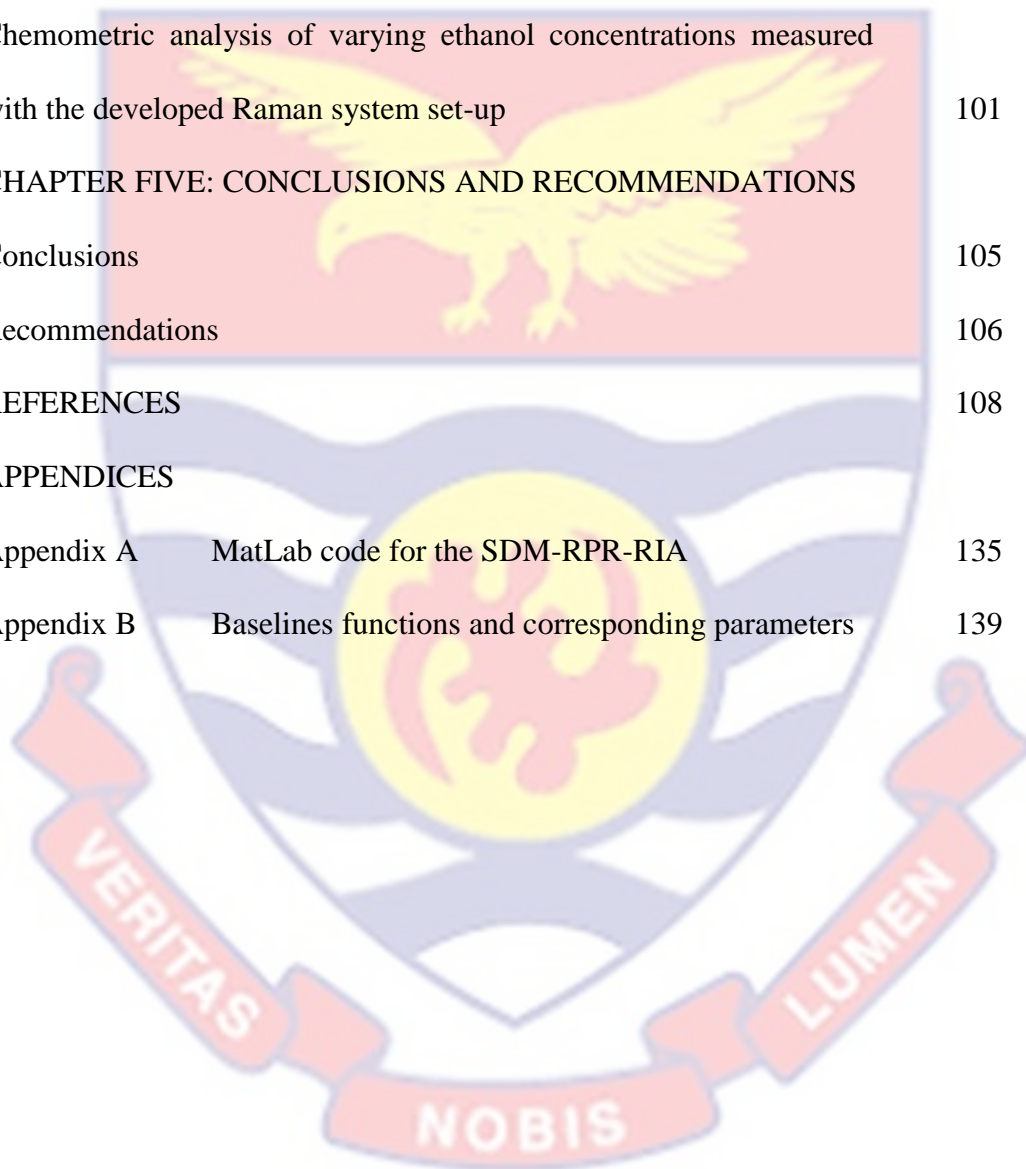


TABLE OF CONTENTS

	Page
DECLARATION	ii
ABSTRACT	iii
ACKNOWLEDGEMENTS	iv
DEDICATION	v
LIST OF TABLES	ix
LIST OF FIGURES	x
LIST OF ACRONYMS	xv
CHAPTER ONE: INTRODUCTION	
Background to the Study	1
Motivation	12
Objectives	14
Organisation of the Rest of the Study	14
CHAPTER TWO: REVIEW OF RELATED LITERATURE	
The interaction of light with matter	16
The scattering processes	17
Raman scattering	19
Raman spectroscopy	20
Raman scattering theory	22
Raman spectroscopy instrumentation	25
Raman set-up configuration	31
Raman set-up calibration	31

Measurement techniques in Raman spectroscopy	33
Raman spectral data representation	38
Raman data analysis	39
Problem of fluorescence contamination	42
Methods for fluorescence suppression	44
Experimental methods for fluorescence suppression	44
Computational methods for fluorescence suppression	49
CHAPTER THREE: METHODOLOGY	
Developed Raman system set-up	56
The Laser source	58
The high pass absorptive edge filter	59
The detection system	60
The auxiliary components	61
Raman system characterisation measurements	63
Test measurements	64
Fluorescence background removal procedure	65
The second derivative method for Raman peak recognition and range independent background subtraction algorithm(SDM-RPR-RIA)	65
Testing the algorithm	70
CHAPTER FOUR: RESULTS AND DISCUSSION	
The developed Raman system setup	74
System characterization measurement	76
System test measurements	80

Fluorescence background removal procedure	83
Retrieved Raman signal from measured spectra using the SDM-RPR- RIA	90
polarisation ratio and polarisation difference	97
Chemometric analysis of varying ethanol concentrations measured with the developed Raman system set-up	101
CHAPTER FIVE: CONCLUSIONS AND RECOMMENDATIONS	
Conclusions	105
Recommendations	106
REFERENCES	108
APPENDICES	
Appendix A MatLab code for the SDM-RPR-RIA	135
Appendix B Baselines functions and corresponding parameters	139



LIST OF TABLES

Table	Page
1 Comparison between holographic notch filters and edge filters	29
2 Data sheet for some Common Bonding Groups and their associated Vibrational Energies	41
3 Lorentzian Function parameters used to generate the Raman spectrum; a_0 is the peak area, a_1 is the peak center position and a_2 is the peak width	71
4 Estimated Prices of Set-up Components	75
5 Fit parameters for Mercury (Hg) and Cyclohexane spectrum using the Developed Raman Spectroscopic System	77
6 Comparison of the performance of RIA, RIA-SG-SR, RIA-SG-RPR and SDM-RPR-RIA under varying SFR conditions	88
7 Samples described according to their structure, peak position and corresponding functional group assignment. References for assigned values are: a.(Spectral Database for Organic Compounds, 2015), b.(McCreery, 2005) and c.(Ananthakrishnan, 1937)	97
8 Summary of Raman peak polarisation characteristics of Ethanol, Pure Water and Benzene	99

- 9 PLS Regression Model Performance Statistics based on correlation coefficient, RMSE and MAPE for the various combinations of the training and test data set

103



LIST OF FIGURES

Figure		Page
1	Light interaction with matter showing the phenomenon of reflection (A), transmission (B), absorption (C) and scattering (D)	16
2	Jablonski Diagram representing Quantum Energy Transitions for Rayleigh and Raman Scattering (Long, 1977)	24
3	Experimental Raman spectra of liquid ethanol and assignment (Kiefer, 2015)	38
4	Using the different characteristics of a molecular band to obtain relevant information for univariate analysis (Renishaw plc, n.d.)	40
5	Schematic diagram of the developed Raman spectroscopic system; A- used for liquid sample measurement and B- used for solid sample measurement.	56
6	Normalized spectrum displaying the spectral characteristics of the 445 nm laser	58
7	Transmission and cut-off properties of the 445 nm long pass filter	59
8	Internal description of the USB 2000 spectrometer with its components (“USB Optical Bench,” n.d.)	60
9	Fibre probe depicting the six around single- fibre leg bundle	

	design (“Fibers & probes,” n.d.)	61
10	Schematic diagram showing ray tracing characteristics of a plano convex lens	62
11	Transmission spectra of different cuvette making materials (“Material & Technical information,” n.d.)	63
12	An example of a collected Raman signal having a polynomial baseline and the second derivative spectrum of the collected	67
13	A flowchart of the second derivative method for Raman Peak Recognition	68
14	Flowchart of the Second Derivative Method for Raman Peak Recognition and Range Independent Algorithm (SDM-RPR-RIA)	70
15	The fifth order polynomial, Gaussian and sigmoidal type of baseline used to test the performance of the second derivative method for Raman Peak Recognition and Range Independent Algorithm (SDM-RPR-RIA)	72
16	Raman spectra of 0.5, 0.05 and 0.005 signal-to fluorescence-ratio (SFR) imposed on the fifth order polynomial baseline	73
17	The developed low cost Raman system setup and components	74
18	The water Raman spectrum and associated noise (insert)	

	used to compute signal to noise ratio (SNR) of the system.	76
19	Fitted spectrum of fluorescence mercury (Hg) lamp to determine resolution of the bare spectrometer	78
20	Fitted spectrum of cyclohexane to determine resolution of the entire system	79
21	Raman spectrum of Liquid (glycerol, n-hexane and methanol) and solid (benzoic acid, urea, and naphthalene) samples measured with the developed system	80
22	Raman spectra of benzene, ethanol, pure water and well water samples with their associated P_{\parallel} (black) and P_{\perp} (red) polarised Raman spectra	81
23	Raman spectra of ethanol measured at different concentrations with the developed Raman system	82
24	Mathematically generated Raman spectrum with 12 Lorentzian peaks on a fifth order polynomial baseline	84
25	Raman signal recovery processes using the second derivative method for Raman Peak Recognition and Range Independent Algorithm (SDM-RPR-RIA)	85
26	Raman spectra recovered from (a) fifth degree polynomial (b) Gaussian and (c) sigmoidal baselines using the second derivative method for Raman Peak Recognition and Range Independent Algorithm (SDM-RPR-RIA)	86
27	Raman spectra recovered from polynomial baselines of (a)	

	1, (b) 0.5, (c) 0.05, (d) 0.005 signal-to-fluorescence ratio (SFR) using the second derivative method for Raman Peak Recognition and Range Independent Algorithm (SDM-RPR-RIA)	87
28	Mathematically generated Raman spectra with signal-to-noise-ratio (SNR) of 10 (red) and 0.1 (black) compared with noise free Raman spectrum (blue)	89
29	A comparison of the weighted correlation coefficient (WCC) between spectra with signal-to-noise ratio (SNR) of 0.01 and 10 for the case of 0.5 and 0.005 SFR after processing with the second derivative method for Raman Peak Recognition and Range Independent Algorithm (SDM-RPR-RIA)	90
30	Benzene Raman spectrum recovery process using the second derivative method for Raman Peak Recognition and Range Independent Algorithm (SDM-RPR-RIA)	91
31	Naphthalene Raman spectrum recovery process using the second derivative method for Raman Peak Recognition and Range Independent Algorithm (SDM-RPR-RIA)	92
32	Benzoic acid Raman spectrum recovery process using the second derivative method for Raman Peak Recognition and Range Independent Algorithm (SDM-RPR-RIA)	93
33	Recovered Raman Spectra of benzene, glycerol, n hexane	

	and methanol	94
34	Recovered Raman spectra of benzoic acid, naphthalene and urea	95
35	Spectrum of benzene molecule showing the effect of both vertical and horizontal polarisation states	98
36	Polarisation difference spectrum (dashed lines) of the two Polarisation states of the well water sample	100
37	Recovered Raman spectrum of varying concentrations of ethanol	101
38	Number of Partial Least Square (PLS) components and their contribution to variation in data set explained percentage-wise	102
39	Prediction assessment of the Partial Least Square (PLS) regression model by (a) Leave one out cross validation method and (b) Blind cross validation method	103
40	Comparison of the relative error determined for each concentration of ethanol based on Leave one out cross validation method and Blind cross validation method	104

LIST OF ACRONYMS

CCD	Charged Coupled Device
D	Depolarisation ratio
DR	Degree of Recovery
FS	Fluorescence Spectroscopy
FT	Fourier Transform
FWHM	Full Width at Half Maximum
MAPE	Mean Absolute Prediction Error
NIR	Near-Infrared
PD-RS	Polarisation Difference Raman Spectroscopy
PLSR	Partial Least Square Regression
r^2	Coefficient of Correlation
RE	Relative Error
RIA	Range Independent background subtraction Algorithm
RIA SG SR	Gauss Seidel Successive Relaxation and Range independent background subtraction Algorithm
RMSE	Root Mean Square Error
RS	Raman Spectroscopy
SDM-RPR-RIA	Second Derivative Method for Raman Peak Recognition and Range independent background subtraction Algorithm
SG-RPR-RIA	Gauss Seidel Successive Relaxation method for Raman Peak Recognition and Range independent background

subtraction Algorithm

SFR Signal-to-Fluorescence Ratio

SNR Signal-to-Noise Ratio

WCC Weighted Correlation Coefficient



CHAPTER ONE

INTRODUCTION

Background to the Study

The use of light and light based technologies in spectroscopy to investigate sample characteristics and probe material properties have invariably become wide spread among researchers in recent years (Aparicio & Harwood, 2013; Ellis, Feher, & Wright, 2005). Spectroscopic techniques often require minimal or no sample preparation. They provide rapid analysis and have the potential to run multiple tests on a single sample since they are nondestructive (Sun, 2008; Wang, 2008; Xu, Riccioli, & Sun, 2015). These advantages particularly apply to nuclear magnetic resonance (NMR), X-ray Emission Spectroscopy, UV-Vis Spectroscopy, Mossbauer Spectroscopy, Infrared (IR) Spectroscopy, Terahertz Spectroscopy (TS), Mass Spectroscopy (MS), Atomic Absorption Spectroscopy (AAS), Inductively Coupled Plasma-Optical Emission Spectroscopy (ICP-OES), etc (Demtröder, 2008; Demtröder, 2013; Parson, 2007; Pavia, Lampman, Kriz, & Vyvyan, 2008).

Optical spectroscopic methods, which use radiations in the optical region of the electromagnetic spectrum to study the effects of the source radiation and its interaction with a material are often preferred (Svanberg, 2012). This is due to the fact that several of the processes in the domain of optical spectroscopy use non-ionizing radiation. They also require reduced space, low cost of instrumentation and are simpler to set-up. This is in contrast to their other counterparts, such as;

Instrumental Neutron Activation Analysis (INAA), Chromatographic techniques, which include Gas Chromatography (GC), and High Performance Liquid Chromatography (HPLC) and Thermogravimetry (Frontasyeva, 2011; Greenberg, Bode, & Fernandes, 2011; Heftmann, 2004).

In optical spectroscopy, reflection, absorption, transmission and scattering properties are studied to unearth the features of the materials such as its molecular composition, crystal structure, scattering coefficient and absorption coefficient. The techniques employed in optical spectroscopic experiments rely on information derived from the electronic transitional, vibrational and rotational energies of the molecules (Hollas, 2004; Svanberg, 2012). In optical spectroscopy, there are two analytical techniques used in determining the above mentioned parameters, these are elemental or atomic spectroscopy and molecular spectroscopy. UV-Vis-NIR Absorption Spectroscopy, Fourier Transform Infrared Spectroscopy (FTIR), Fluorescence Spectroscopy (FS) and Raman Spectroscopy (RS), represent some of the common measurement techniques used in molecular spectroscopy. However, the usage of RS is gradually dominating in research and applications. This is because of the numerous advantages RS has over the other molecular spectroscopic techniques.

For instance, infrared spectroscopy as identified with optical spectroscopy employs the use of radiation sources of relatively longer wavelength (> 700 nm) to provide vibrational information of the molecules present in a given sample matrix (Colthup, 2012; Nakamoto, 1977). Effective detection in the infrared region requires that samples are prepared with Nujol oil or Potassium Bromide

(KBr) to avoid the absorption of water which mars the measured spectra (Harwood, Moody & Harwood, 1989). Also, a specialized chamber is required to perform experiment in IR spectroscopy. These procedures make Infrared spectroscopy a little cumbersome as compared to Raman spectroscopy (RS). In RS special sample preparation is not required and the use of a specialized chamber is also not necessary. Again, aqueous substances can easily be studied using RS since water is a weak Raman scatterer (Lewis & Edwards, 2001; Smith, 1990).

Fluorescence Spectroscopy (FS) is another common optical technique in which emissions due to the actual absorption of photons into an atom is analyzed (Sauer, Hofkens, & Enderlein, 2010). Fluorescence emission is caused by electronic transitions of atoms and occurs in the near ultraviolet and optical range of the electromagnetic spectrum (300 nm – 700 nm). The technique is suitable for analyzing molecules because of its sensitivity and specificity (Lakowicz, 2006). However, fluorescence emission is limited by its dependence on the excitation frequency or wavelength. Generally not all substances do fluoresce for a particular excitation. This makes FS a frequency dependent phenomenon whereas Raman emission occurs independently of the excitation frequency. RS has several advantages over FS, Firstly RS is able to provide a unique signature for every bond in a molecular species. This is because each bond is characterised by a resonant vibrational energy which is unique to a particular molecule. Secondly Raman spectra are very narrow and bond-specific while fluorescence spectra have broad wavelength spread, indicating that only certain “types” of atoms are present

in the sample but not specifically what bond structures these atoms constitute in the sample. Thirdly, in FS the fluorescence intensity can be linked to concentration of certain solute in a solution, but not the concentration of a particular bond type as seen with RS.

Absorption measurement techniques can equally be used to investigate the presence of molecular species having energies which are in resonance with the spectral line(s) of the radiation source (Knee, 1996). Some examples of Absorption Spectroscopy measurement techniques include; Tunable Diode Laser Absorption Spectroscopy (TDLAS), Differential Optical Absorption Spectroscopy (DOAS), Wavelength Modulation Spectroscopy (WMS) and Differential Absorption and Lidar (DIAL) (Platt & Stutz, 2008; Sigrist, 1994). In order to obtain specific absorption lines for different species using Absorption spectroscopy, excitation sources with several wavelengths and optical materials are required. This hampers the ability to perform multi elemental detection (Parson, 2007; Sigrist, 1994). RS on the otherhand is advantageous over absorption spectroscopy because in RS a mixture of species and their concentrations can be simultaneously measured without the need for different wavelengths of the excitation sources or extra optical components.

The phenomenon of RS was discovered and named after the Indian scientist Sir Chandrasekhara Venkata Raman. He won a Nobel Prize for this work in 1930 (Long, 1988; Singh, 2011). He experimented with sunlight, by passing it through a photographic filter to create a monochromatic source and noted that a changed frequency of scattered light emanated from a sample exposed to the

monochromatic light source (Raman, & Krishnan, 1928). Today, the procedure has been improved with the invention of powerful lasers (Maiman, 1960). Rapid development in filter and detector technologies is also enabling weak inelastic Raman scattered photons to be detected with much ease. These inelastic scattered photons are observed as spectral peaks so that by analyzing the location and amplitude of these peaks in the spectrum, chemical composition of the sample can be identified (Lewis & Edwards, 2001; McCreery, 2005). A linear relationship also exists between concentration of the sample and the intensity of the Raman peaks, which makes system calibration simple (Sinfield & Colic 2012). The intensities of Raman peaks can also be compared in the polarized and cross-polarized states to determine the orientation and symmetry of a material (Crawford, Silva, York, & Li, n.d.).

Raman spectroscopy is fast advancing, for instance, in the field of cellular biology. It has been used successfully for discriminating between normal and malignant cells in cancer studies (Haka et al., 2005; Movasaghi & Rehman, 2007; Nijssen et al., 2002). Others have applied RS in the study of infected and uninfected blood cells for early diagnosis of malaria (Carter, 2007; Webster, Tilley, Deed, McNaughton & Wood, 2008). In Pharmacology, RS has been combined with imaging techniques to map the composition of drugs to aid uniformity in batch manufacturing processes (Wartewig & Neubert, 2005; Henson & Zhang, 2006; Šašić, 2007). The use of Raman LIDAR techniques continue to serve several benefits in the remote sensing of atmospheric gaseous species such as O₂, Water Vapor, NO₂, CO, CO₂, SO₂, etc (Grant, 1991; Wilczak, Gossard,

Neff, & Eberhard, 1996). Carter et al., (2005), as well as Gaft and Nagli (2008) have also reported the use of RS in the detection of explosive making constituents such as; TNT, PETN, and some other contraband drugs. Remarkably, these substances can be identified using the RS technique without unsealing their containers. Some of these detections were reported to have been conducted from a distance. This implies that hazardous substances can be safely handled by law enforcement and quality control officers using Raman spectroscopy.

There are a number of studies where RS has been used to examine adulteration in foods, fuels and beverages. It has also been used to aid in detecting forgery in works of art, to scrutinize composition of archeological findings and to investigate crime in forensics without necessarily destroying the evidence (Chalmers, Edwards, & Hargreaves, 2012; Edwards & Chalmers, 2005; López-Díez, Bianchi, & Goodacre, 2003; Yang & Ying, 2011). These and several other applications of RS give an indication of the promising capabilities of RS not only as a subject matter for academic research but also an essential tool for industry and society as a whole.

Despite the promising usefulness of Raman Spectroscopy, its applicability is limited due to the high cost associated with a commercial Raman system. The price of portable Raman spectrometers ranges from \$20,000 to \$60,000 for bench top models. Low cost Raman systems under \$5000 have been reported for undergraduate laboratories (Bisson, Parodi, Rigos & Whitten, 2006; DeGraff, Hennip, Jones, Salter, & Schaertel 2002). The cost of such systems is relatively

expensive considering the low contribution of the national budget to academic and research activities in developing countries (Quartey, 2005).

Apart from the drawback in usage due to cost, Raman spectroscopy suffers two order limitations related to the measurement technique. These limitations include low number of observed photons providing less intense spectral lines and interference by fluorescence emission (Lieber & Mahadevan-Jansen, 2003; Zhao, Carrabba & Allen, 2002; McCreery, 2005). The fluorescence emission usually occurs as intense broad envelope which submerges the small, narrow and weak Raman spectral lines (McCreery, 2005; Auguié, Reigue, Le Ru, & Etchegoin, 2012). In order to enhance the weak signals, several experimental procedures which include Coherent Anti Stokes Raman Spectroscopy (CARS), Surface Enhanced Raman Spectroscopy (SERS) and Tip Enhanced Raman Spectroscopy (TERS) have been developed. In CARS, two laser beams are used to generate a coherent anti-Stokes frequency beam, which enhances the signal by resonance (Tolles, Nibler, McDonald & Harvey, 1977). In the SERS approach, Raman-active molecules that have been adsorbed onto certain specially prepared metal surfaces cause an increase in the intensity of Raman signal from the regularly observed order of 10^4 and 10^6 to as high as 10^8 and 10^{14} (Blackie, Ru & Etchegoin, 2009; Le Ru & Etchegoin, 2008; Moskovits, 2005). The TERS approach is similar to SERS. In TERS a metallic tip coated with silver or gold of an Atomic Force Microscope (AFM) is used to enhance the Raman signals of molecules found in the tip's locality (Deckert-Gaudig & Deckert, 2009). In a review by Schultz (2014), TERS was reported as having sensitivity down to the single

molecular level. Ferraro and Nakamoto (2012) discussed several other enhancement procedures such as the Hyper Raman Spectroscopy (HRS), Resonance Raman Spectroscopy (RRS) and Stimulated Raman Spectroscopy (SRS).

The limitation resulting from intense fluorescence emissions submerging the Raman peaks is equally been pursued in quite a number of studies using either experimental techniques or computational methods to retrieve the Raman signal from fluorescence interference. One of the commonly reported experimental techniques involves the use of tunable diode lasers in a process known as Shift Excitation Raman Difference Spectroscopy (SERDS) (Martins et al., 2010; Sowoidnich & Kronfeldt, 2012). SERDS has evolved into other forms which includes Shift Excitation Raman Difference Spectroscopy Difference Deconvolution Method (SERDS – DDM) and Instantaneous Shifted – Excitation Raman Difference Spectroscopy (iSERDS) (Osticioli, Zoppi & Castellucci, 2006; Osticioli, Zoppi & Castellucci, 2007; Kiefer, 2014). Adami and Kiefer (2013) reported a cost effective type of SERDS with Light Emitting Diodes (LED) as an alternative to the use of a tunable Laser in a technique abbreviated as LED-SERDS. Another experimental means by which fluorescence emission in RS can be avoided is with the use of time gating techniques referred to as Time Resolved Raman Spectroscopy (TRRS) (Efremov, Buijs, Gooijer & Ariese, 2007). TRRS exploits the different time scales of the Raman ($\sim 10^{-12}$ s) and fluorescence ($\sim 10^{-9}$ s) processes by using fast cameras to capture only the Raman photons. Fluorescence can also be avoided experimentally by purposefully choosing an

excitation source having a wavelength that will produce Raman scattering either beyond (> 700 nm) or below (< 300 nm) the fluorescence region. To achieve this, a Near Infrared (NIR) or deep Ultraviolet excitation source is employed (Patil, Pence, Lieber & Mahadevan-Jansen, 2014). NIR excitation sources are used because the relative energy of photons in the NIR region is too low to excite electronic transitions and cause fluorescence emission. Alternatively, a deep UV laser source with wavelength below 270 nm will effectively avoid fluorescence since most molecules will re-emit fluorescence photons in the wavelength range greater than 300 nm whereas the excited Raman photons will occur below 300 nm (Asher & Johnson, 1984). Employing deep UV excitation also has the advantage of providing a large Raman cross-section which leads to resonance enhancement of the Raman signals (Asher, Ludwig & Johnson, 1986). The use of polarisation Raman Spectroscopy (PRS) has been found to be very efficient in selectively discriminating Raman photons from fluorescence photons based on their polarisation differences (Auguié et al., 2012; Le Ru, Schroeter & Etchegoin, 2012). The fluorescence photons do not conserve the polarisation state of the exciting source as do the Raman photons (Angel et al., 1984).

Even though most of the above procedures have proven effective in retrieving the Raman peaks, their implementation require sophisticated and expensive instrumentation. For instance, the tunable radiation source used in SERDs and the specialized detectors used in TRRS adversely increase the cost and add up to making the system more complicated rather than simple and cost effective. Using NIR excitation means a tradeoff between intensity and

fluorescence, whereas the use of UV excitation leads to enhanced but not well resolved Raman signals. UV radiations are also harmful and relatively expensive (Chalmers et al., 2012; Smith & Dent, 2013; Svanberg, 2012).

With the advancement in computers and software technology, fluorescence background removal using computational methods are rapidly being improved (Phillips & Hamilton, 1996; Schulze et al., 2005; Liland, Almøy & Mevik, 2010; Wei, Chen & Liu, 2015). The computational methods are cost effective alternatives to the experimental techniques. These procedures are generally offline but some studies have suggested the possibility of on-line or real time application due to rapid processing time (De Luca, Mazilu, Riches, Herrington, & Dholakia, 2009). A number of studies have reported of these computational methods used to retrieve the Raman spectra from the intense fluorescence background. These include manual estimation using visual inspection (Jirasek, Schulze, Yu, Blades & Turner, 2004), full matrix methods such as orthogonal signal correction (Luypaert, Heuerding, Massart & Vander Heyden, 2007), multiplicative signal correction (Geladi, MacDougall, & Martens, 1985), frequency domain methods such as fast fourier transform (Mosier-Boss, Lieberman, & Newbery, 1995), wavelet transform (Hu et al., 2007) and rolling cycle filtering (Brandt, Brovko, Chikishev, & Paraschuk, 2006). There are also derivative preprocessing methods such as computing first and second order derivatives (Leger & Ryder, 2006; Mosier-Boss et al., 1995) and polynomial fitting (Huang et al., 2003; Leger & Ryder, 2006; Lieber & Mahadevan-Jansen, 2003; Vickers, Wambles & Mann, 2001; Zhao, Lui, McLean & Zeng, 2007).

Other techniques are based on statistical methods, including maximum entropy and principal component analysis (Hasegawa, Nishijo & Umemura, 2000; Schulze et al., 2005).

Among the computational methods the polynomial fitting method due to its simplicity is predominately used (Lieber & Mahadevan-Jansen, 2003). This method estimates fluorescence background with the help of a single polynomial function. The order of the polynomial function is selected to best represent the contour of the background to be subtracted from the measured spectrum. A shortcoming to this procedure is the subjectivity in choosing the degree of the polynomial. This choice is largely based on empirical experience. Again, the line shapes of the extracted Raman spectra are found to vary significantly with the change in the degree of the polynomial function. To offset these limitations Krishna, Majumder and Gupta, (2012) proposed the Range Independent background subtraction Algorithm (RIA). RIA uses a zero order Savitsky Golay filter which works iteratively to entirely eliminate the high frequency components in a raw spectrum leaving only the low frequency component (baseline). However Chen, Wei, Zhang, Wu, and Li, (2015) have shown that the RIA process is a bit subjective because it relies on certain parameters that are subjectively selected. Their study also reveals that the RIA process leads to the introduction of spurious peaks; it is not able to efficiently recover Raman peaks from signals with very low signal-to-fluorescence Ratio (SFR) and comes along with a huge cost for computational time. A method known as RIA-SG-RPR has been proposed by Chen et al., (2015) to compensate for the limitations of RIA. In this method the

peak with maximum amplitude within the spectrum is identified and used as an intrinsic criterion for convergence to avoid subjectivity. A Gauss Seidel Successive Relaxation procedure is also used for the iterative smoothing to improve the computational time. However, successful implementation of the RIA–SG–RPR algorithm requires the user to specify the SFR of the spectrum. Full automation of the RIA-SG-RPR algorithm is therefore hampered considering the fact that the SFR parameter is approximately estimated by visual inspection.

Motivation

Raman spectroscopy has evolved to become a potent research technique for qualitative and quantitative spectral analysis. It is envisioned as “one of the most powerful, versatile and fascinating tools for the investigation of matter” (Laserna, 2001). This is because it has the ability to provide unique fingerprints of substances in real time (Ellis et al., 2012) and it is adaptable for use in severe harsh places or conditions (Goncharov & Crowhurst, 2005; Lin, Santoro, Struzhkin, Mao & Hemley, 2004). The technique is suitable for studies and applications that are of benefit to academia, industry and society in general. A major challenge hampering its usage is the cost of the system (Abhyankar & Subramanian, 1995; Galloway, Ciolkowski & Dallinger, 1992; Lorigan, Patterson, Sommer, & Danielson, 2002). Nonetheless, attempts continue to be made in achieving a low cost Raman system. Some of these attempts have been reported in literature (Abhyankar & Subramanian, 1995; Bisson et al., 2006; Degraff et al., 2002; Galloway et al., 1992; Lorigan et al., 2002). In most of these reports the spotlight has been on reducing the price of the components for the

instrumentation by focusing solely on either using a cheaper light source (Adami & Kiefer, 2013; Greer, Petrov & Yakovlev, 2013), or the detector (Li & Deen, 2014) or a reduction in the number of optical components involved (Bisson et al., 2006; Somerville, Le Ru, Northcote & Etchegoin, 2010). With all these attempts, the recently reported price of a low-cost Raman system still hovers around \$5000 (Bisson et al., 2006; Degraff et al., 2002). This is relatively expensive to be afforded by research laboratories and educational institutions in developing and third world countries. But with the use of a relatively cheap 445 nm diode laser, enhanced signals can be obtained because of the inverse fourth power relation between intensity and wavelength. A detector unit of compact integrated spectrometer with CCD readout can be employed. This device (i.e. CCD) is now cheaply available and provides unprecedented convenience for spectral assessment. The associated fluorescence backgrounds usually encountered with visible lasers can be eliminated computationally using an efficient computational method without extra cost in instrumentation. In entirety, it is expected that the cost of such a system for Raman spectroscopy will reduce drastically. With a reduction in cost of Raman systems, research and education capabilities using Raman spectroscopy will be kindled among developing countries where this novel technique is prospective for new discoveries and improved learning.

Objectives

General Objective

The general objective of this research was to design and develop a low-cost Raman spectroscopic system to study liquid and solid samples

Specific Objectives

The specific objectives to be achieved in this study were to design a Raman system comprising a dual configuration (90^0 and Backscattering) for signal acquisition from both liquid and solid samples, to incorporate a fully automated preprocessing computational method that improves upon the RIA-SG-RPR algorithm for fluorescence removal, and to perform test measurements with the developed system where the Raman spectra of known samples will be measured to establish the validity of the set-up.

Organisation of the Rest of the study

The rest of the study is structured in four chapters as follows. Chapter two is devoted to the review of related literature. This provides support for the study. In this section the historical and theoretical explanations of the phenomenon is reviewed here. The Raman spectroscopy technique, its applications and limitations have been mentioned as well. Chapter three details the methods and procedures as well as materials used in Raman spectroscopy. In this chapter the system characteristics and the method used for analysis have been explained. In Chapter four the results obtained from all the measurements that were conducted

with the system are discussed and compared with references from the literature. Chapter five gives a summary of key findings, the conclusion and recommendations for future work.



CHAPTER TWO

REVIEW OF RELATED LITERATURE

The key concepts involving Light matter interaction, light scattering and Raman spectroscopy will first be reviewed in this chapter. This will be followed by a review of processing and analysis methods used in this study.

The Interaction of Light with Matter

An interaction of light with a sample leads to an aurora of phenomena which include absorption, reflection, scattering and transmission as shown in Figure 1. These phenomena could be studied for useful information regarding the light, the matter or even the surrounding condition of the matter (Feynman & Zee, 2006; Parson, 2007).

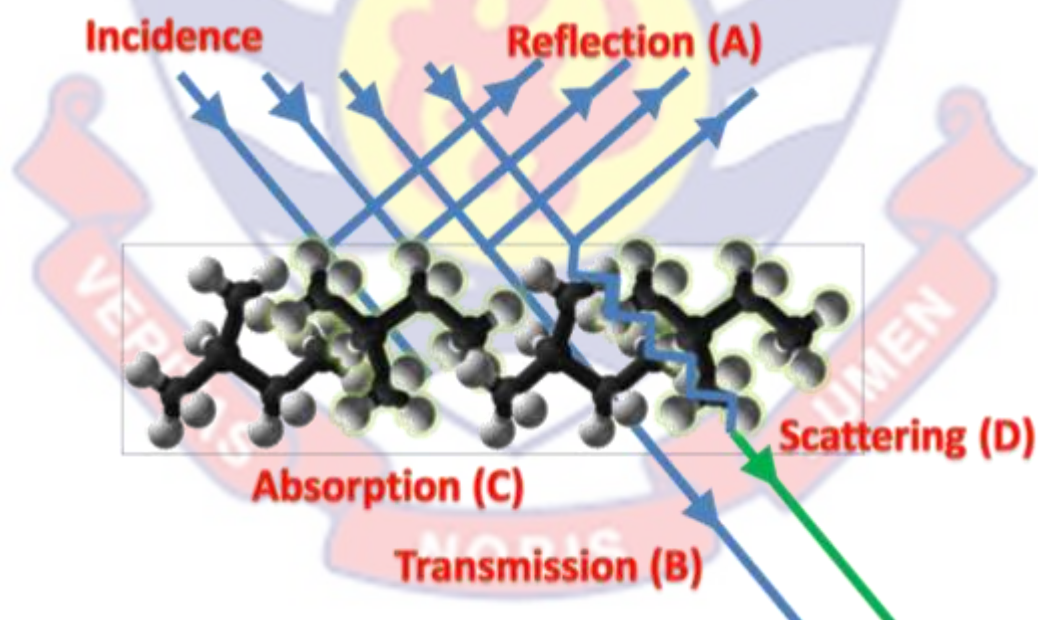


Figure 1: Light interaction with matter showing the phenomenon of reflection (A), transmission (B), absorption (C) and scattering (D)

Upon light's interaction with a sample, if the energy of the incident photon corresponds to the energy gap between the ground state and an excited state, the photon may be absorbed and the material promoted to the higher energy state. This change leads to the loss of energy of radiation from the light which is measured in absorption spectroscopy. The absorbed light energy becomes the excitation energy of the sample and it may end up being dissipated either through thermal degradation producing heat or lost through a radiative decay process producing fluorescence or phosphorescence. However, it is also possible for the photon to interact with the sample and scatter from it. In this case there is no need for the photon to have an energy which matches the difference between two energy levels of the molecule. The scattered light is used to study various properties of the sample. Finally the sample may behave transparently for the light to passing straight through it without interacting with the sample (Demtröder, 2008; Pavia et al., 2008).

The Scattering Processes

An important family of light-matter interaction processes involves the simultaneous (instantaneous) absorption of an incident photon and emission of another photon. Such processes are called scattering processes, and the emitted photon is called the scattered photon (Le Ru & Etchegoin, 2008). The scattering processes can be divided into two types: Linear (elastic) and non-linear (inelastic) scattering. Linear scattering mechanisms cause the transfer of some or all of the optical power contained within one propagating mode to be transferred linearly (proportionally to the mode power) into a different mode. With all linear

processes, there is no change of frequency on scattering. Nonlinear scattering effects are observed usually at high optical power levels. This nonlinear scattering causes the optical power from one mode to be transferred in either the forward or backward direction to the same, or other modes, at a different frequency causing a disproportionate attenuation. Nonlinear phenomena are useful in the field of optical amplification. Linear scattering comprises of Rayleigh and Mie scattering and non linear scattering comprises of Brillouin and Raman scattering (Senior & Jamro, 2009).

Rayleigh scattering, which is also referred to as molecular scattering (Strutt, 1899) occurs when the wavelength of the incident light is somewhat larger than the molecules, or particles. This type of scattering is proportional to the fourth power of the frequency (Senior & Jamro, 2009). Mie scattering occurs when the wavelength of the incident light is less or comparable with the size of the molecules, or particles. For Mie, the scattered intensity which has an angular dependence is mainly in the forward direction. It is not strongly wavelength dependent (varies from λ^{-4} to about λ^{-2} for large particles) (McCartney, 1976) and it is typical to be observed when the scattering inhomogeneity size is greater than $\lambda/10$. Turbidimetry and Nephelometry are two ways by which Mie scattering can be used to monitor particles sizes and shape parameters in ambient air and water. Mie scattering also affects atmospheric visibility (Xu, 2001).

Brillouin scattering is a nonlinear phenomenon in which the incident photon produces a phonon of acoustic frequency as well as a scattered photon. This leads to an optical frequency shift which varies with the scattering angle

because the frequency of the sound wave varies with acoustic wavelength. The frequency shift is maximum in the backward direction, reducing to zero in the forward direction making Brillouin scattering a backward process (Senior & Jamro, 2009). There are other types of light scattering that involve transfer of different forms of energy between the molecule and the radiation field. These include quasielastic (dynamic) light scattering two-photon absorption, and Reflective-refractive (Surface) scattering (Church & Takacs, 1995). However, the most dominant scattering technique used for molecular identification is Raman scattering (Smith & Dent, 2013).

Raman Scattering

In some optical scattering processes, photons absorbed by molecules (or atoms) are re-emitted with different frequency. This phenomenon is called the Raman Effect which provides vibration, rotation and other information about the material. The emitted photons differ in energy and the molecule is either promoted to a higher vibrational or rotational level of the ground electronic state, or demoted to a lower level. The transitions in which the molecule gains vibrational or rotational energy is called Stokes Raman scattering and it usually predominate over transitions in which energy is lost called anti-Stokes Raman scattering. The reason is that resting molecules populate mainly the lowest levels of any vibrational modes. The strength of anti-Stokes scattering increases with temperature, and the ratio of anti-Stokes to Stokes scattering provides a way to measure the effective temperature of a molecule (Senior & Jamro, 2009).

Raman scattering is similar to Brillouin scattering except that a high-frequency optical phonon rather than an acoustic phonon is generated in the scattering process. Also, Raman scattering can occur in both the forward and backward directions, and may have higher optical power threshold than the Brillouin threshold in a material (Senior & Jamro, 2009). The Raman Effect provides vibration, rotation and other information about the material. It can be applied to analyze crystallinity, orientation, polymerization kinetics, etc (Bhaumik, 1967).

Raman Spectroscopy

Description

The measurement and analysis of the signals (photons) arising from the Raman Effect is called Raman spectroscopy. Raman spectroscopy was discovered in 1928 by the Indian physicist Sir Chandrasekhara Venkata Raman (Singh, 2011). In his experiment, he focused sunlight using a narrow band photographic filter to scatter dust-free vapour and block the unscattered light. With his eyes as the detector, He found that a small amount of light had changed the frequency and passed through the second filter. This 'New Type of Secondary Radiation' was named after him (Raman and Krishna, 1928). The discovery led him to receive a Nobel Prize (Physics) in 1930. The 'New Type of Secondary Radiation' was named after him. Three years before the phenomenon of Raman scattering was discovered experimentally, Kramers and Heisenberg (1925) had predicted the same phenomenon. The prediction by Kramers and Heisenberg was explained

using a semi classical theory in which the scattering molecule is treated quantum mechanically and the radiation field treated classically. The semi classical theory was extended to a whole quantum theory to include quantization of the radiation field by Dirac (1927). Several other authors have since then gone further to explain the Raman Effect based on vibrational wavepackets (Craig & Thirunamachandran, 1984; Myers, 1997; Parson, 2007).

Until the discovery and development of the laser, early research in Raman Spectroscopy was concentrated on the development of better excitation sources. This is because Raman scattering requires intense and highly monochromatic sources. Mercury sources and mercury lamps suitable for Raman spectroscopy were initially designed and used. Eventually, the Ar⁺ (351.1 - 514.5 nm), Kr⁺ (337.4-676.4 nm) and more recently the Nd-YAG (1064 nm) laser sources were developed for use with Raman spectroscopy. Development of detection systems for Raman measurements begun and progressed with the use of photographic plates, photoelectric detectors and then cooled photomultiplier. A combination of photographic and photoelectric detectors was also developed and used until the recent upsurge in the development of Charged Couple Devices. The Monochromator, especially the double monochromator and later, a triple monochromator were also developed for the efficient removal of stray light during Raman measurement. Most notable commercial systems use Holographic gratings and Notch filters for the same purpose as the monochromator. Alternatively, Raman spectra can be obtained by the method of Fourier Transform (FT) when using an infrared source (Ferraro & Nakamoto, 2012).

Today the experimental usefulness of Raman spectroscopy have gone beyond stationed equipments occupying large laboratories to portable hand held devices which are far more convenient for practical applications in field measurements.

Raman Scattering Theory

According to Svanberg (2012), when a molecule is subjected to an electric field (E), the electric field induces an electric dipole moment (P) in the molecule. The relation between P and E is expressed as

$$P = \alpha E \quad (1)$$

Where α is the polarizability tensor. The expression for an oscillating electric field P is given by $E_0 \sin(2\pi\nu t)$ hence

$$P = \alpha E_0 \sin(2\pi\nu t) \quad (2)$$

If a molecule vibrates, its polarizability varies. This is because, the polarizability depends on the orientation of the molecule with regard to the field thus the polarizability of the molecule will also vary as the molecule rotates. It can therefore be stated that for the vibrational motion:

$$\alpha = \alpha_0 + \alpha_{lv} \sin(2\pi\nu_{vibr}t) \quad \alpha_{lv} \ll \alpha_0 \quad (3)$$

and for the rotational motion:

$$\alpha = \alpha_0 + \alpha_{lr} \sin(2\pi 2\nu_{rot}t) \quad \alpha_{lr} \ll \alpha_0 \quad (4)$$

The variation in this case occurs at twice the rotational frequency ν_{rot} . This is due to the fact that the polarizability is the same for opposite directions of the field. If an external oscillating field of frequency (ν) is applied, there will be a coupling between the applied and the internal oscillation. This coupling becomes evident if either equations (3) or (4) is inserted into equation (2) to give

$$P = \alpha_o E_0 \sin(2\pi\nu t) + (\frac{1}{2}) \alpha_{iv} E_0 [\cos 2\pi(\nu - \nu_{vibr}) t - \cos 2\pi(\nu + \nu_{vibr}) t] \quad (5)$$

for vibrational motion and

$$P = \alpha_o E_0 \sin(2\pi\nu t) + (\frac{1}{2}) \alpha_{ir} E_0 [\cos 2\pi(\nu - 2\nu_{rot}) t - \cos 2\pi(\nu + 2\nu_{rot}) t] \quad (6)$$

for rotational motion.

The first term in equations (5) and (6) defines Rayleigh scattering. This is because polarisation varies at the frequency ν and re-radiates light of the same frequency. The next set of two terms occurs as side bands on both sides of the Rayleigh shifted from the Rayleigh frequency by the vibrational frequency and twice the rotational frequency. These two side bands represent the Stokes and the Anti-Stokes bands. The strength of the both the Stokes and Anti-stokes band is about 10^{-3} less as compared to the Rayleigh line. It is evident that the Raman Effect occurs only when the polarizability is changed in the process ($\alpha_1 \neq 0$) whereas the polarizability remains unchanged in the process for Rayleigh scattering ($\alpha_1 = 0$).

Figure 2 shows a Jablonski diagram of some energy exchange processes. It is observed that for a normal Raman scattering process, a molecule is excited from its ground state (E_o) to a virtual state when illuminated by incident radiation

such as a laser. A virtual state is not a stationary quantized energy level and does not also correspond to any eigenvalue hence the molecule decays very fast with the emission of a photon. Molecules with an initial state in the lowest vibrational state of the ground state ($E_0, \nu = 0$) corresponds to the Stokes Raman scattering where as the anti-Stokes Raman scattering starts from the higher vibrational energy level ($E_0 + h\nu_m$) of the ground state.

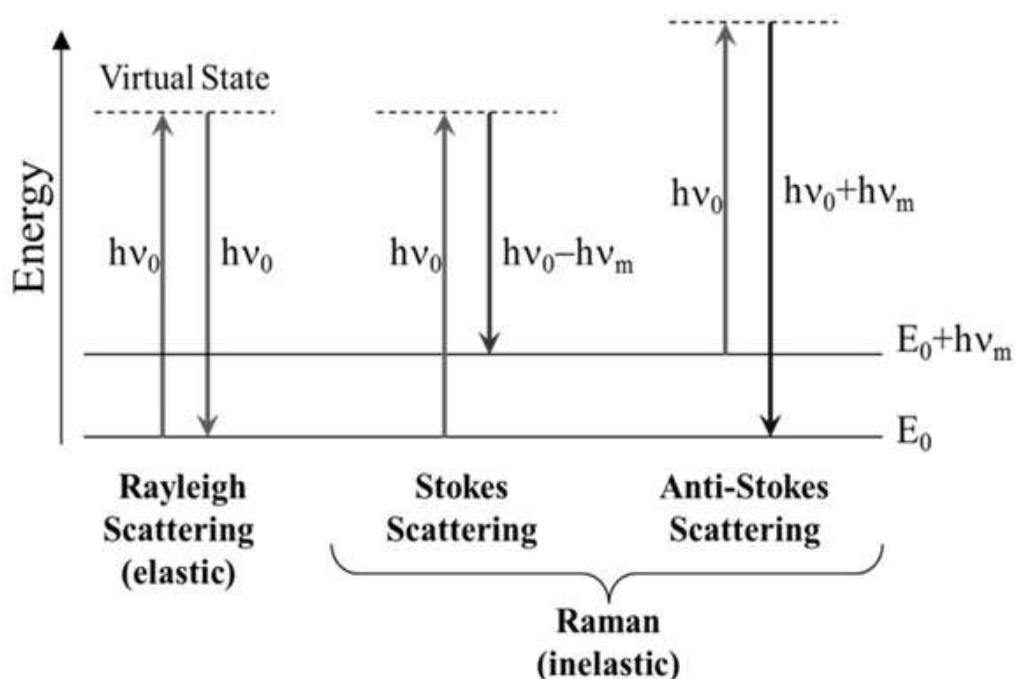


Figure 2: Jablonski Diagram representing Quantum Energy Transitions for Rayleigh and Raman Scattering (Long, 1977)

Even though the Raman scattering efficiency is very low, if the frequency of the excitation is close to the frequency of a particular electronic transition, then scattering enhancements of up to 10^6 can be achieved. This effect is referred to as Resonance Raman scattering (Knee, 1996).

Raman Spectroscopy Instrumentation

Spectral setups in spectroscopy reflect three basic requirements for instrumentation. These include a radiation source, an analyzer and a detection system. The radiation source creates a perturbation in the analyzer which is captured by the detecting system for interpretation or further analysis. The choice of each of these components and the setup arrangements are considered based on the specific purpose the assembled instrument will serve. Raman signals are very weak, hence additional optical components and sophisticated setup configurations may be employed to enhance signals or enable easy detection or both (Svanberg, 2012).

Radiation source

The light source basically required to induce Raman scattering must be intense, focusable and highly monochromatic. Arc lamps have been used in the past but recently laser light sources have become more preferred due to their intense, coherent, less diverging and monochromatic properties. In the book *Modern Raman Spectroscopy* (Smith & Dent, 2013, p.182) it is explained that “Since Raman scattering is recorded as a shift from one specific excitation frequency, if the excitation line covers a range of frequencies, each peak in the spectrum due to the Raman scattering will also cover a range of frequencies. Thus, broadening of the peaks occurs even before natural line broadening from the molecular processes is taken into account. Thus, a good monochromatic source is essential for the best results.”

The monochromaticity of a laser, especially Gas and dye lasers can be enhanced by using a laser line filter to clean them of other wavelengths that hitherto may have been suppressed. Other features such as tunability and pulse generation makes lasers an essential and unique component for Raman spectroscopy as applied in Modulation Raman spectroscopy, Time Resolved Raman spectroscopy and in LIDAR Raman techniques (Platt & Stutz, 2008; Efremov et al., 2007). It must be noted that diode lasers have made Raman spectroscopy practically useful for field, Laboratory and industry applications. This is because of their simplicity, low cost, less power requirement and extreme efficiency across a large range of wavelengths (Vandenabeele, 2013). These comparative advantages make Diode lasers good candidates for the implementation in cost effective setups.

The intensity of the Raman Scattering (I_s) is related to the wavelength (λ) by an inverse fourth power (Senior & Jamro, 2009; Svanberg 2012). The mathematical expression for this relation is

$$I_s \propto \lambda^{-4} \quad (7)$$

Ultraviolet (UV) excitation sources have low wavelength, hence they are suitable in providing enhanced scattering. But their practical use is limited due to effects such as sample degradation and relatively high cost of UV excitation sources. Alternatively, Infrared (IR) sources within the region 700nm to 2300nm can be considered. Firstly because of the rich information they provide and also because IR excitation sources limits the effect of florescence degradation (Patil et

al., 2014). Using IR sources equally have limitations. These include low scattering intensity, with poor spectral resolution and sensitivity. Detector problems are also prevalent when using IR sources due to poor efficiency of CCDs in the IR region. Fourier Transform (FT) spectrometers using linear semi conductors have been found to be a good substitute to CCDs, only that FT spectrometers demand higher acquisition time (Smith & Dent, 2013; Ferraro & Nakamoto, 2012).

Analyzer

In the description of the basic instrumentation for Raman spectroscopy, the Analyzer is used to refer to the sample under investigation. Usually the laser is focused onto a small portion of the sample so that much concentration of the light will generate considerable inelastic scattering for detection. The means by which the radiation is delivered to the sample can either be unguided or guided as used in optical fiber probes. Optical instruments like the microscope, the telescope, etc have been adapted for use in Raman spectroscopic studies. The novelty of Raman spectroscopy is that, the analyzer (sample), needs very little or no special preparation at all. They can be studied either within or without their containing vessels in any state be it liquid, solid, gas, vapour, paste, gel or powders (Lewis & Edwards, 2001; Smith, 1990).

Detection system

The detection system for Raman spectroscopy consists of the filter and detector device. A good detection system in Raman spectroscopy requires a filter

unit that is able to effectively separate the predominant elastic Rayleigh scattered light from the inelastic Raman scattered light. The detector unit must also have the ability to resolve observed peaks since overlapping and convolved peaks can severely compromise the spectral assignment in an investigated sample. Monochromators, edge filters and specially designed holographic notch filters are some of the optical components used to effectively separate elastic scattered light from the inelastic scattered light. These devices are coupled with systems such as photomultiplier tubes, array detectors using CCD, Single Photon Avalanche Diode (SPAD) and Complementary Metal Oxide Semiconductor (CMOS) to help with signal detection (Lewis & Edwards, 2001; Smith & Dent, 2013). Monochromators have been used a lot in the past for effective Rayleigh light rejection and to separate the Raman scattered light into their component colors. In single line detection like the PMT, the monochromator usually has its filter unit on a motorized system. This enables the different energies of light to be collected per rotation of the motor in some defined order. Raman systems employ two to three stage type monochromator. The first monochromator mainly separates the frequency-shifted Raman scattering from the other radiation. The second monochromator increases the dispersion and separates the individual Raman peaks. The third further increases the resolution of each of the peaks making them more refined (Ferraro & Nakamoto, 2012). Even though monochromator based systems enable the recording of Raman scattering as close to the exciting line as is possible at about 10 cm^{-1} from the exciting line they can really be a cumbersome component in the Raman spectroscopic system.

Filter unit

Technological advancement has enabled the development of effective notch and edge filters for use in Raman Spectroscopy. Notch filters are designed to suppress the central Rayleigh line and allow for both the Stokes and Anti-Stokes bands to be observed simultaneously. Notch filters, because of their small sizes are advantageous to use in portable spectrometers. Some instruments use both the notch filter and monochromator to improve the efficiency in detection and resolution of the system (Ferraro & Nakamoto, 2012).

Edge filters operate by absorbing or reflecting all the energies below or above a specific wavelength. An edge filter operates as a low pass filter when it allows only the lower energies to be detected. To operate as a high pass filter, the edge filters absorb or reflect all the energies above a specific wavelength and allow only the higher energies to be detected. In Table 1, holographic notch filters and edge filters have been compared and contrasted.

Table 1

Comparison between Holographic notch filter and Edge filters

Edge Filter	Holographic notch filter
Has very narrow transition width	Relatively large transition width
Measures either Stokes or Anti-Stokes shifts only	Simultaneously measure Stokes and Anti-Stokes shifts
Rejects laser line completely	Rejection is angle dependent
Virtually infinite lifetime	Finite lifetime

Detector device

Detectors are special electronic devices that transform the photon energies to observable features either on a photographic plate or a computer. Common examples are Photomultiplier Tubes (PMT), SPADs, CMOS & CCD. Comparatively, CCD's are less expensive. The CCD devices used as detectors is a sectored piece of silicon in which each sector is separately addressed to the computer. They are arranged in an array of pixels, multi channels as opposed to single channel analyzers like the PMT, each of which can be individually addressed. In this way, it is possible to discriminate each frequency of the scattered light and therefore construct a spectrum. With CCDs it is possible to perform both time resolved signal acquisition and imaging simultaneously (Carter, & Pemberton, 1995; Deckert, Kiefer, Umopathy, & Hamaguchi, 1994).

Weak scattering makes Raman signal detection challenging in the infrared region. The CCDs also work less efficiently in this region. Hence Fourier Transform (FT) instruments employing semi-conductor mostly Silicon (Si), Indium Gallium Arsenide (InGaAs) or Germanium (Ge) detectors are used. In this type of experiment the spectral data are acquired as an interferogram and Fourier techniques are used in the transform the interferogram into spatial domain for analysis. To avoid dark current noise most of the CCD and FT spectrometers are thermally cooled using liquid nitrogen. Current developments in detector technologies enable electrical cooling which ensures long integration time and simple designs of the spectrometer (Long, 1977; Ferraro & Nakamoto, 2012).

Raman Setup Configuration

There are two setup configurations (90° and 180°) mainly used in Raman spectroscopy measurements. The 90° system collects the light a perpendicular position from the incident light. In the 180° configuration, the laser is delivered through the collection lens and the scattered light is collected back through the same direction (Smith & Dent, 2013; Vandenabeele, 2013). Each of the configurations as well include several other optical components such as mirrors and lenses for directing and focusing light unto the sample or collecting scattered light from the sample to the detector. Since the light is scattered as a sphere, the larger the cone of light which can be collected the better. Consequently large lenses or lenses with short focal lengths are used to cover the largest practicable angle. Due to aberrations and some other defects associated with lenses sometimes a mirror system such as a Cassegranian system or a silvered sphere is used (Smith & Dent, 2013).

Raman Setup Calibration

Wavelength scale calibration

Wavelength scale of the spectrometer is calibrated using the different peaks from a spectral calibration lamp or a fluorescent discharge lamp. An experimentally determined spectrum from any of these lamps is compared with standard nominal wavelength positions of that same lamp specified by either the manufacturer or in literature. Sensitivity calibration for intensity measurement can equally be achieved by dividing the standard nominal wavelength positions with

the experimentally recorded one to obtain a correction curve. All spectra that are eventually measured will then be multiplied by this correction curve before evaluation (Klinteberg, Andreasson, Sandström, Andersson-Engels, & Svanberg, 2005)

Sensitivity

Sensitivity of a system is generally expressed as the ratio of the signal of a standard sample to the root means square noise level (American Society for Testing and Materials [ATSM], 1993). In several reports, the Raman band of water is used in measuring the signal-to-noise ratio (SNR). Some of the reasons for using water are because; the Raman band of water is inherently reproducible and does not degrade with time. Also, water is convenient to obtain in a pure state so no preparation or dilution is required. This allows comparisons to be made with high confidence levels across laboratories. The Raman band is a low-level signal, providing a good test for both the optics and the electronics of an instrumental system (Photon Technology International [PTI], 2005).

To determine the sensitivity of a system, the Raman signal for water is first measured, and then the noise is measured in a region where the signal is negligible. The noise level can be estimated as the extreme peak values of the noisy trace either by determining the peak-to-peak amplitude of the noise and then dividing this value by 5 to convert it to an approximate root mean square (RMS) value or otherwise determine the Standard Deviation (SD) of the range selected for the noise. The SNR is calculated using the expression

$$SNR = \frac{\text{Signal Intensity}}{\text{SD of Noise}} \quad (8)$$

Resolution

The resolution characteristic of a system simply determines how well the system is able to discriminate the peaks in a spectrum from each other (DeNoyer & Dodd, 2002). For a Raman system the instrument response is a combination of the resolution of the bare spectrometer combined with the linewidth of the excitation laser. To determine the resolution of the bare spectrometer, the strongest peak of the Hg spectrum which is initially measured and fitted to a Lorentzian curve to determine the Full Width at Half Maximum (FWHM). Similarly the full instrument response is determined by using the system to measure the Raman spectrum of a sample with very narrow peaks such as Cyclohexane. This is because Cyclohexane reportedly has an extremely narrow Raman line which is not easily resolved by a spectrometer (McCain, Gehm, Wang, Pitsianis, & Brady, 2006). A Lorentzian function is then fitted to the narrowest peak of the Cyclohexane spectrum to determine the FWHM. The measured linewidth, then, is approximately the full instrument response.

Measurement techniques in Raman spectroscopy

Since its discovery, Raman spectroscopy has evolved in several forms for diverse applications in different fields. These include Resonance Raman Spectroscopy, Surface Enhanced Raman Spectroscopy, Tip Enhanced Raman

Spectroscopy, Hyper Raman Spectroscopy, Coherent Anti Stokes Raman Spectroscopy, Raman Optical Activity, among several other techniques.

Resonance Raman Scattering (RRS) is the most common of all types of measurement techniques used in Raman spectroscopy. In RRS a laser source is chosen such that it has an excitation frequency close to that of an electronic transition. Ideally, a tuneable laser with its frequency chosen to correspond exactly to the energy difference between the ground vibrational state and the first or second vibronic state of the excited state is used. When the frequency of the exciting beam is close to the frequency of an electronic transition, scattering enhancements of up to 10^6 can be observed (Knee, 1996). This makes RRS a very sensitive and selective technique. At resonance conditions, it is possible to get electronic as well as vibrational information from the sample. One key reason this technique has become important is that the molecules give rise to good Raman scattering rather than intense fluorescence (Ferraro & Nakamoto, 2012; Svanberg, 2012).

Surface enhanced Raman spectroscopy (SERS) effect is about amplifying Raman signals by several orders of magnitude greater than 10^{12} (Moskovits, 2005; Le Ru & Etchegoin, 2008; Blackie et. al., 2009). The amplification of the signals in SERS comes mainly through the electromagnetic interaction of light with metals, which produces large amplifications of the laser field through excitations generally known as Plasmon resonances. Plasmon resonances refer to effects associated with the interaction of electromagnetic radiation with metals (Le Ru & Etchegoin, 2008). For effective detection with SERS, the molecules to be detected

known as the probe must be in close proximity to the surface of the metal known as the SERS substrate. Two metals most used for SERS are Gold and Silver; this is because they provide the largest enhancement or amplification (Le Ru & Etchegoin, 2008). The substrates are tentatively classified into three main classes as Metallic particles in solution, planar metallic structures, and Metallic electrodes. SERS is a promising subject of intense research. It has been exploited as an analytical tool capable of boosting the sensitivity of Raman experiments to the point of detecting a single molecule (Le Ru & Etchegoin, 2008).

Tip enhanced Raman spectroscopy (TERS), is basically identical to SERS, in this case the SERS substrate is brought to the probe, rather than the conventional transfer of the probe onto the substrate. This is achieved by creating a 'hot-spot' between a metallic tip and a substrate (Deckert-Gaudig & Deckert, 2009; Sonntag, Pozzi, Jiang, Hersam & Van Duyne, 2014; Stöckle, Suh, Deckert & Zenobi, 2000). The tip normally comes from a scanning tunneling microscope (STM), or an atomic force microscope (AFM). Similar to SERS, TERS has been reported to achieve single molecule detection (Schultz, 2014).

In Hyper Raman spectroscopy (HRS), an intense beam of radiation is focused onto the sample. This is usually achieved using a 1064nm Nd YAG laser. With sufficient power two photons interact with one molecule then a virtual state is created at double the frequency of the laser excitation. Raman scattering from this virtual state to an excited vibrational state of the ground state is called hyper Raman scattering (Ferraro & Nakamoto, 2012). An advantage of HRS is that because Raman scattering from a 1064 nm laser has too low a frequency to be

detected using a CCD camera and usually requires an interferometer and FT spectrometer. The hyper Raman effect becomes useful in obtaining Raman scattering with this low frequency laser i.e. 1064 Nd YAG and also reduces fluorescence greatly. The main disadvantage is that hyper Raman scattering is very weak, and very high laser powers are required to achieve effective scattering. This is usually achieved with pulsed lasers. Such an arrangement is likely to cause an unacceptable amount of heating and sample degradation in many systems (Ferraro & Nakamoto, 2012)

Coherent anti stokes Raman spectroscopy (CARS) is among the most widely used nonlinear technique in Raman spectroscopy. In the CARS technique, a number of laser excitation sources are required. In its most standard form, three different laser sources are used. The first beam creates a virtual state just like any ordinary Raman scattering. The frequency of the second beam is chosen to have a frequency equal to that which would be scattered in spontaneous Stokes Raman scattering. This stimulates the creation of an excited vibrational state. The third laser is finally used to excite the molecule to a second virtual state. Scattering from this second virtual state, which returns the molecule to the ground state, is what gives the technique its name CARS (Chabay, Klauminzer & Hudson, 1976; Maker & Terhune, 1965; Tolles et al., 1977) This effect can be somewhat simplified by using only two lasers. It should be noted that unlike ordinary Raman scattering, CARS is emitted in specific directions and has to be detected in these directions. A considerably simplified version of the CARS system is more practical has been developed. The procedure uses laser light from two lasers

which is sent co-linearly and in phase down a microscope. The sharp focus of the microscope removes the difficulty with co-linear beams and still provides sufficiently effective phase matching to obtain effective CARS at the focus. This makes these systems much simpler for the average spectroscopist. One advantage of CARS is that it is an anti-Stokes process making it fluorescent-free. However, in solution, there is an appreciable background associated with CARS that limits the value of this advantage (Smith & Dent, 2013).

In Raman Optical Activity (ROA) a beam of plane polarized light generated by a laser and a polarizer is passed through a device such as a photoelastic modulator to create circularly polarized light. The beam created alternates between left circularly polarized (lcp) and right circularly polarized (rcp) light. When this light interacts with a chiral molecule, more scattering will occur from either the lcp or rcp beam depending on which fits with the helix which can be traced on the chiral molecule. The difference in intensity between these beams is Raman optical activity (ROA). This technique is proving very effective in that not only does it provide information on chirality, it also selectively identifies particular features within a protein such as the degree of folding occurring within it. The use of fast effective modulators to achieve this circular polarisation has been a key to the development of ROA (Barron, Zhu & Hecht, 2006).

Raman Spectral Data Representation

The Raman spectrum of a sample is obtained as peaks with different intensities spread over a wavelength scale. Peaks in the Raman spectrum correspond to vibrational modes of the molecule. Figure 3 shows an example of a Raman spectrum consisting mainly of peaks with their intensities expressed as function of wavenumber (cm^{-1}) which is otherwise known as Raman shifts (cm^{-1}).

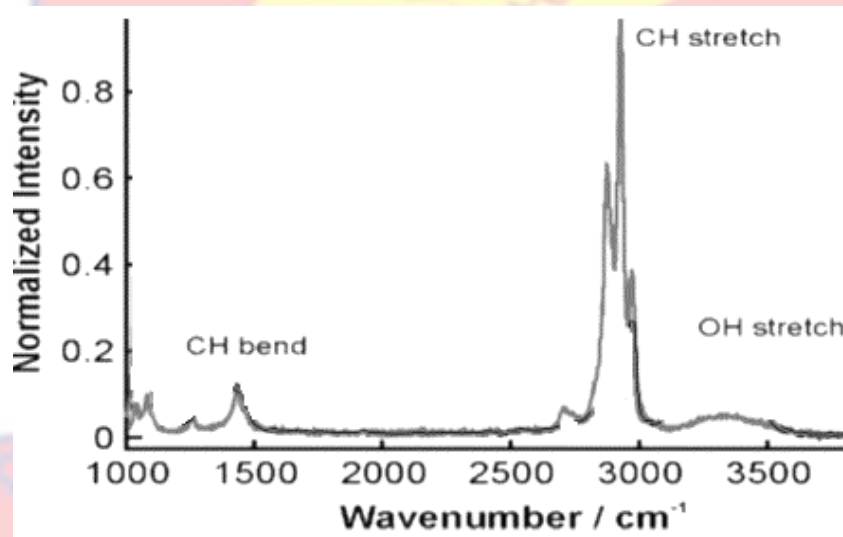


Figure 3: Experimental Raman spectra of liquid ethanol and assignment (Kiefer, 2015)

The Raman shift of a peak is equal to the vibrational energy of the corresponding mode. In most systems the wavelength axis needs to be converted from the conventional units of wavelength (nm) to Raman shifts (cm^{-1}). Generally, the conversion from wavelength to Raman shifts is done using the expression;

$$v = \left[\frac{1}{\lambda_{laser}(nm)} - \frac{1}{\lambda_{emitted}(nm)} \right] \times 10^7 \text{cm}^{-1} \quad (9)$$

Here $\lambda_{laser}(nm)$ is the wavelength of the incident photons and $\lambda_{emitted}(nm)$ is the wavelength of emitted radiation from the scattered photons. The result of conversion from nm into cm^{-1} , ν , is the energy of the vibrational mode. The total intensity scattered by a given vibrational mode is therefore the integrated intensity of the corresponding Raman peak. However, not every vibrational mode, leads to strong Raman scattering, and the Raman intensity varies from mode to mode (Le Ru & Etchegoin, 2008).

Raman Data Analysis

The essential interest for a Raman spectroscopist is to obtain the spectrum and draw inferences from it. These inferences can be used for qualitative and quantitative analysis. Qualitative analysis is more concerned with identification of the types of bonding groups, their position or location and sometimes the number present in a sample. On the other hand, the quantitative analysis focuses on determining how much of a particular sample is present. Information used in both quantitative and qualitative analysis is based on univariate and/or multivariate statistical methods. Univariate methods use a single value for the determination of the property of interest. Figure 4 shows some of the information that can be obtained based on the different properties of interest such as band width, band position, and etcetera, to be used in a univariate analysis.



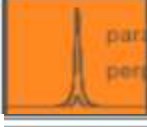



Band parameter		Information
	Characteristic Raman frequencies	Identification (material composition)
	Compare characteristic Raman frequencies	Differentiation
 parallel perpendicular	Intensity variation with changing polarisation	Crystallographic orientation
	Variation in absolute / relative intensity	Absolute / relative concentration
	Variation in Raman band width	Crystallinity; Temperature
	Variation in Raman band position	Stress state

Figure 4: Using the different characteristics of a molecular band to obtain relevant information for univariate analysis (Renishaw plc, n.d.)

A common application of univariate analysis is in specifying the bonding or functional groups present in a sample. Table 2 provides a list of some these bonding groups and their associated vibrational energies in Raman shifts.

Table 2

Data sheet for some Common Bonding Groups and their associated Vibrational Energies

High wavenumber Region		Fingerprint Region	
Group	Raman Shifts (cm ⁻¹)	Group	Raman Shifts (cm ⁻¹)
≡C – H	3300	O – O	970
– O – H	3400	≡ C – C ≡	900
= N – H	3350	≡ C – F	1100
= C = O	1700	≡ C – Cl	650
– C ≡ N –	2100	≡ C – Br	560
– C ≡ C –	2050	≡ C – I	500
= C = C =	1650	Si – O – Si	550

Usually the spectral region between 500 and 1800 cm⁻¹ is labeled as the fingerprint region and can be used for discriminatory purposes (Joshi, 2012). A new alternative to analysis is to use bands that are away from the laser line in the high wavenumber region (2800 cm⁻¹ – 3600 cm⁻¹) in studies known as High Wavenumber Region (HWR) Raman Spectroscopy (Lin, Cheng & Huang, 2012; Mo et al., 2009). The bands present in the HWR are related to hydroxyl (O–H), alkyl (CH, CH₂, CH₃) Carbonyl (C=O) and Amino (NH) vibrations. Methyl (CH₃) and methylene (CH₂) groups exhibit two forms of vibration (bending and stretching). This brings about peaks occurring at 1455 cm⁻¹ for CH₂ bending (Scissoring mode) as well as 1460 cm⁻¹ and 1375 cm⁻¹ for the CH₃ asymmetric

and CH₃ symmetric bending (umbrella mode) respectively. Peaks occurring as a result of mode stretching are found at the positions of 2950 cm⁻¹ for the CH₃ asymmetric stretch as well as 2925 cm⁻¹ and 2850 cm⁻¹ for the CH₂ asymmetric and symmetric stretch respectively (Smith, 2015). The Hydro Oxyl functional group (OH) vibration occurs between 3100 cm⁻¹ to 3650 cm⁻¹. It is an outstanding feature found in substances made up of organic acids (-COOH), water aqueous substances (H-OH) and Alcohols (R-OH). Other vibrational bonds within the HWR can be found in the Table 2.

Even though univariate methods are useful in spectral analysis, multivariate methods also present very competent ways for sample analysis. Multivariate methods use relationship between properties within a spectrum and between different spectra to precisely and accurately make a determination, discrimination or prediction. Some of the multivariate methods include Principal Component Analysis (PCA), Partial least square regression analysis (PLS-R), Partial Least Square Discrimination Analysis (PLS-DA), and Single Value Decomposition (SVD) (Ferraro & Nakamoto, 2012).

To a large extent, the Raman spectrum of a molecule as a whole is a unique fingerprint of that molecule. Therefore Raman measurements carried out in most experiments is used mainly for comparative purposes. However, quantitative information can be obtained from single peaks with the relevant data treatment.

Problem of Fluorescence Contamination

A major challenge associated with analysing the Raman spectral data is the contamination of the spectra by fluorescence emission (Lieber & Mahadevan-Jansen, 2003; Zhao et al., 2002). Fluorescence emission occurs if the incident photons have enough energy to excite the electrons between quantized states. As the electrons return to a lower and more stable energy level, their energies can be dissipated through various mechanisms releasing either light or heat. The fluorescence phenomenon is the feature that is observed as light in the visible part of the electromagnetic spectrum (Lakowicz, 2006).

There are several ways by which Raman scattering differs from fluorescence, even though, both processes occur almost simultaneously within a sample. First, Raman involves an increase in the vibrational energy of the bonding atoms, while fluorescence is an emission due to the actual absorption of the photons into a single atom. Secondly, Raman emission lines are much narrower than fluorescence emission spectra. Raman lines for small molecules in solution typically have widths on the order of 10 cm^{-1} as compared with the broad spectrum covered by fluorescence. Thirdly, Fluorescence emission spectra of many molecules are essentially independent of the excitation frequency, whereas Raman lines shift linearly with the excitation frequency so as to maintain an unvarying value between the excitation and the scattering frequency. Also, fluorescence typically has a lifetime of several nanoseconds and is of higher intensity whereas, Raman scattering has a lifetime a little over a millisecond but with lower intensity. This can be explained by the fact that it takes less time for

the photons to inelastically scatter than to be first absorbed by the atom and then reemitted again. Lastly, It is common for fluorescent photons to be shifted to the longer wavelength region (Red shift or Stokes shift) whereas, Raman photons occur in either directions from the excitation (stokes and anti-stokes region) (Sinfield & Colic, 2012).

Methods for Fluorescence Suppression

When fluorescence occurs it is seen as a broad background which overshadows the Raman peaks. The effect of the background is seen in its signal-to-fluorescence ratio (SFR). SFR is defined as the ratio of the intensity of the tallest Raman peak to its baseline height. The mathematical expression for SFR is

$$SFR = \frac{\text{Raman peak maximum} - \text{Raman peak minimum}}{\text{baseline maximum} - \text{baseline minimum}} \quad (10)$$

SFR of very high values are desired; otherwise for lower value SFR, the fluorescence backgrounds must be removed to enable good spectra. Reports by several researchers have provided techniques for resolving this challenge. Wei et al., (2015) grouped the fluorescence suppression techniques to include; time-domain, frequency-domain, wavelength-domain and computational methods. The review also makes mention of various Raman enhancement techniques and other unconventional methods.

Experimental methods for fluorescence suppression

Time domain methods

Time-domain techniques depend on the use of pulsed lasers with ultra-short laser pulses. These take advantage of the fact that Raman scattering and fluorescence background signal have slightly different response in the time scale. Fluorescence has a much longer lifetime (\sim ns) than the Raman signal (\sim ps to fs). Therefore, the quickly arriving Raman scattered light from late arriving fluorescence emission of a sample excited by ultrafast pulses could be separated temporally. A well-chosen temporal gate with an appropriate gate width enables excellent detection of the Raman signals while minimizing the fluorescence contribution. Various time-domain methods have been established, which are based on the Kerr gate (Matousek, Towrie, Stanley & Parker, 1999), photomultiplier tube (Watanabe, Kinoshita & Kushida, 1985), intensified charge coupled device (ICCD) camera (Ariese, Meuzelaar, Kerssens, Buijs & Gooijer, 2009 ; Efremov et al., 2007; Martyshkin, Ahuja, Kudriavtsev & Mirov, 2004), complementary metal-oxide-semiconductor (CMOS) detectors (Kostamovaara, Tenhunen, Kögler, Nissinen, Nissinen & Keränen, 2013) and streak camera (Tahara & Hamaguchi, 1993).

Frequency domain methods

Another method for suppressing fluorescence in Raman measurements is the frequency-domain method (Bright & Hieftje, 1986; Genack, 1984). This method of measurement is of two common types, namely frequency domain

demodulation (Bright & Hieftje, 1986) and frequency-domain phase nulling (Rusciano, De Luca, Sasso, & Pesce, 2007). Frequency domain demodulation method is rooted in the different behaviour in the response between fluorescence and Raman scattering under high frequency modulation. At high-frequency fluorescence behaves like a low-pass filter and cannot follow the high-frequency modulation. This results in amplitude demodulation and phase shift relative to the excitation light. In comparison, Raman scattering can instantaneously follow the high-frequency modulation of the excitation light. Hence the Raman and fluorescence signals can be discriminated by extracting the high-frequency (mostly, Raman) or low-frequency (mostly, fluorescence) components from the output of the detector. The Raman and fluorescence signals from the sample can be detected separately with a lock-in amplifier also known as a phase-sensitive detector by setting an appropriate phase delay. To achieve this, the detector must be set as out of phase (90 degrees) with respect to the fluorescence emission. In this manner, the fluorescence-free signal is obtained with a minimal decrease in the Raman signal (Wirth & Chou, 1988).

Wavelength-domain methods

The wavelength domain methods are based on Kasha's theory (Kasha, 1950). From the theory, the wavelength of a Raman peak closely follows the wavelength of the excitation source while the fluorescence peak wavelength does not vary significantly with the excitation wavelength. The wavelength-domain methods take advantage of this theory to remove fluorescence while enhancing very weak Raman signals dominated by fluorescence. Common wavelength-

domain methods include Shifted Excitation Raman Difference Spectroscopy (SERDS) (Martins, et. al., 2010; Sowoidnich & Kronfeldt, 2012), Wavelength Modulated Raman Spectroscopy (WMRS) (De Luca et al., 2009) and Subtracted Shifted Raman Spectroscopy (SSRS) (Bell et al., 2000).

SERDS requires an excitation laser source with at least two different narrow emission lines spectrally separated, preferably a tunable source. This method produces two Raman spectra excited by two slightly shifted laser lines. Because the fluorescence spectrum is insensitive to the slight shift in the excitation laser wavelength, the contribution of fluorescence is cancelled out by the differentiation, resulting in difference (derivative) spectrum. To retrieve the actual Raman spectrum, several mathematical methods can be used to reconstruct a normal Raman spectrum from the raw difference spectrum, The SERDS method offers several distinct advantages such as improved signal-to-noise ratio (noise=1/frequency) and shortened data acquisition. Additionally, it ensures the effective removal of strong fluorescence background as well as, other sources of systematic or random noises.

Wavelength modulated Raman spectroscopy (WMRS) uses an excitation light source whose excitation wavelength can continuously be modulated. Multichannel lock-in detection is then used to suppress the fluorescence background (De Luca et al., 2009). The WMRS technique takes advantage of the fact that fluorescence background is unchanged during modulation whereas a periodical modulation of the excitation wavelength causes modulation in the

Raman wavelengths. By this approach WMRS is able to effectively distinguish the Raman signal from fluorescence background.

Subtracted shifted Raman spectroscopy (SSRS) uses the slight change in the Raman spectrum achieved by employing two different grating positions. This leaves the fluorescence background nearly unchanged. By subtracting the two spectra a difference spectrum is obtained. The difference spectrum can be converted into a more recognizable and conventional form of reconstruction. The advantage SSRS and WMRS have over SERDS is the waiving in the requirement of a tunable laser source (Bell & Bourguignon, 1998).

Polarisation domain methods

Polarisation domain methods take advantage of the different responses in Raman scattering and fluorescence to polarisation modulation. The polarisation dependence of the excitation light with polarized Raman bands and fluorophore with low fluorescence anisotropy enables the discrimination between Raman molecules from that of fluorescence. This is because Raman scattering in symmetric vibrations is related to the polarisation of incident light (Angel et al., 1984; Auguié et al., 2012; Le Ru et al., 2012; McCreery, 2005).

The polarisation measurement is done by placing a polarizing plate between the laser and the sample to rotate the polarisation of the beam. The two polarisation states (parallel and perpendicular) can be observed when a polarisation analyzer is placed between the sample and the collection fiber optic. Depolarisation ratio is measured by analyzing plots of intensity for the two

polarisations states. The depolarisation (D) measurement takes the ratio of the peak intensity of a particular Stokes band when the polarizer is rotated perpendicular (P_{\perp}) to the peak intensity when the polarizer is parallel (P_{\parallel}) to the polarized laser light (Long, 1977). This is expressed mathematically as

$$D = \frac{P_{\perp}}{P_{\parallel}} \quad (11)$$

The depolarisation ratio, D, indicates whether the scattered light's polarisation state has been preserved ($D < 0.5$) for symmetric vibrations or destroyed ($D > 0.75$) for asymmetric vibrations. When the depolarisation ratio measurement is combined with the Stokes band frequency (i.e. energy) and point group theory, the structure of small molecules and bond force constants can be determined (Signorell & Reid, 2011). Another use of the polarisation effect is its ability to recover Raman features obscured by the effect of fluorescence contamination. The process is known as polarisation Difference Raman Spectroscopy (PD-RS). The recovery is achieved by a careful measurement and subtraction of the P_{\perp} polarisation from that of the P_{\parallel} polarisation (i.e. $P_{\parallel} - P_{\perp}$), so that the intensity of the fluorescence feature which remains unaffected in both polarisation states can be eliminated. A measure of how well the signal is recovered is called the degree of recovery (DR). DR is computed using the expression,

$$DR = \frac{R_2/F_2}{R_1/F_1} \quad (12)$$

Where R_1/F_1 is the ratio of the Raman peak intensity to the fluorescence background intensity before recovery and R_2/F_2 is the ratio of the Raman peak to the fluorescence peak after recovery (Le Ru et al., 2012).

Computational Methods for Fluorescence Suppression

In addition to experimental methods for fluorescence suppression, there are several computational methods which have been widely adopted for processing measured Raman spectra directly to remove any fluorescence background (Phillips & Hamilton, 1996; Schulze et al., 2005; Liland et al., 2010). The following sub-topics describe some of the computational methods mentioned in literature.

Derivative method (DM)

The use of derivatives for the identification of peaks and the rejection of baselines has been reported in a number of studies (Brown, Vega-Montoto & Wentzell, 2000; Griffiths, King, Hubbard, Schwing-Weill & Meullemeestre, 1982; Leger & Ryder, 2006; Mosier-Boss et al., 1995; Sastry & Singh, 1987). The first derivative represents the slope(s) of a spectrum. Because the slopes of a background are generally lower than those of signal peaks, taking the first derivative of a spectrum will discriminate against slowly varying values. The second derivative and higher derivatives have proven to practically attain reliable positions of Raman peaks, good peak width estimation and also the true Raman peaks from an intense fluorescence background (Zhang, Chen & Liang, 2010). It must be noted that the derivative methods have the ability to enhance noise in a

spectrum. Also these methods can distort the Raman line shape and require complex mathematical fitting algorithm to reconstruct the Raman spectra (Vo-Dinh & Masters, 2004).

Fourier transform method (FTM)

The implementation of Fourier methods for baseline correction is very common among spectroscopy researchers (Atakan, Blass & Jennings, 1980; Mann & Vickers, 1987; Mosier-Boss et al., 1995). Fourier transform methods assume that a given spectrum (or dataset) can be decomposed into a series of frequency varying sine and cosine functions. The Fourier transform is then used to decompose a spectrum into a sum of sine and cosine waves of different frequencies. A plot of amplitude as a function of frequency will reveal which frequencies are contributing most to the spectrum. Hence, baseline (low-frequency), signal (mid-frequency), and noise (high-frequency) components within the spectrum can be observed and separated by application of a low-pass, band-pass, or high-pass filter to the Fourier domain spectral data to eliminate unwanted spectral components. This ensures that only those frequency components contributing to the signal are retained while discarding all others. When the frequency components of the Raman spectra and noise features are not well separated, the Fourier transform method can produce severe artifacts (Vo-Dinh & Masters, 2004).

Wavelet transform method (WTM)

The wavelength transform method (WTM) can be used instead of a Fourier transform method. The WTM represents a given function as a sum of wavelets (Ehrentreich & Sümmchen, 2001; Hu et al., 2007; Ramos & Ruisánchez, 2005; Cai et al., 2001). These wavelets are localized in space and also in frequency. Wavelets have a unique feature of spatial localization which is not found in their sinusoidal counterparts (sine, cosine). This makes wavelets more suited to representing a large class of signals. For example, spectra can be represented with far fewer wavelets than sinusoids. Wavelets also offer the potential to discriminate between high frequency noise, low-frequency baseline, and mid-frequency signals because it allows for a representation of spectra at different resolution scales.

Noise median method (NMM)

The noise median method (NMM) is a computational technique that estimates the baseline as the median value in a moving window. In this method, the baseline is estimated as the median value of all those points within a window of a given size. The points of the chosen window are first ranked ordered; the median value is then the middle value of the set, implying that there are as many points greater than the median as there are smaller than the median. A suitably large window is used so that in the presence of a peak some of the numbers above the median are much greater (in value or intensity) than they would be in the presence of a noise. Under these conditions, there would be neither more nor

fewer points above the median. If the window chosen is too narrow relative to the signal, it leads to errors in baseline determination (Friedrichs, 1995).

Threshold based classification (TBC)

Threshold-based classification (TBC) is an automatic peak recognition technique in which the derivative of the spectrum is squared and then a polynomial fitting is applied to the remaining spectral regions in order to obtain an estimate of the baseline. The fit is subsequently removed from the original spectrum to produce a baseline-corrected result (Dietrich, Rüdell, & Neumann, 1991).

Polynomial based methods

Among the computational methods, the polynomial fitting method is the popular and most widely used (Vickers et al., 2001; Zhang et al., 2010). The method estimates fluorescence background with the help of a single polynomial function and subtracts from the raw spectrum to obtain the true Raman spectrum. The order of the polynomial function is selected to best represent the contour of the background to be subtracted from the measured spectrum. A setback to this procedure is the subjectivity in choosing the degree of the polynomial. This choice is largely based on empirical experience. Again, the line-shape of the extracted Raman spectrum is found to vary significantly with the change in the degree of the polynomial function. To reduce the dependence of the spectra on the polynomial order, Lieber and Mahadevan-Jansen (2003) proposed a modified multi-polynomial fit (ModPoly)-based iterative algorithm. The algorithm was

further improved by Zhao et al., (2007) to take care of spectra with high noise or less intense Raman peaks. Although the modified polynomial-based algorithms are superior to most of the remaining background subtraction algorithms in their simplicity, effectiveness and the ability for automation is limited by sensitivity to the choice of the spectral region to be used in the fit. Thus, selection of different start and stop wavenumbers leads to Raman spectra of significantly different line shapes and intensities (Krishna et al., 2012)

Recently, the range independent background subtraction algorithm (RIA) was developed by Krishna et al., (2012). This method estimates the fluorescence background by a modified iterative fitting procedure. RIA is reported to efficiently suppress the fluorescence background without any peak distortions or inclusions of spurious peaks in the data. RIA also operates indifferently with respect to the selected range of the data to be processed. It equally shows indifference in its performance for different types of spectral backgrounds. RIA attests to two fundamental limitations. The first being that it takes relatively longer time for processing and the other is that it has lowering performance on spectral backgrounds with varying signal-to-background Ratio (SBR). To offset the limitation by longer computation time, Chen et al., (2014) developed the Savitsky Golay-Successive Relaxation (RIA-SG-SR) method based their iteration instead on a modified Savitsky-Golay method to achieve faster convergence. However, both RIA and RIA-SG-SR algorithms fall short to being able to effectively retrieve Raman peaks from spectra having lower SBR. The reason for this limitation is attributed to the choice of the two extra artificial Raman peaks

whose height is used as the criterion for convergence. Chen et al., (2015) in a novel fluorescence subtraction algorithm, named the RIA-SG-RPR algorithm, describe a method in which the criterion of convergence is intrinsically chosen to minimize subjective human intervention. This method shows better recovery efficiency at very low SBR values. Nevertheless, in the RIA-SG-RPR algorithm, a user intervention is required to specify the SBR value to be incorporated into the algorithm making the process not fully automated for practical applications.

Other computational methods

Besides all the above mentioned methods, there exist numerous other computational methods that have been reported for fluorescence suppression. Principal component analysis methods (Hasegawa et al., 2000), artificial neural networks (ANN) methods (Schulze et al., 2005), Composite (Linear-Sine-Cosine) baseline methods (CBM) (Synovec & Yeung, 1985), maximum entropy methods (MEM) (Fischer, Hanson, Dose & Von Der Linden, 2000; Phillips & Hamilton, 1996; Von der Linden, Dose & Fischer, 1996), signal removal methods (SRM) (Ralston & Wilcox, 1968; Vekemans, Janssens, Vincze, Adams & Van Espen, 1995) and spectral shift methods (SSM) are just but a few of some of the techniques reported in literature.

CHAPTER THREE

METHODOLOGY

A detailed description of a Raman system set-up, system characterization measurement, test measurement and a procedure for fluorescence background removal is presented in this chapter.

The Designed Raman System

Schematic diagram of the setup used in this work is shown in Figure 5. This setup allows the implementation of two configurations. It includes a 90° configuration for measuring of liquid samples and a backscattering configuration for measuring solid samples.

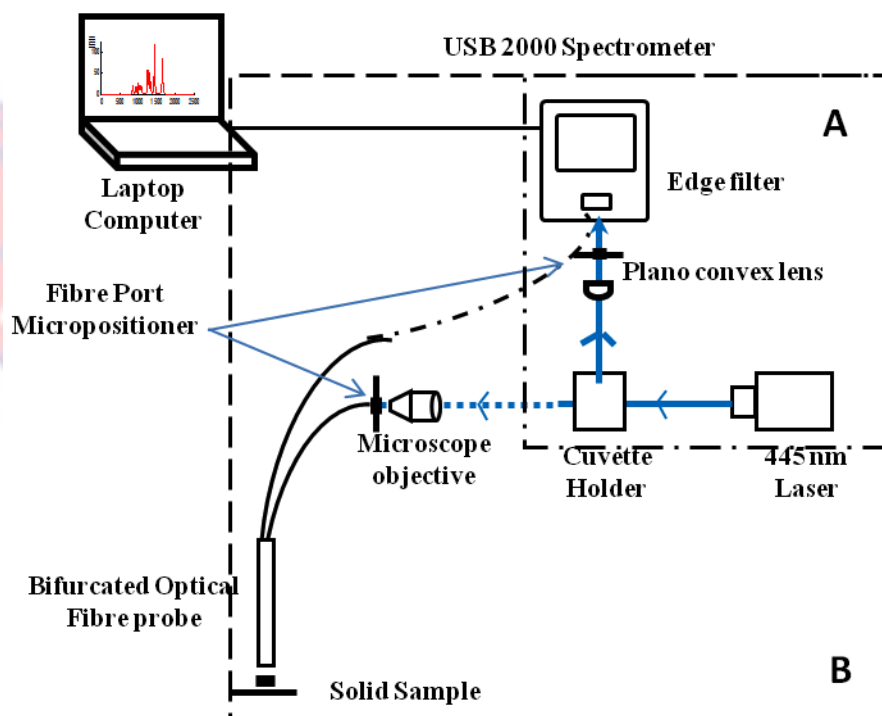


Figure 5: Schematic diagram of the designed Raman spectroscopic system; A- use for Liquid sample measurement and B- use for Solid sample measurement.

The setup components include a 445nm diode laser source, a high pass absorptive edge filter and a CCD based detector system. Auxiliary components include an optical fibre cable, bifurcated optical fibre probe, fibre port, focusing lens, quartz cuvette and a microscope objective lens are used in the setup.

Raman spectrum of a sample is measured using the system by passing light directly from the 445 nm laser into the sample. For liquid samples the light is passed into the standard quartz cuvette cell and the scattered light is collected at a 90° angle from the laser beam path. For solid samples the quartz cuvette is removed from the laser beam path to allow light to be coupled into the Bifurcated optical probe for the backscattered light to be collected and directed into the detector. In both cases, the plano convex lens collects and focuses the scattered light into the detector via the fiber optic coupling. The high pass edge filter placed before the detector effectively rejects the Rayleigh scattered light.

When in operation, a black box mimicking a dark room is used to surround the sample, filter, lens, and fiber optic coupling in order to prevent external light from reaching the spectrometer. In the spectrometer, light is dispersed by a reflecting grating unto a CCD array detector. The electronics cable from the spectrometer leads to the PC through a USB port. This enables observation of the spectrum using the OOI Base 32 software in real time. The protocol for data collection is such that a dark spectrum (with laser light blocked) is initially stored and subtracted from the overall signal using the same integration time as used for the sample spectrum. Also, before recording the spectrum of each

sample, the cuvette is first filled with water to observe the water Raman band which occurs between 3300 cm^{-1} to 3500 cm^{-1} at an intensity of ~ 120 (a. u.). For all the measurements conducted in this study, the integration time was set to 300 ms of which 120 spectra were acquired for 60 seconds and the average computed.

The Laser Source

A continuous wave diode laser source with a 100 mW maximum output power emitting at a wavelength of 445 nm was used as the single source of radiation in the set-up.

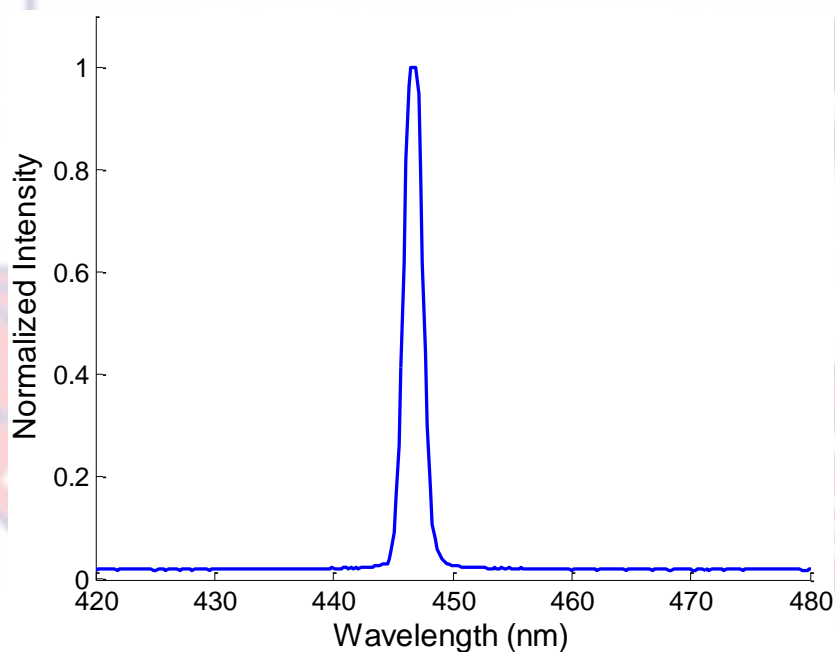


Figure 6: Normalized spectrum displaying the spectral characteristics of the 445 nm laser

The laser was supplied by O-Like (100 mW 445 nm laser module, China). It is equipped with a laser diode driver requiring an input voltage and current of 12 V and 2 A, respectively, with TTL modulation of 0 to 20 KHz. Experimentally

determined spectral characteristics of the laser are shown in Figure 6. The peak centre wavelength of the laser is 446.5 nm and the linewidth (FWHM) is 1.61 nm.

The High Pass Absorptive Edge Filter

An intense elastic Rayleigh scattered light which accompanies the weak Raman signals was suppressed using a 445 ± 6 nm long-pass absorptive edge filter (GG-445) from Edmund Optics. The long-pass edge filters transmit wavelengths greater than 445 nm in the long wave region. It has a diameter of 12.5 mm and spectral transmittance of 93%. Figure 7 shows the transmission characteristics of the long pass filter.

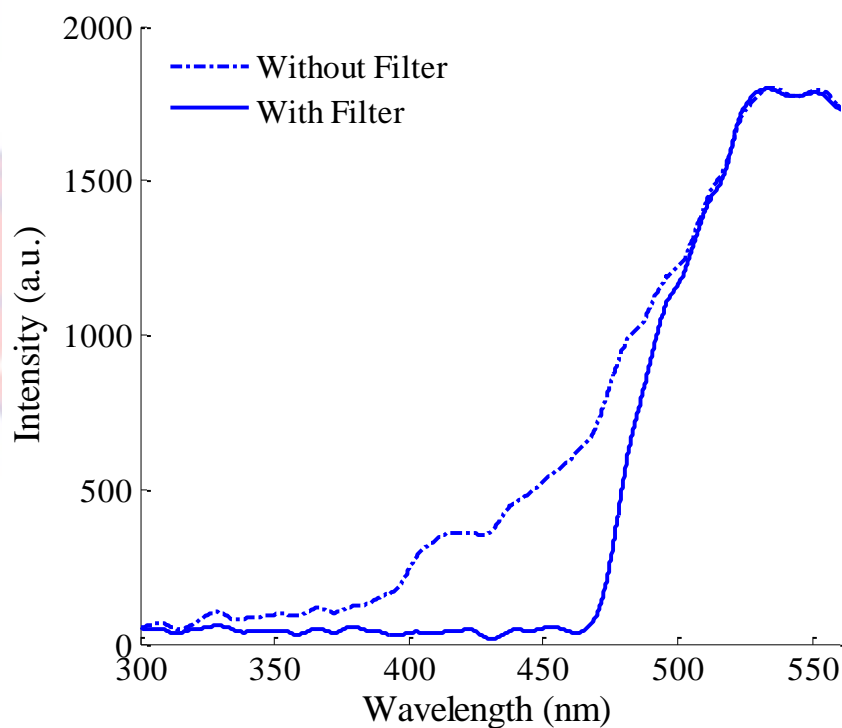


Figure 7: Transmission and cut-off properties of the 445 nm long pass filter

The Detection System

In this work the CCD based USB 2000 spectrometer (USB2000, Ocean Optics) was used to detect the Raman scattered light. It operates on low power characteristics of 100 mA at 5 V. The spectrometer is sensitive to photon activity in the range of 200 nm to 1100 nm. When in operation an optical fibre cable acts as an entrance slit through which light enters. The light is dispersed by an asymmetric cross Czerny-Turner optical bench unto a 2048-element, linear silicon CCD array detector (Sony ILX511). Data from the CCD detector is acquired by choosing from 1 ms to 60 ms as integration time (USB Optical Bench, n.d.). The data collected is transformed into digital information and passed to the 001Base 32 spectrometer operating software of the Ocean Optics USB 2000 spectrometer on the PC for visualization.

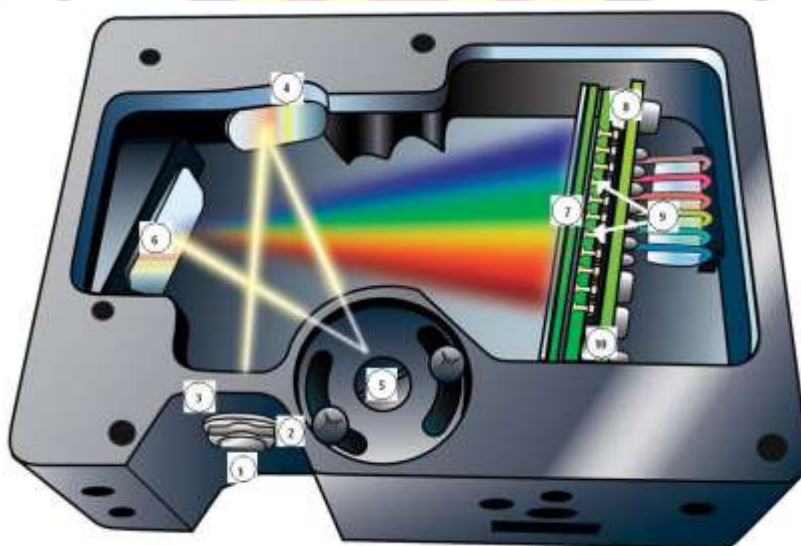


Figure 8: Internal description of the USB 2000 spectrometer with its components (“USB Optical Bench,” n.d.)

The 001Base 32 spectrometer operating software is a 32-bit user-customizable for advance acquisition and display program. It displays measurements in real-time which allow the user to make selections and changes. The software is fully computer controlled for data acquisition and a large number of data can be saved automatically and exported to other software platforms for further analysis.

The Auxiliary Components

The experimental set-up included a 50 cm metallic jacketed multimode Ocean Optics lab grade optical fibre cable. The optical fibre cable (QP600-2-UV-BX, Ocean Optics) was used for the transmission of scattered light from the sample into the spectrometer. For measurement with solid samples, the bifurcated optical fibre probe (R400-7-VIS-NIR, Ocean Optics) shown in Figure 9 was used. The probe has a six (6) around one fibre bundle design. The 600 μm probe comes with a 3.175 mm (1/8") diameter ferrule and 76.2 mm (3") probe ferrule length. It performs best when the 6-fibre leg is connected to the light source and the single-fibre leg is connected to the spectrometer.



Figure 9: Fibre probe depicting the six around single- fibre leg bundle design (“Fibers & probes,” n.d..)

A fibre port micropositioner (PAF-SMA-5-B, Thor Labs) was used to provide an easy-to-use platform for coupling light into and out of the optical fibres. The port has a six-degree-of-freedom fibre collimator and coupler (5 axes, plus rotation). Using the fibre port micropositioners enabled stable alignment and locking mechanism for the fibres. Maximum coupling of the light into the bifurcated optical fibre probe was achieved with the aid of a 40× magnification with 0.65 numerical aperture microscope objective (O4OAS016, Melles Griot).

Light scattered by the sample was collected using a single plano convex lens. The nature of light transmission in the single plano convex lens is as shown in Figure 10. The short focus (3 mm) enabled it to be brought as near as possible to the sample to economize the space while reducing the number of the optical components used in the set-up as well.

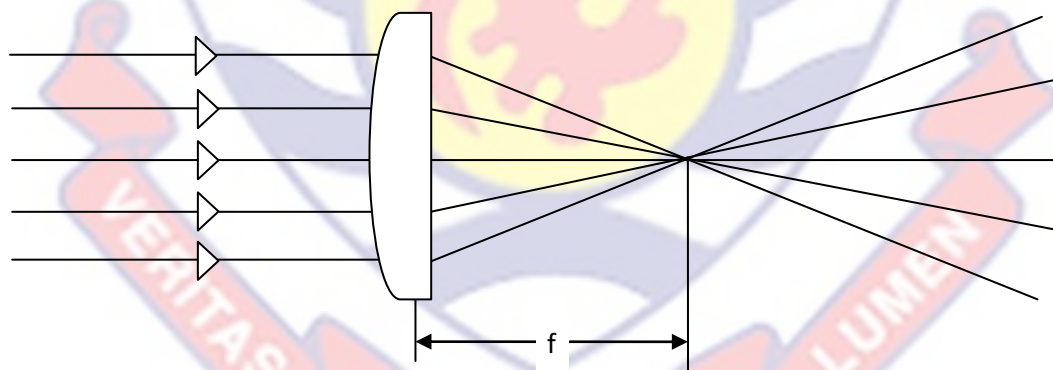


Figure 10: Schematic diagram showing ray tracing characteristics of a plano convex lens

Aqueous samples were studied in a precision cuvette made of quartz suprasil (104F-QS, Hellma Group). The quartz cuvette has a volume of 1400 μl

and transmits light efficiently between wavelengths of 200 nm to 2500 nm as shown in the transmission spectral graph of Figure 11.

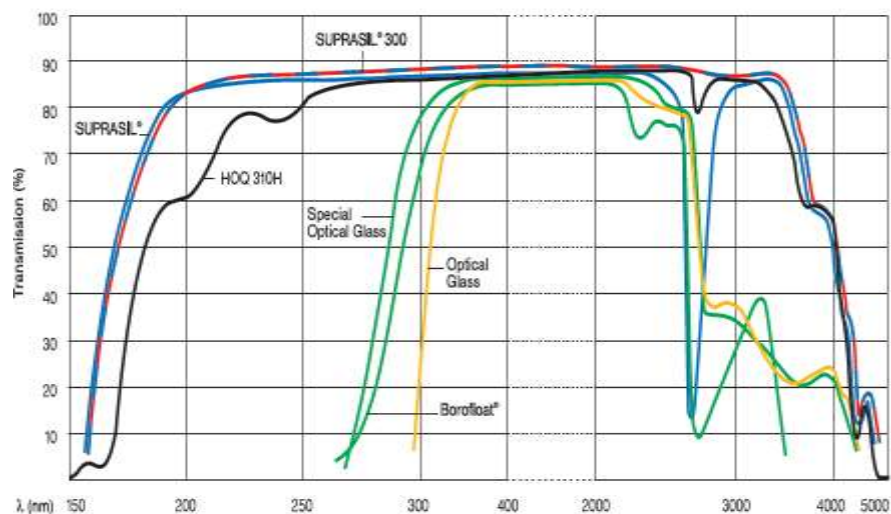


Figure 11: Transmission spectra of different cuvette making materials (“Material & Technical information,” n.d.).

Raman System Characterization Measurements

Several measurements were performed in order to characterize the performance of the system. These include the calibration of the spectrometer, sensitivity and system resolution. Calibration of the spectrometer was done using the peak centre wavelength of the water Raman peak. This was measured and compared with reported nominal wavelength position of water Raman peak from literature (McCreery, 2000).

The sensitivity of the system was determined by measuring signal-to-noise ratio (SNR). Similarly the Raman signal produced by water was used for this measurement. The Raman signal was measured at 510 nm and the noise was measured in a region where the signal was negligible. The noise level was

estimated using the standard deviation (SD) of the noisy trace between 600 nm and 700 nm. The expression used in calculating SNR is as shown in equation (13)

$$SNR = \frac{\text{Signal Intensity}}{\text{SD of Noise}} \quad (13)$$

The resolution of the system was determined by first measuring the spectrum of the bare spectrometer using a mercury (Hg) source. Secondly, the system was used to measure the Raman spectrum of cyclohexane. The most intense and narrow peaks found in these two spectra was fitted to a Lorentzian function. The full-width-at-half maximum (FWHM) was determined from the fit, and analyzed.

Test Measurements

The functionality of the Raman spectroscopic system was evaluated in its utility for studying samples of known chemical constituents. The samples used were aqueous samples including deionized water, ethanol, methanol, benzene, hexane, cyclohexane, paraffin, and acetone, as well as, solid samples including benzoic acid, naphthalene and urea. The system was also tested for molecular concentration estimation. This was achieved by mixing ethanol (99.9%) with deionized water in varying concentrations by volume (95%, 90%, 80%, 70%, 60%, 50% and 30%). Measurements were conducted and repeated twice for each of the sample concentrations to obtain a trial and test data sets for further analysis with partial least square regression analysis.

The system was again used to measure the polarizability of the water, benzene and ethanol samples. The polarisation measurement was done by placing a polarizing plate before the sample and an analyzing plate before the detector. The polarisation states of the sample were observed by rotating the analyzer in either parallel or perpendicular directions to the polarizing plate. Measurement results were analyzed based on depolarisation ratio and the polarisation difference, explained in chapter 2.

Fluorescence Background Removal Procedure

After a desired spectrum has been acquired, the intensity and wavelength data of that spectrum was exported from the 001Base32 Software into a commercial software package MATLAB (MatLab, 2012) for further processing. At this stage the entire spectrum was subjected to a pre-processing procedure to recover the Raman signals from the broad fluorescence backgrounds which is in this case considered as noise. The underlining algorithm for preprocessing was the second derivative method for Raman peak recognition and range independent algorithm (SDM-RPR-RIA).

The second derivative method for Raman peak recognition and range independent algorithm (SDM-RPR-RIA)

When light interacts with a sample, the total signal collected $S_R(\nu_1)$ at frequency ν_1 can generally be expressed as;

$$S_R(\nu_1) = L + R(\nu_1) \quad (14)$$

L , represents the fluorescence or noisy component which remains as a constant with the change in the excitation frequency. $R(\nu_1)$ represents the Raman signal which is very much dependent on the excitation frequency. Since L does not change with excitation frequency, it behaves as a constant term in the equation. $R(\nu_1)$ also represents fast changing peaks described generally by a Lorentzian profile (Meier, 2005) given as;

$$R(\nu_1) = \frac{a_0}{1 + \left(\frac{\nu_1 - a_1}{a_2}\right)^2} \quad (15)$$

$a_0, a_1,$ and a_2 represent the amplitude, position and width (FWHM) of the Lorentzian peak profile. By differentiating equation (14) twice with respect to ν_1 , the constant term L is eliminated and the result obtained for the second differential of the signal collected will comprise solely of the $R(\nu_1)$ term in its derivative form. Equation (14) therefore becomes,

$$S_R(\nu_1)'' = R(\nu_1)'' \quad (16)$$

Where, $S_R(\nu_1)''$ is the second derivative of $S_R(\nu_1)$, and $R(\nu_1)''$ Consequently, differentiating equation (15) twice, and substituting into equation (16) yields equation (17)

$$S_R(\nu_1)'' = \frac{8a_0(\nu_1 - a_1)^2}{a_2^4 \left(1 + \left(\frac{\nu_1 - a_1}{a_2}\right)^2\right)^3} - \frac{2a_0}{a_2^2 \left(1 + \left(\frac{\nu_1 - a_1}{a_2}\right)^2\right)^2} \quad (17)$$

The differentiation of the experimental data represented by $S_R(v_1)$ was done numerically using the point-to-point difference method suggested by O'Haver (1997). This is given as;

$$\frac{d^2 S_R}{dv_1^2} = \frac{S_{R_{i+1}} - 2S_{R_i} + S_{R_{i-1}}}{\Delta v_1^2}, \quad v_{1_i}' = v_{1_i} \text{ (for } 2 < i < n - 1 \text{)} \quad (18)$$

A pictorial illustration of the second derivative method is shown in Figure 12, using some Lorentzian peaks over a broad polynomial baseline. In Figure 12, it can be observed that after the second differentiation, the polynomial baseline disappears completely leaving only the peaks in their derivative form.

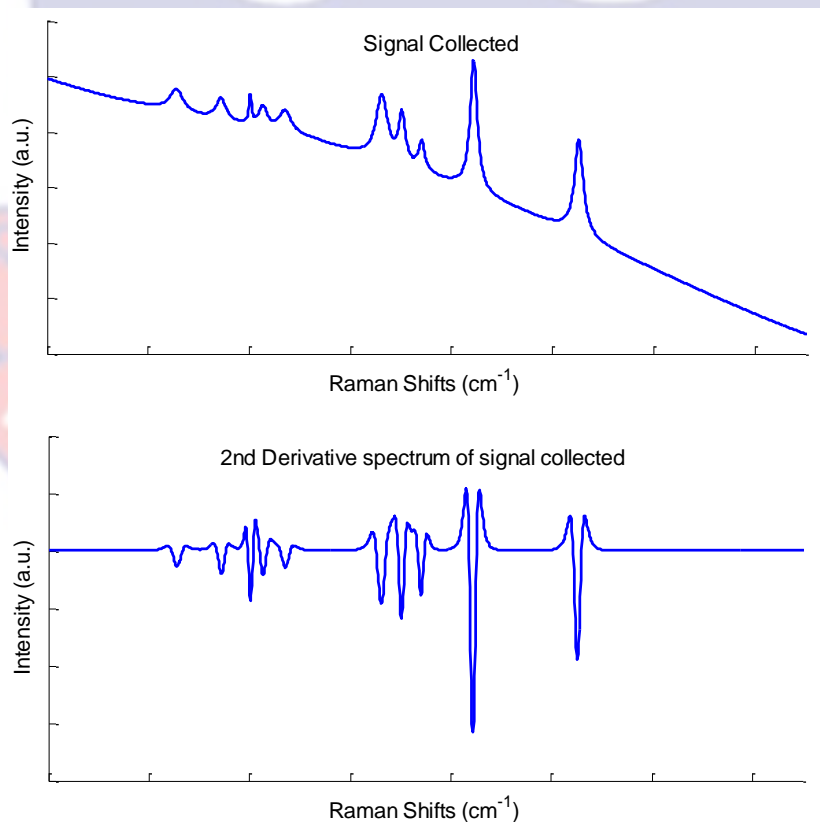


Figure 12: An example of a collected Raman signal having a polynomial baseline and the second derivative spectrum of the collected signal

Intensity-wise, the peak having the maximum intensity in the original spectrum will correspond to the peak with the lowest minima in the 2nd derivative spectrum. Equation (17) is used to fit the peak with the lowest minima in the 2nd derivative spectrum. The fitting is done using a Levenberg-Marquardt nonlinear least square fitting routine (Marquardt, 1963).

The derivative profile contains all the information present in the original measured spectrum, with the fluorescence background been eliminated. However, parameterization and visualization of the spectrum in a more conventional form is mandatory for comparative analysis (Rosi et al., 2010). Hence, the second derivative method is used as a means of identifying and obtaining the amplitude of the Raman peak with the maximum intensity. This value then serves as an intrinsic criterion of convergence in the subsequent iteration procedure. A flowchart of the second derivative method for Raman peak recognition (SDM-RPR) is shown in Figure 13.

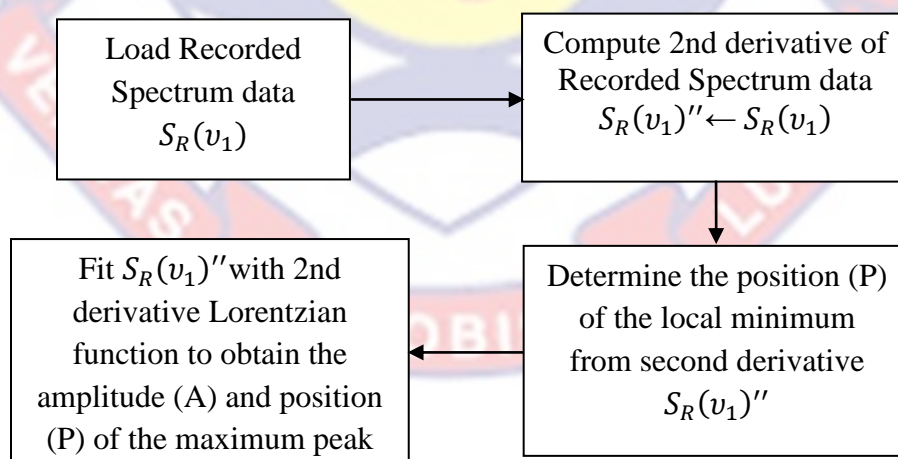
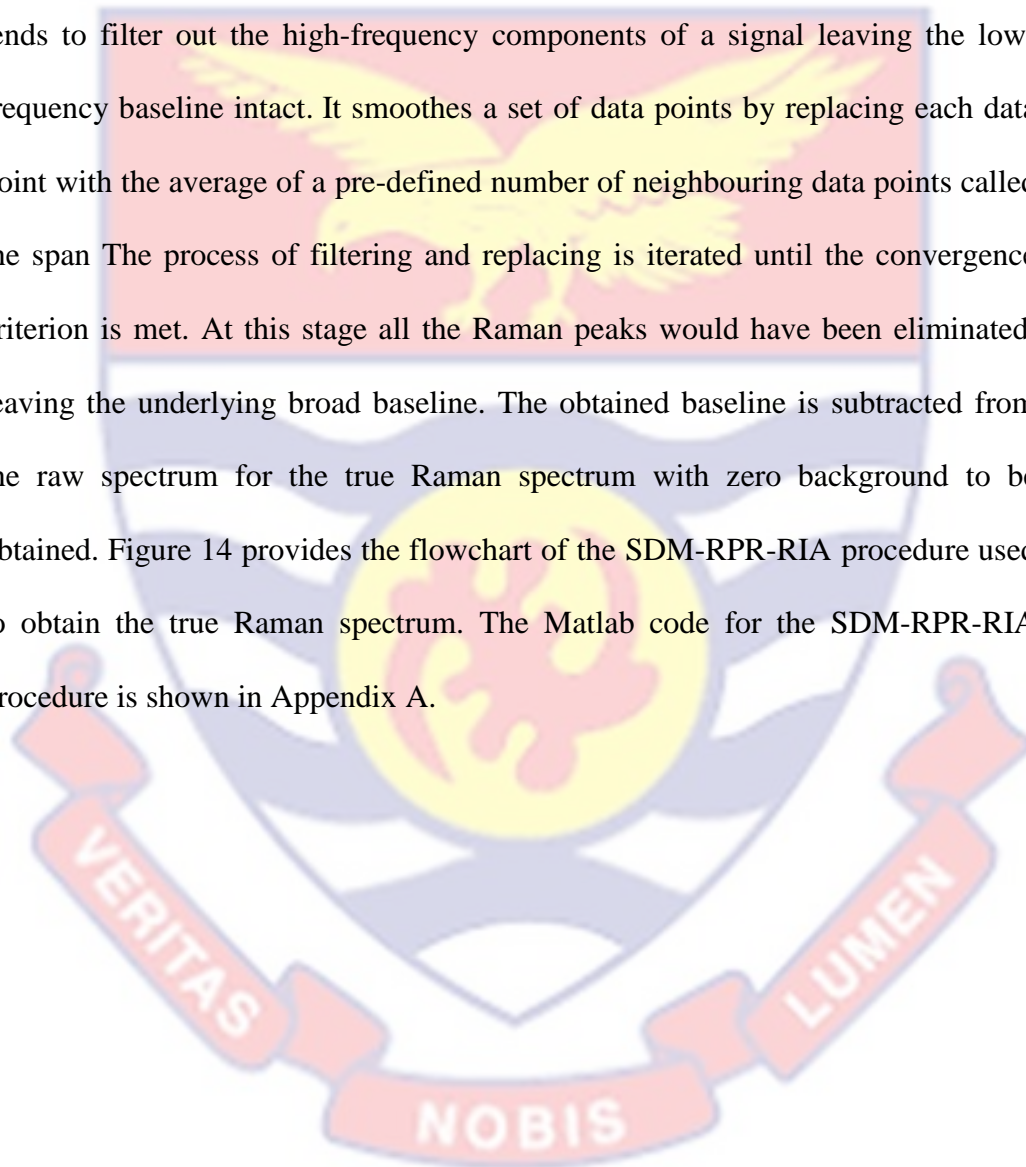


Figure 13: A flowchart of the second derivative method for Raman peak recognition

Following the derivation of the amplitude of the maximum Raman peak, the whole spectrum ($S_R(\nu_1)$) is subjected to a modified iterative smoothing based on moving point average (MPA). The MPA method is a zero-order Savitsky Golay filter and is equivalent to a low pass filter (Krishna et al., 2012). A low pass filter tends to filter out the high-frequency components of a signal leaving the low-frequency baseline intact. It smoothes a set of data points by replacing each data point with the average of a pre-defined number of neighbouring data points called the span. The process of filtering and replacing is iterated until the convergence criterion is met. At this stage all the Raman peaks would have been eliminated, leaving the underlying broad baseline. The obtained baseline is subtracted from the raw spectrum for the true Raman spectrum with zero background to be obtained. Figure 14 provides the flowchart of the SDM-RPR-RIA procedure used to obtain the true Raman spectrum. The Matlab code for the SDM-RPR-RIA procedure is shown in Appendix A.



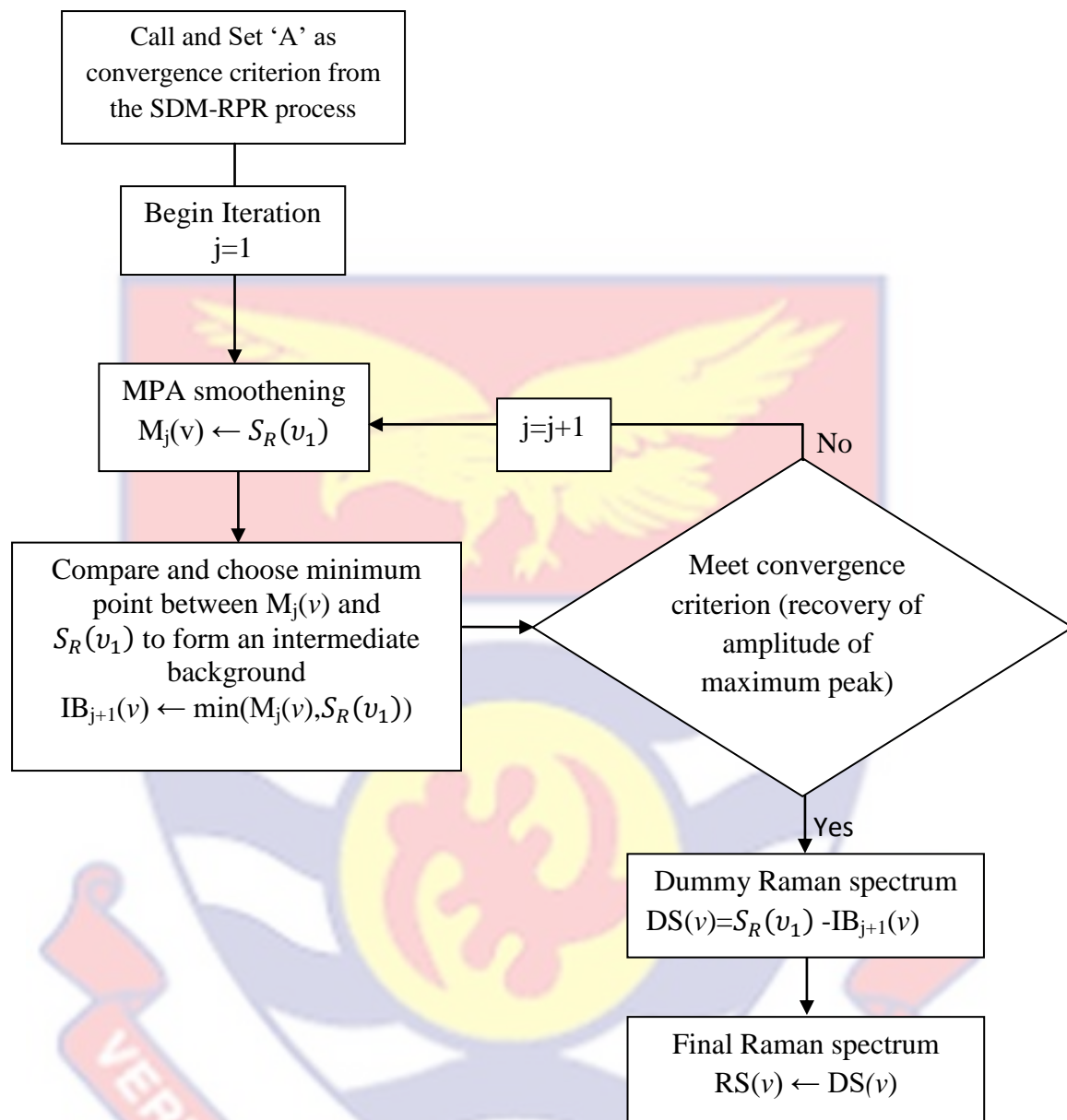


Figure 14: Flowchart of the second derivative method for Raman peak recognition and range independent algorithm (SDM-RPR-RIA)

Testing the algorithm

A mathematically generated Raman spectrum using the parameters of Lorentzian function shown in Table 3 was used for the development and

validation of the SDM-RPR-RIA. With these values a series of 12 Lorentzian peaks on a null baseline was generated.

Table 3

Lorentzian Function Parameters used to generate the Raman Spectrum; a_0 is the peak area, a_1 is the peak center position and a_2 is the peak width

a_0 (a.u.)	a_1 (cm ⁻¹)	a_2 (cm ⁻¹)
20.32	856	31
19.91	944	23
25.02	1002	6
19.07	1027	20
20.36	1071	30
1.93	1123	79
27.80	1259	24
33.01	1265	26
44.01	1302	16
25.81	1341	14
117.67	1444	17
85.40	1652	21

These peaks were placed on a fifth order polynomial baseline to mimic a typical raw tissue Raman spectrum. In practical situations dissimilar baselines can be observed. The performance of the algorithm was tested on three additional baselines including an exponential baseline, a Gaussian baseline, and a sigmoidal baseline. Figure 15 shows the nature of all the four types of baselines used in the simulation. The function equations and parameters of these baselines are found in Appendix B.

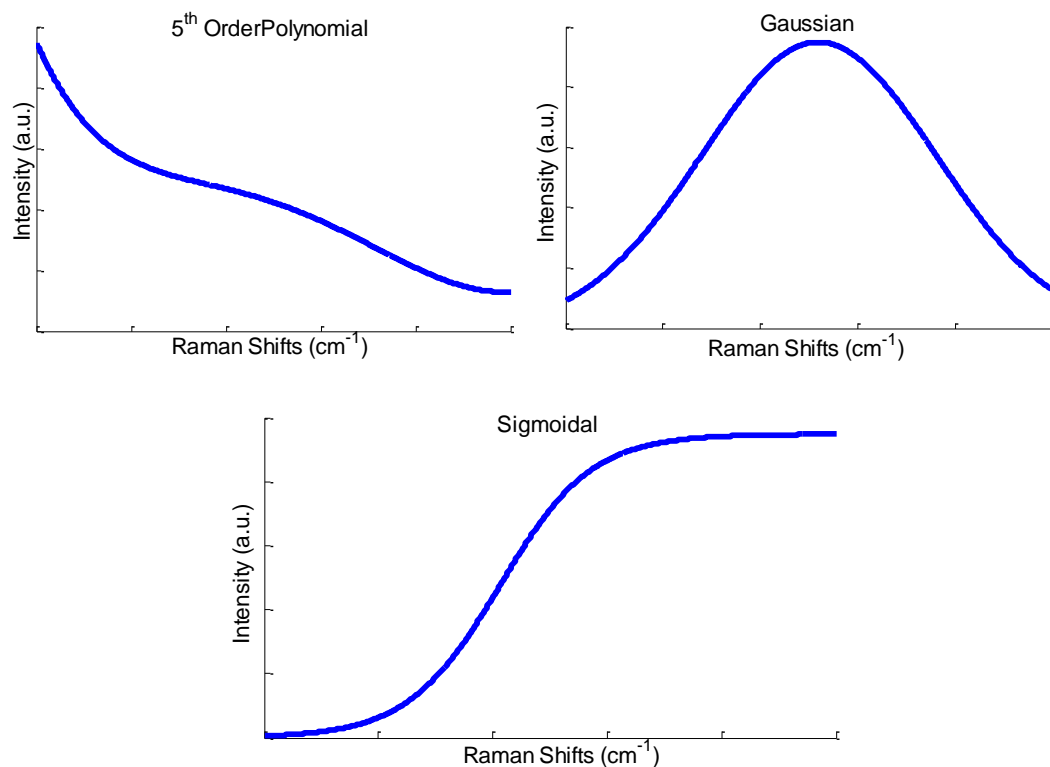


Figure 15: The fifth order polynomial, Gaussian and sigmoidal type of baselines used to test the performance of the second derivative method for Raman peak recognition and range independent algorithm (SDM-RPR-RIA)

A good background subtraction algorithm should accurately recover peaks embedded in a spectrum irrespective of the signal-to-fluorescence ratio (SFR). Especially, for very low values of the SFR. SFR is the ratio of the intensity of the tallest Raman peak to its baseline height. Mathematically, SFR is expressed in equation (10). The SFR values used in this study for the testing ranged from 0.5 to 0.005. A Raman spectrum of varying SFRs on the fifth order polynomial baseline is illustrated in Figure 16.

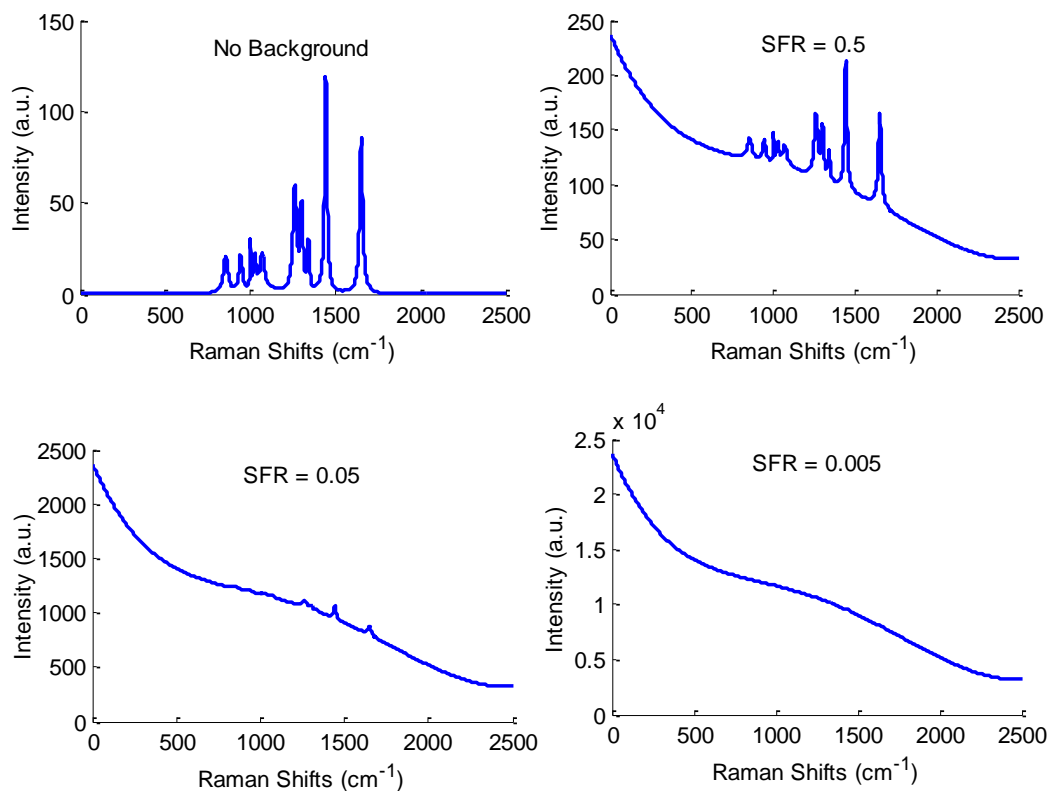


Figure 16: Raman spectra of 0.5, 0.05 and 0.005 signal-to-fluorescence ratio (SFR) imposed on the fifth order polynomial baseline

The SDM-RPR-RIA was evaluated quantitatively on the basis of the Weighted Correlation Coefficient (WCC). This was compared with results from literature. The SDM-RPR-RIA was again assessed on how well it can recover signals from a noisy spectrum. Raman spectra with signal-to-noise ratio (SNR) between 0.01 and 10 were generated and used for the assessment. These levels of SNRs were generated with a constant level of Gaussian (white) noise having a standard deviation of 1.

CHAPTER FOUR

RESULTS AND DISCUSSION

This chapter describes the performance characteristics of both the designed Raman system and mathematical processing algorithm developed in this study. The results obtained with the developed system in measuring the Raman spectrum of known samples have been discussed. Additional functionalities of the developed Raman system including chemometrics and polarisation measurements have also been analyzed.

The Raman System setup

Figure 17 depicts the developed Raman system setup in operation. The approximate cost of the components for the developed Raman setup is summarized in Table 4.

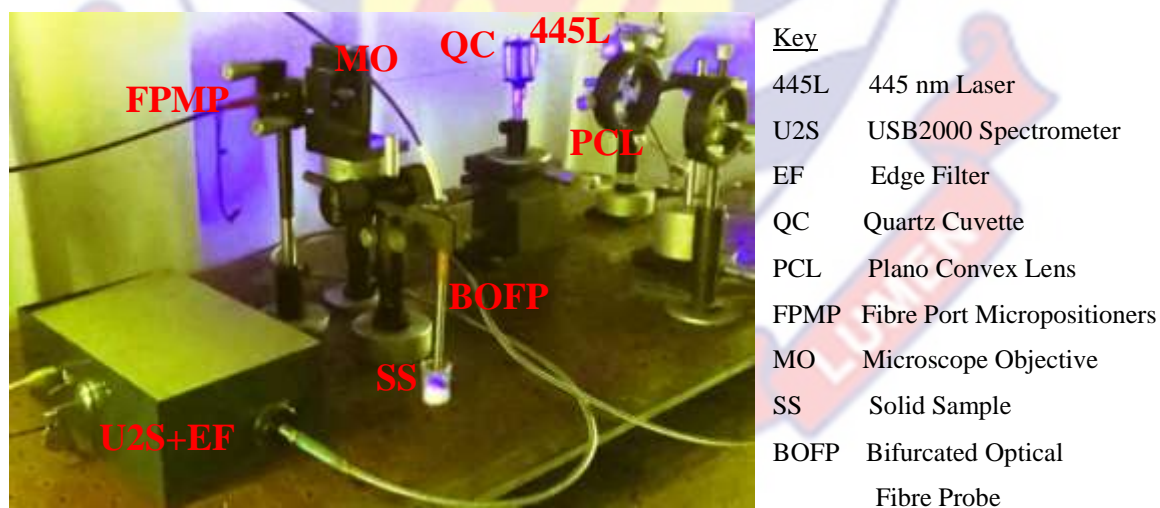


Figure 17: The developed low cost Raman system setup and components

Table 4

Estimated Prices of Set-up Components

Component	Cost (\$)
CCD Based Spectrometer	2000
Diode Laser	100
Long pass Edge filter	425
Fiber probe	460
Laptop	300
Total	3285

The total amount of \$3285 shows a reduction in the cost of our developed system as compared with recently reported low cost Raman systems (Bisson et al., 2006). Young, Stuart, Lyandres, Glucksberg, and Van Duyne (2004) report of a similar cost effective setup using a 10 mW laser pointer as the source with a total cost of \$3668. However, their type of system requires a band pass filter to achieve narrow bandwidth and a SERS substrate to enhance the Raman signals. These inclusions invariably make their system much more expensive than reported. Here the source in our case is a 100 mW, 445 nm diode laser. The diode laser is solely capable of enhancing the Raman signals because of its lower wavelength and high power, hence ignoring the need for a SERS substrate. The dimensions of the developed Raman system setup are within a 30x15x10 cm³ space on an optical bread board. With this space the entire setup can easily be developed into portable miniature device. The advantages of a commercial Raman system may supersede this relatively inexpensive setup. However, for many applications, such as blood glucose monitoring, drinking water testing, forensics, remote field defense sensing and environmental sampling, this setup presents an

appreciable alternative. Additionally, the low cost miniaturized system will facilitate research and learning capabilities in Raman spectroscopy among scientists and students in developing countries.

System Characterization Measurement

The specific characterization parameters measured include the wavelength axis calibration, sensitivity of the system based on SNR and system resolution. Figure 18 describes the spectrum of the water and associated noise of the system (insert).

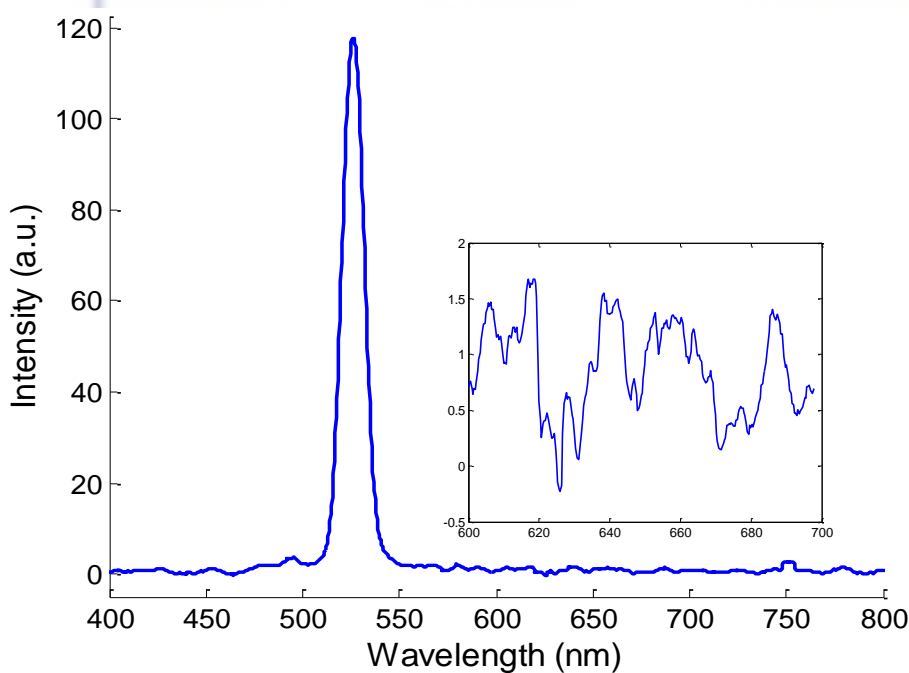


Figure 18: The water Raman Spectrum and associated noise (insert) used to compute signal-to-noise ratio (SNR) of the system

The peak centre wavelength occurs at 532.9 nm (i.e., between 3300 cm^{-1} to 3500 cm^{-1}). This is in excellent agreement with standard Raman band position for water (Lawaetz & Stedmon, 2009). The maximum attainable intensity in

arbitrary units for the water Raman peak using the developed Raman system was ~120. These parameters showed almost no variations at all times during measurements. It is therefore possible for comparison to be made between measurements over different periods in time.

A quantitative spectral analysis with Raman spectroscopy requires a Raman spectrum having high SNR. The absolute intensity of the water Raman signal is 117 and the standard deviation of the noisy spectrum is 0.448. By using Equation (13), the SNR of the system was computed to be 278. Even though most commercial systems report higher SNR values the developed Raman system, the value obtained is estimable as it will still enable very prominent Raman signals to be observed. The SNR can further be improved by several spectra accumulations and signal averaging. The SNR is also a factor that enhances reproducible measurements.

Table 5

Fit Parameters for Mercury (Hg) and Cyclohexane Spectrum using the developed Raman spectroscopic system

Material	Fit parameters for most intense peak		
	Peak position (nm)	Resolution (nm)	r^2
Mercury (Hg)	545.1	7.81	0.9929
Cyclohexane	512.9	4.68	0.9945

Table 5 summarizes the results for the fitting parameters of the most intense peak of the mercury and Cyclohexane spectra shown in Figure 19 and Figure 20, respectively.

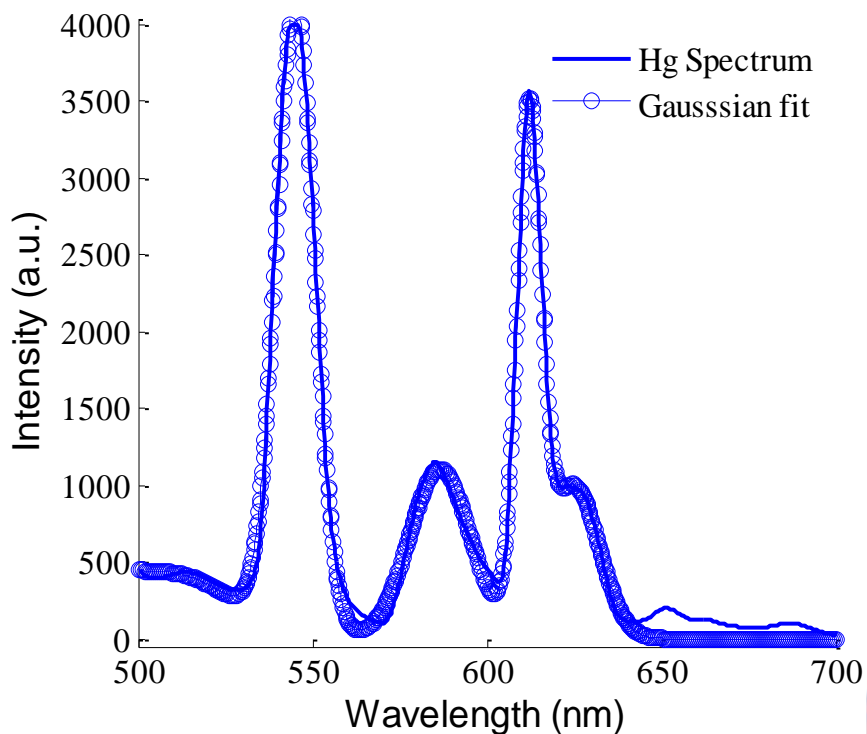


Figure 19: Fitted spectrum of fluorescence mercury (Hg) lamp to determine resolution of the bare spectrometer

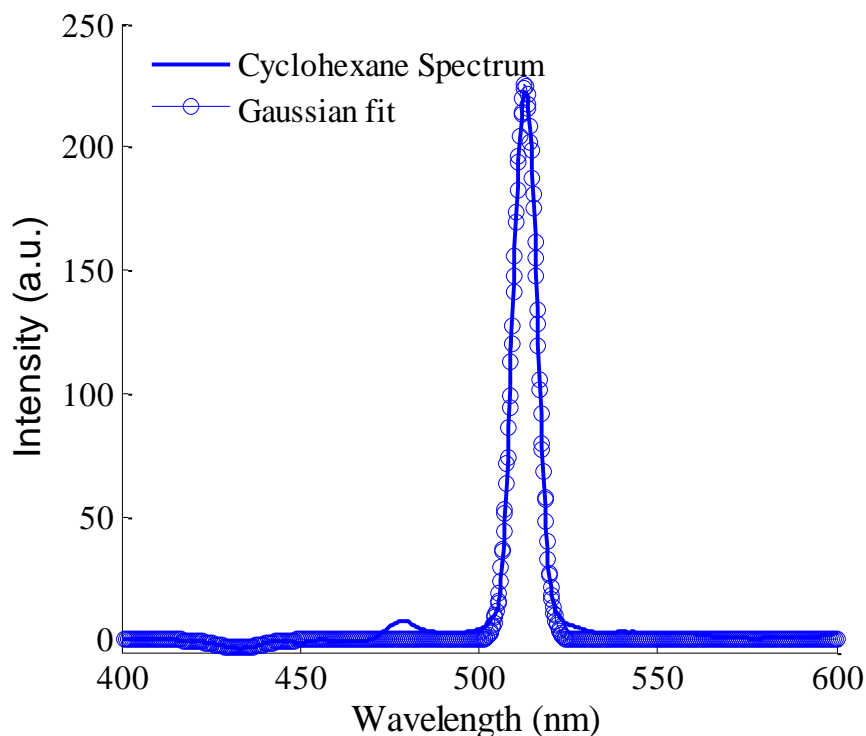


Figure 20: Fitted spectrum of Cyclohexane to determine resolution of the entire system

The values indicate a very low resolution by the developed Raman spectroscopic system. The implication is that it will be difficult to observe individual peaks in the Raman spectrum with this system as most of the peaks will be convolved rather than been resolved. That notwithstanding, mathematical procedures for signal enhancement such as Fourier Self Deconvolution (FSD) and Line shape Optimization Maximum Entropy linear Resolution (LOMEP) can be used to resolve those spectral peaks (Saarinen & Kauppinen, 2002). These methods are cost effective and avoid the need for additional instrumentation.

System test measurement

Figure 21 shows the Raman spectrum of known samples measured with the developed system. The spectra recorded include both liquid and solid samples. Generally, the liquid samples have very small backgrounds indicating minimal fluorescence contamination as compared to the solid samples.

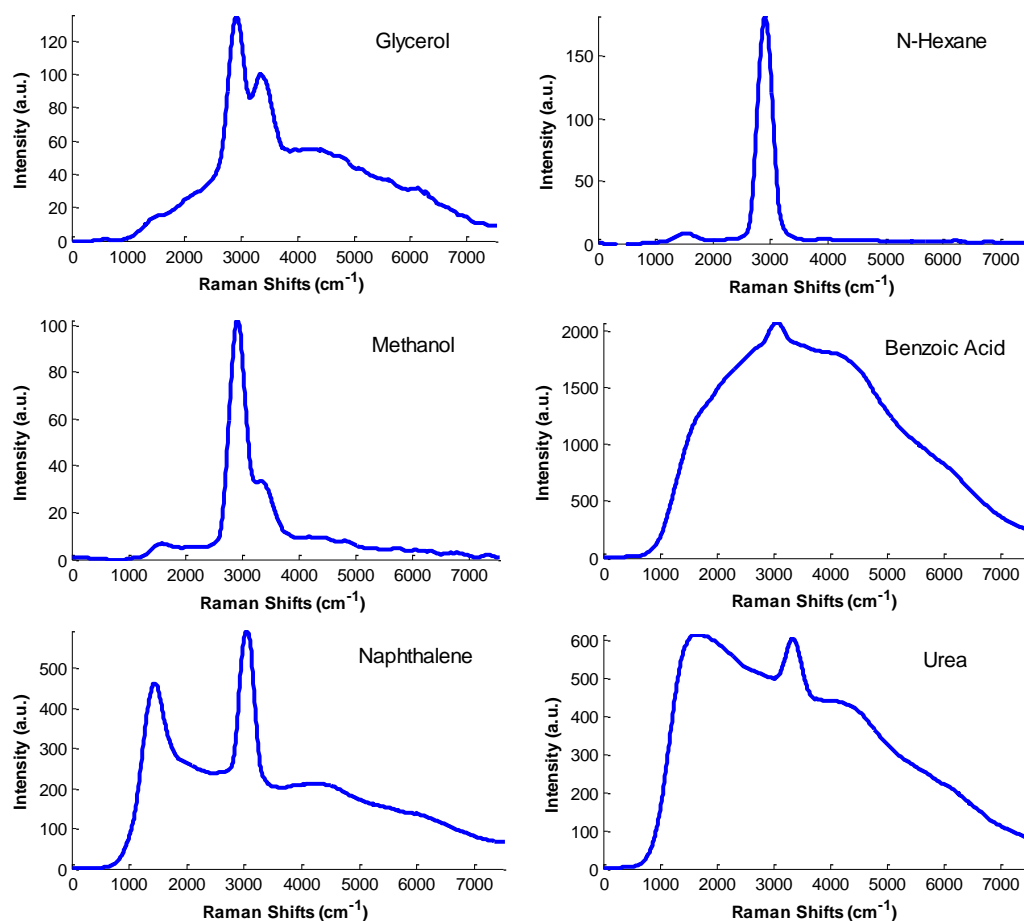


Figure 21: Raman spectrum of liquid (glycerol, n-hexane and methanol) and solid (benzoic acid, urea, and naphthalene) samples measured with the developed system

The spectra of benzene, ethanol and water samples studied for their parallel and perpendicularly polarized Raman spectra are shown in Figure 22. The

figure describes the Raman spectra of the samples when there is no polarizer and when the polarizer and analyser are placed in either parallel (P_{\parallel}) or perpendicular (P_{\perp}) positions. From Figure 22 it can be observed that the fluorescence background intensity remains almost unchanged in both the P_{\parallel} and P_{\perp} spectra, whereas, the Raman peak intensities decrease substantially for the P_{\perp} spectra. As explained by Angel et al., (1984), the fluorescence intensity remains unchanged because fluorescence photons unlike Raman photons are not polarized to be affected by the change in polarisation state of the laser.

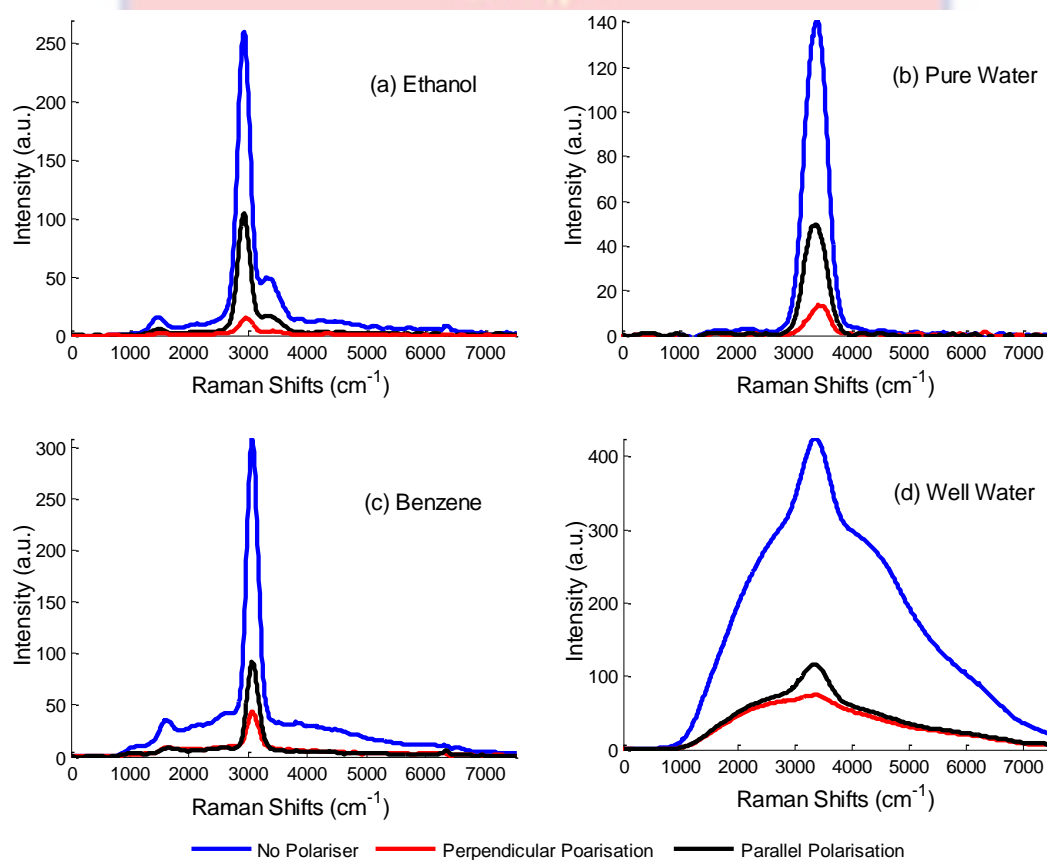


Figure 22: Raman spectra of benzene, ethanol, Pure water and well water samples with their associated P_{\parallel} (black) and P_{\perp} (red) polarised Raman spectra

In Figure 22d, the Raman spectrum of well water sample is almost obscured by the broad and huge fluorescence background. The fluorescence background feature is due to the presence of dissolve organic matter (DOM) content in the water (Lawaetz & Stedmon, 2009). The SFR of the spectrum is 0.5. This indicates an average fluorescence background which is twice the size (amplitude) of the Raman peak. A spectrum with SFR value of 0.5 or below complicates peak detection especially by visual inspection. It is therefore, not surprising that the peak occurring around 3350 cm^{-1} is almost obscured by the broad and huge fluorescence feature.

Figure 23 describes the spectra of varying concentrations of ethanol measured with the developed Raman system.

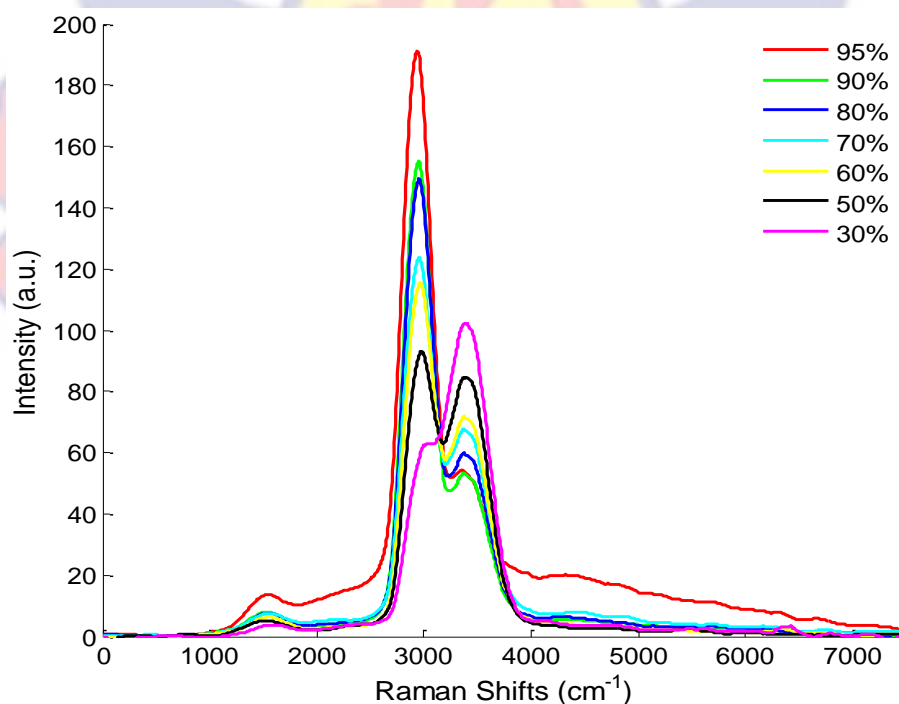


Figure 23: Raman spectra of ethanol measured at different concentrations with the developed Raman system

Even though the spectra recorded have some amount of fluorescence background, the variations in the different concentrations can still be seen. This affirms the capability of the developed Raman system for the evaluation of sample concentration or sample dilution.

Fluorescence Background Removal Procedure

The fluorescence background found in all the measurements recorded with the developed Raman system setup were removed with the proposed second derivative method for Raman peak recognition and Range independent background algorithm (SDM-RPR-RIA) prior to any further analysis. The performance of the SDM-RPR-RIA with respect to Raman signals of different baseline types, SFR and SNR, is first described. This is followed by the description of how the SDM-RPR-RIA was used in the recovery of Raman peaks from the Raman spectra initially measured with the developed Raman setup.

Figure 24 is a mathematically generated Raman spectrum with a fluorescence background. It comprises 12 Lorentzian peaks superimposed on a fifth degree polynomial baseline.

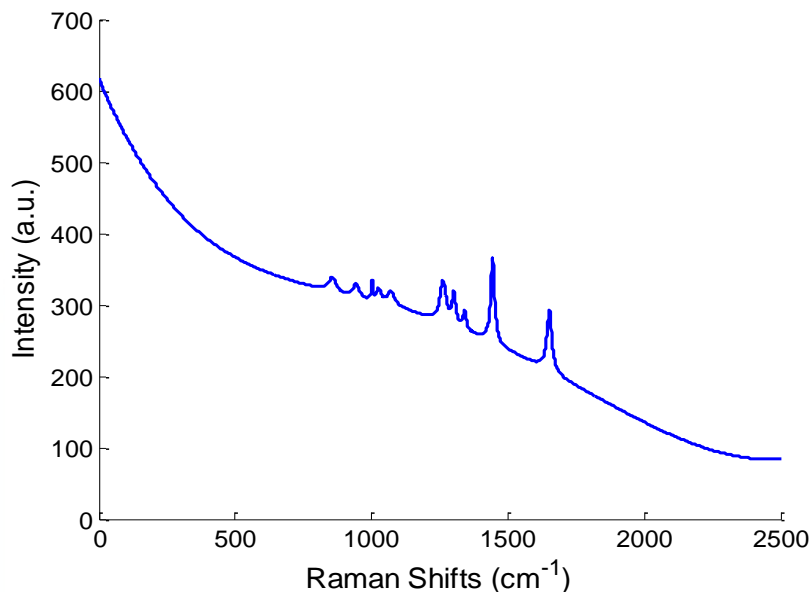


Figure 24: Mathematically generated Raman spectrum with 12 Lorentzian peaks on a fifth order polynomial baseline

The processes for the recovery of the Raman spectrum from the fluorescence background as described in Figure 25. In Figure 25a the mathematically generated Raman spectrum and its second derivative is shown. In Figure 25b, the derivative spectrum is fitted to obtain the amplitude of the maximum peak. Figure 25c is the result of processing with the SDM-RPR-RIA. Figure 25d shows how successfully the SDM-RPR-RIA has been able to estimate the fifth order polynomial baseline. The baseline is subtracted from the mathematically generated Raman spectrum with fluorescence background. The recovered Raman spectrum is compared with the original Raman spectrum in Figure 25d. The SDM-RPR-RIA is seen to successfully recover Raman peaks from its intense background. The novelty of the SDM-RPR-RIA has to do with the non-subjective manner in which the criterion of convergence is chosen. As stated earlier the RIA method required the use of two artificial peaks. The RIA-

SG-RPR method also requires the user to specify the SFR value. In the proposed SDM-RPR-RIA no user intervention is required since all parameters used are generated by the algorithm. This makes the SDM-RPR-RIA more robust for recovery of Raman spectra as compared to the other algorithms. In effect, the SDM-RPR-RIA makes a suitable candidate for full automation implementation.

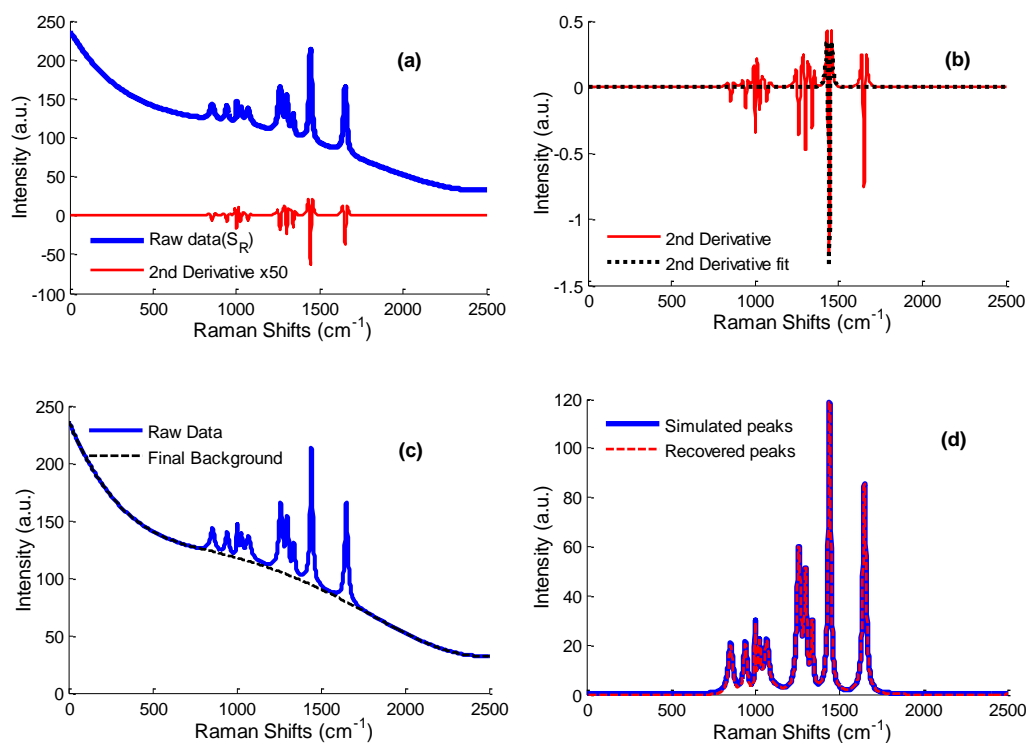


Figure 25: Raman signal recovery processes using the second derivative method for Raman peak recognition and range independent algorithm (SDM-RPR-RIA)

Figure 26 shows the raw Raman spectra for each of the baselines on which the SDM-RPR-RIA was tested. The recovered spectrum is shown beneath each baseline. Following the application of the SDM-RPR-RIA, it can be seen from Figure 26 that, in all the three cases there is complete recovery of the Raman

peaks with almost no obvious distortions or artifacts. This exemplifies the effectiveness of the SDM-RPR-RIA in estimating spectral baselines irrespective of the type.

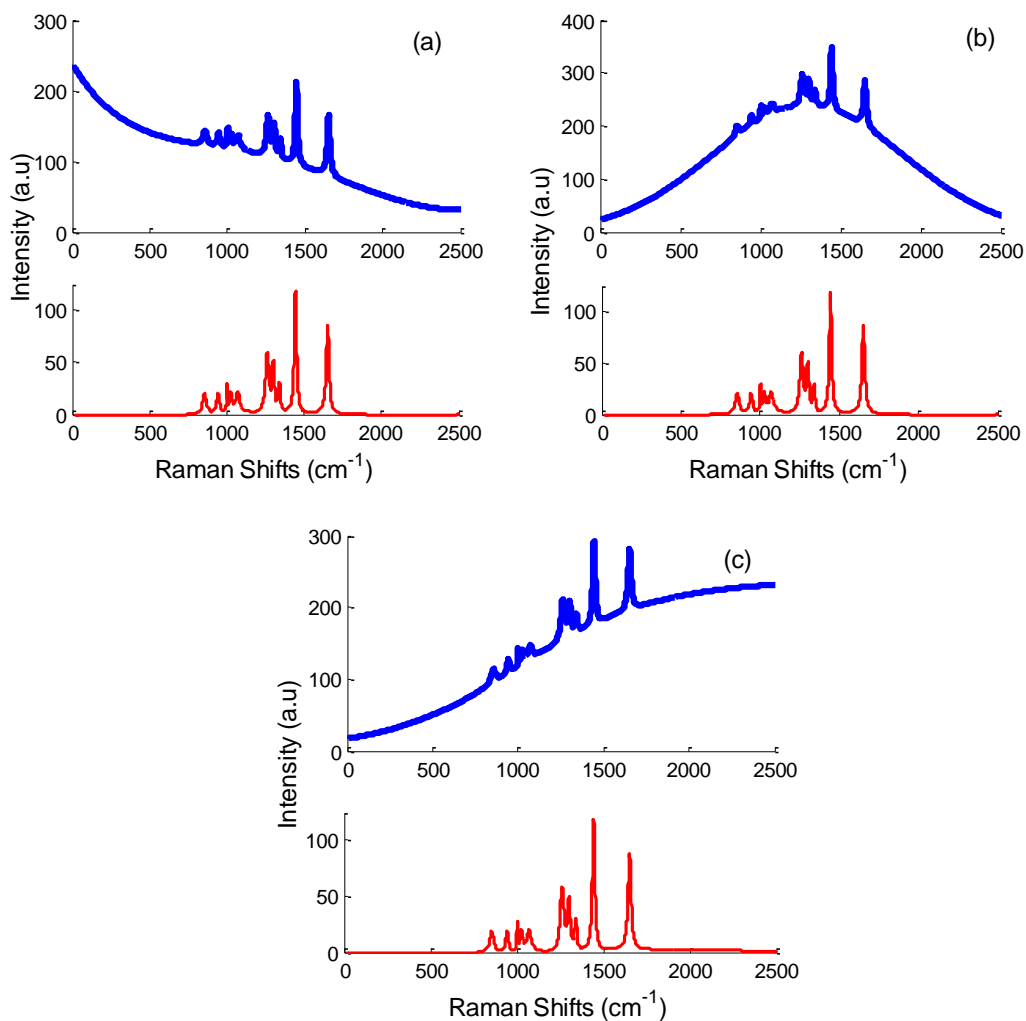


Figure 26: Raman spectra recovered from (a) fifth degree polynomial (b) Gaussian and (c) sigmoidal baselines using the second derivative method for Raman peak recognition and range independent algorithm (SDM-RPR-RIA)

Figure 27 shows SFRs of 1, 0.5, 0.05 and 0.005 with their corresponding recovered spectrum. Visual examination of the different spectra shows the Raman

peaks gradually disappear with lower SFR values. The subtraction-recovered Raman spectra in Figure 27 give evidence of how the SDM-RPR-RIA faithfully retrieves Raman peaks without any apparent distortions.

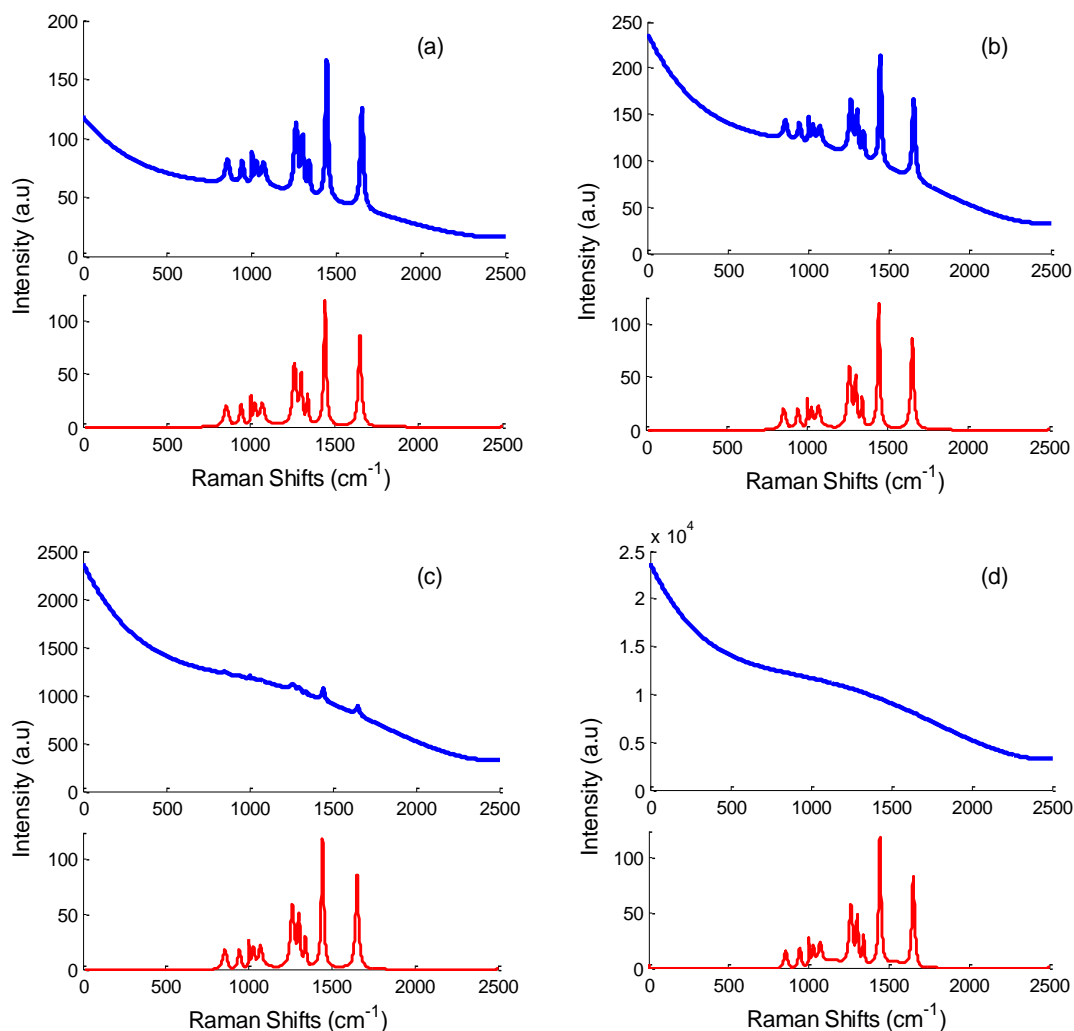


Figure 27: Raman spectra recovered from polynomial baselines of (a) 1, (b) 0.5, (c) 0.05, (d) 0.005 signal-to-fluorescence ratio (SFR) using the second derivative method for Raman peak recognition and range independent algorithm (SDM-RPR-RIA)

The performance of the SDM-RPR-RIA was further determined quantitatively on the basis of the weighted correlation coefficient (WCC). A

higher WCC means a better match between the generated and the recovered Raman spectra (Griffiths & Shao, 2009). The implication is that recovered spectra actually reveal the “molecular fingerprint” which is of crucial importance in the application of Raman spectroscopy assessment. Table 6 shows the results of SDM-RPR-RIA as compared to results obtained for RIA, RIA-SG-SR and RIA-SG-RPR as reported by Chen et al., 2015.

Table 6
Comparison of the performance of RIA, RIA-SG-SR, RIA-SG-RPR and SDM-RPR-RIA under varying SFR conditions

Baseline Type	Algorithm Type	WCC		
		0.5	0.05	0.005
5th Degree Polynomial	RIA		0.9830	0.9811
	RIA-SG-SR		0.9812	0.9798
	RIA-SG-RPR		0.9870	0.9871
	SDM-RPR-RIA	0.9992	0.9987	0.9921
Gaussian	RIA		0.9830	0.1057
	RIA-SG-SR		0.9809	0.1252
	RIA-SG-RPR		0.9870	0.9876
	SDM-RPR-RIA	0.9990	0.9946	0.8797
Sigmoidal	RIA		0.9829	0.8574
	RIA-SG-SR		0.9814	0.6942
	RIA-SG-RPR		0.9870	0.9870
	SDM-RPR-RIA	0.9902	0.9625	0.8710

From Table 6, for 0.05, all the four methods achieve nearly the same recovery performance with the proposed SDM-RPR-RIA performing better especially for the Gaussian and Polynomial baseline. However, for SFRs below 0.05, the RIA-SG-RPR shows better recovery than the proposed SDM-RPR-RIA.

Since the SDM-RPR-RIA uses the second derivative approach in detecting peaks and considering the fact that derivatives have the potential of enhancing noise, it was worthwhile assessing the performance of the algorithm based on its performance to recover spectra with SNR. Figure 28 portrays a noiseless spectra (blue) with two other spectra having a SNR of 10 (red) and 0.01 (black).

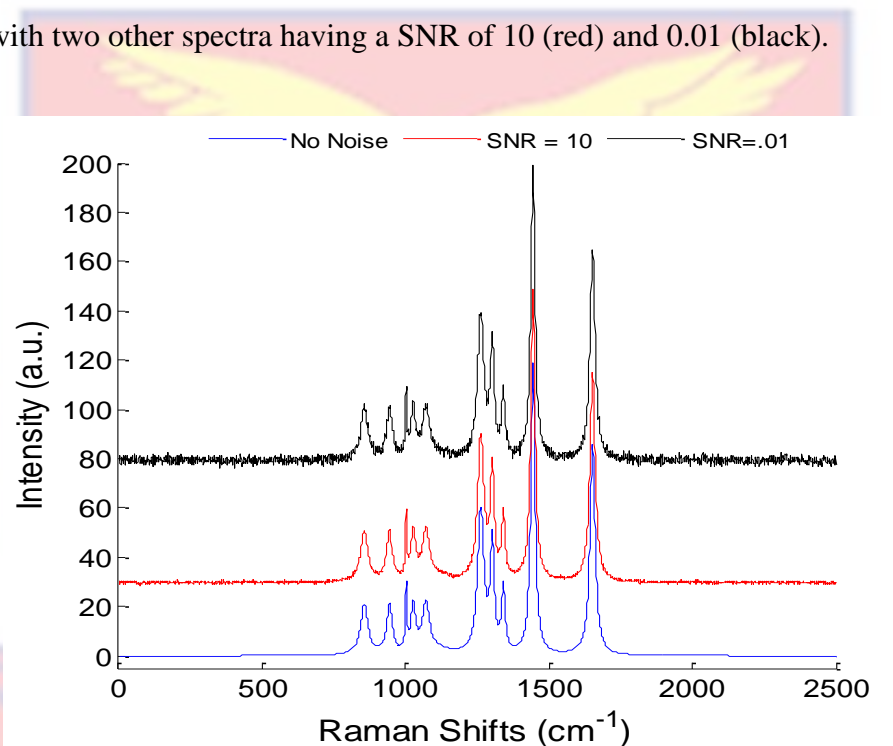


Figure 28: Mathematically generated Raman spectra with signal-to-noise ratio (SNR) of 10 (red) and 0.1 (black) compared with noise free Raman spectrum (blue)

In Figure 29, the recovery of the spectra with SNR levels of 10, 0.1 and 0.01 are compared based on their WCC values with a spectrum without any added noise. Comparatively, the algorithm shows almost the same performance even with very challenging noisy situations and varying background conditions. It must be noted that in the SDM-RPR-RIA, the second derivative spectrum of each of

these spectra were smoothed with a Savitsky Golay smoothing algorithm of 10 iterations before Raman signals are recovered.

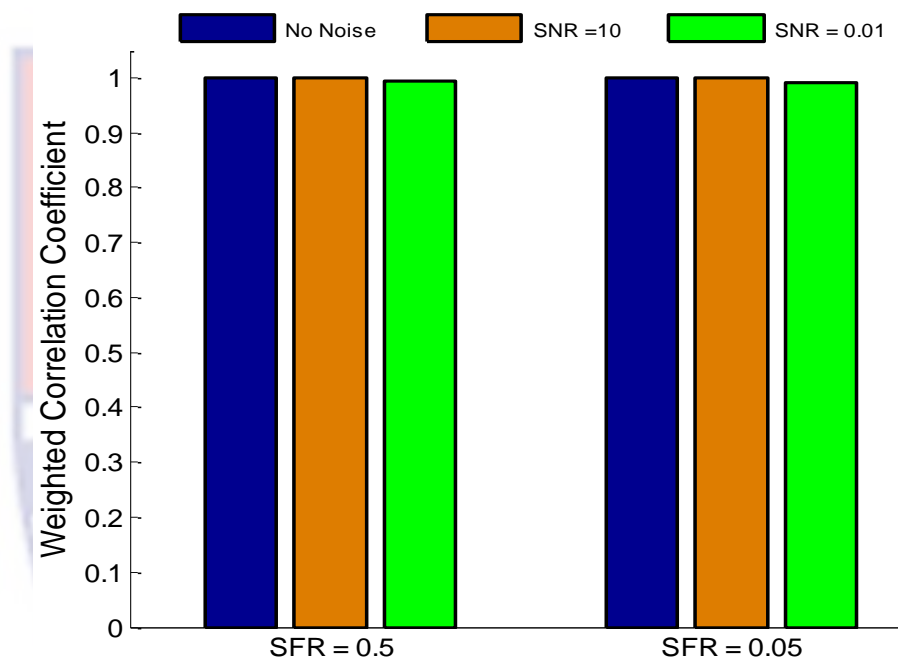


Figure 29: A comparison of the weighted correlation coefficient (WCC) between spectra with signal to noise ratio (SNR) of 0.01 and 10 for the case of 0.5 and 0.005 SFR after processing with the second derivative method for Raman peak recognition and range independent algorithm (SDM-RPR-RIA)

Retrieved Raman signal from measured spectra using the SDM-RPR-RIA

Figure 30-32 exemplifies how the SDM-RPR-RIA operates when applied to spectra recorded with the developed low-cost Raman system. Three cases of a small SFR (Benzene, 3.29), medium SFR (Naphthalene, 0.74) and a huge SFR (Benzoic acid, 0.06) are considered. In Figure 30 a very high SFR is observed for Benzene. This presents less difficult situation for the SDM-RPR-RIA to recover the benzene Raman spectrum. In contrast, Naphthalene and Benzoic acid

demonstrate a relatively complicated case of intense fluorescence contamination. Especially in the case of the Benzoic acid (Figure 32), the peaks which hitherto were unobservable have become prominent as a result of preprocessing with the SDM-RPR-RIA.

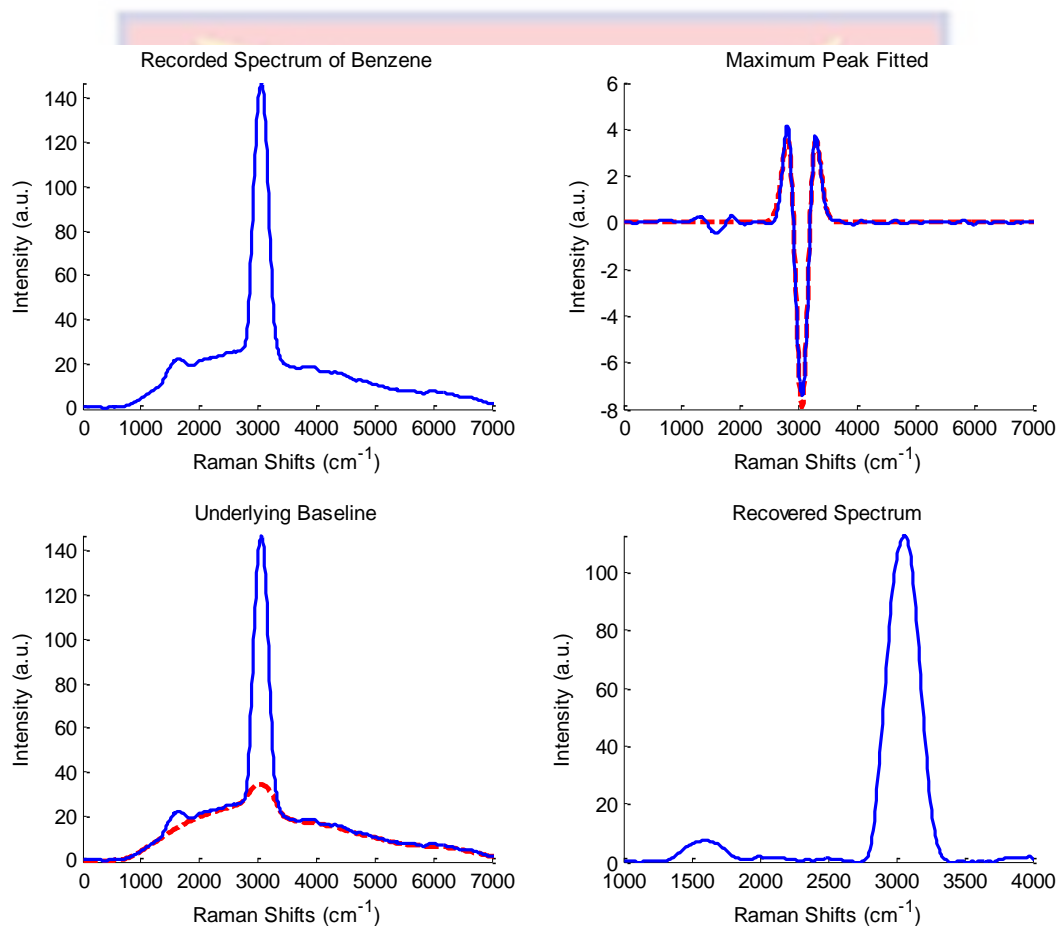


Figure 30: Benzene Raman spectrum recovery process using the second derivative method for Raman peak recognition and range independent algorithm (SDM-RPR-RIA)

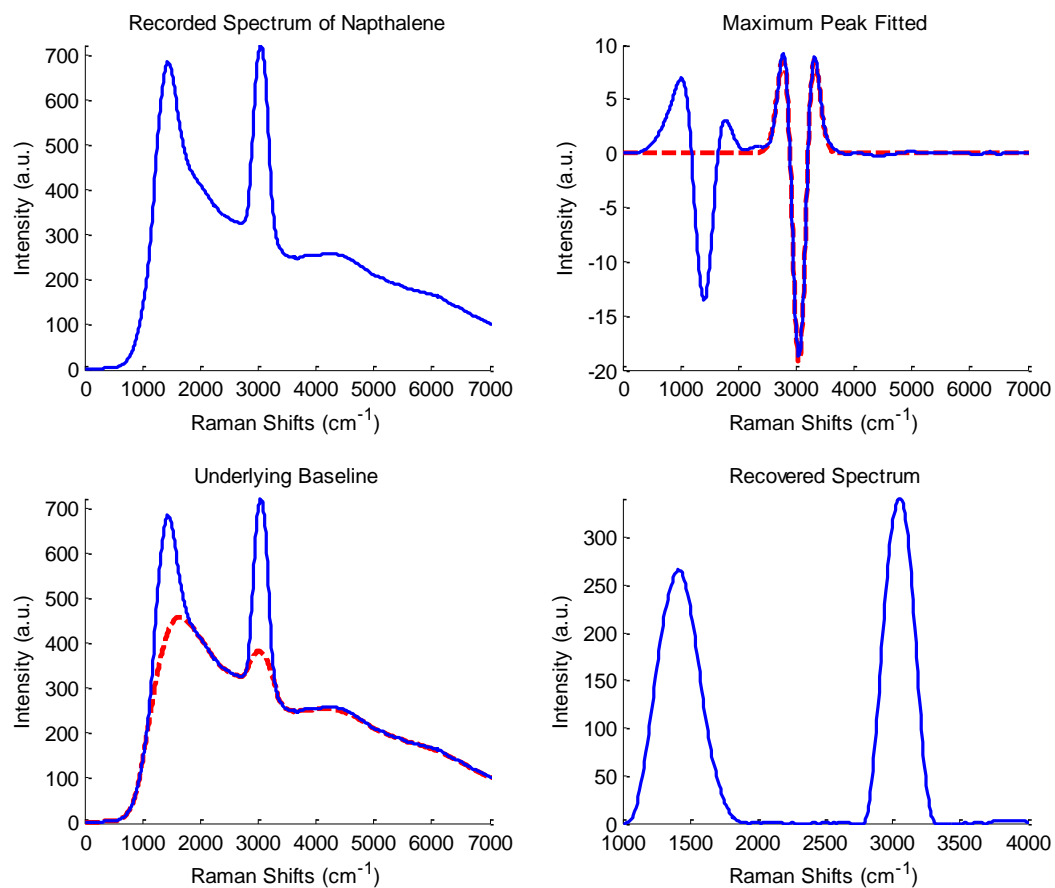


Figure 31: Naphthalene Raman spectrum recovery process using the second derivative method for Raman peak recognition and range independent algorithm (SDM-RPR-RIA)

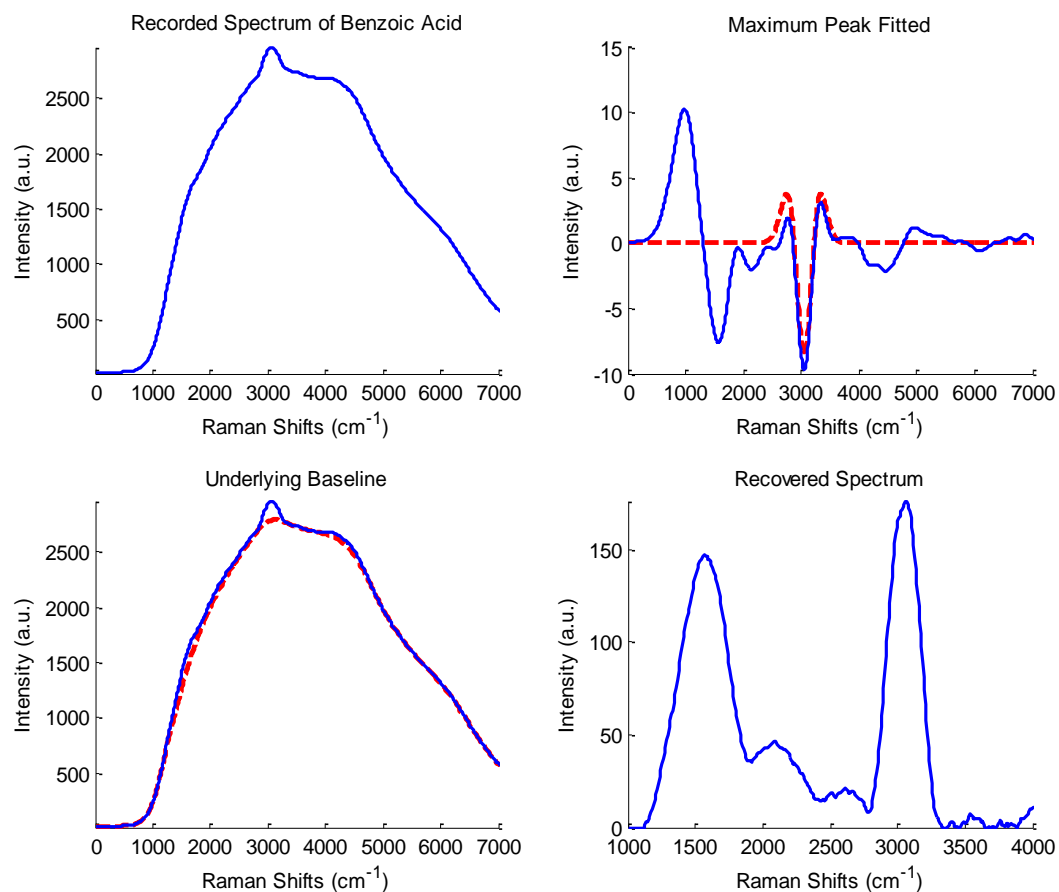


Figure 32: Benzoic Acid Raman spectrum recovery process using the second derivative method for Raman peak recognition and range independent algorithm (SDM-RPR-RIA)

The recovered Raman spectra of the samples tested with the developed Raman system setup are shown in Figure 33 and 34. The peaks in the spectra have been labeled with their corresponding centre wavelength positions. This is to ensure ease in comparing the samples based on their unique spectral features.

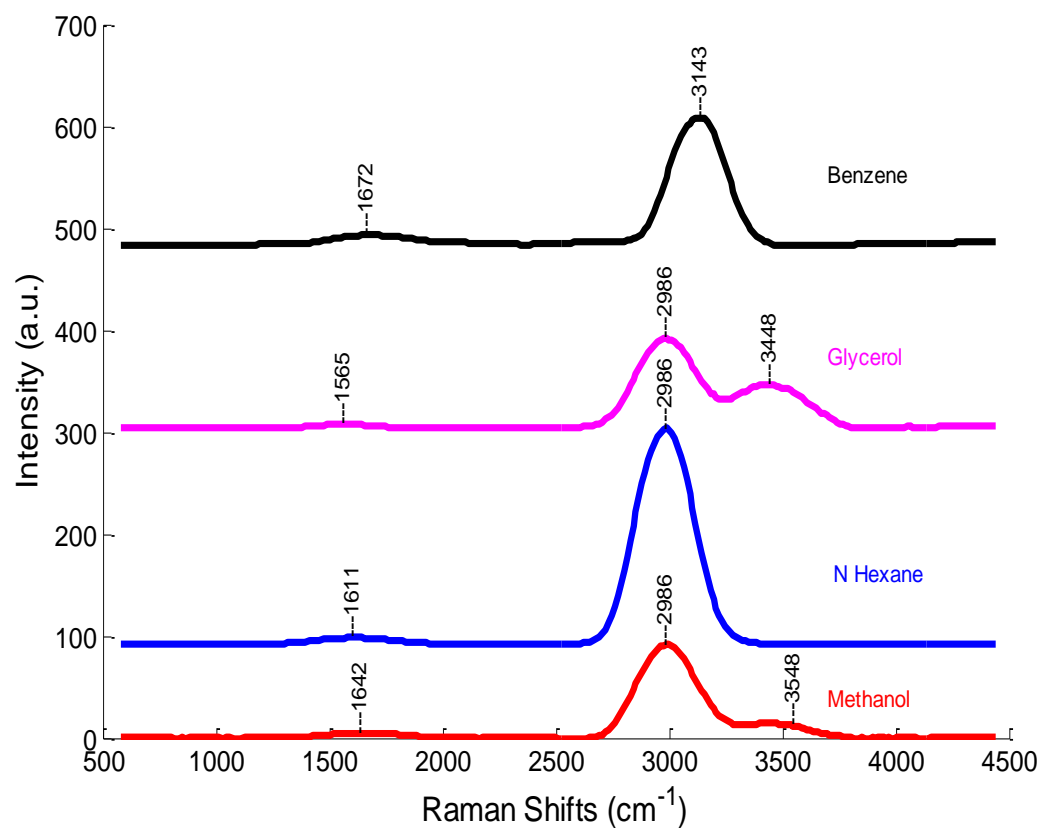
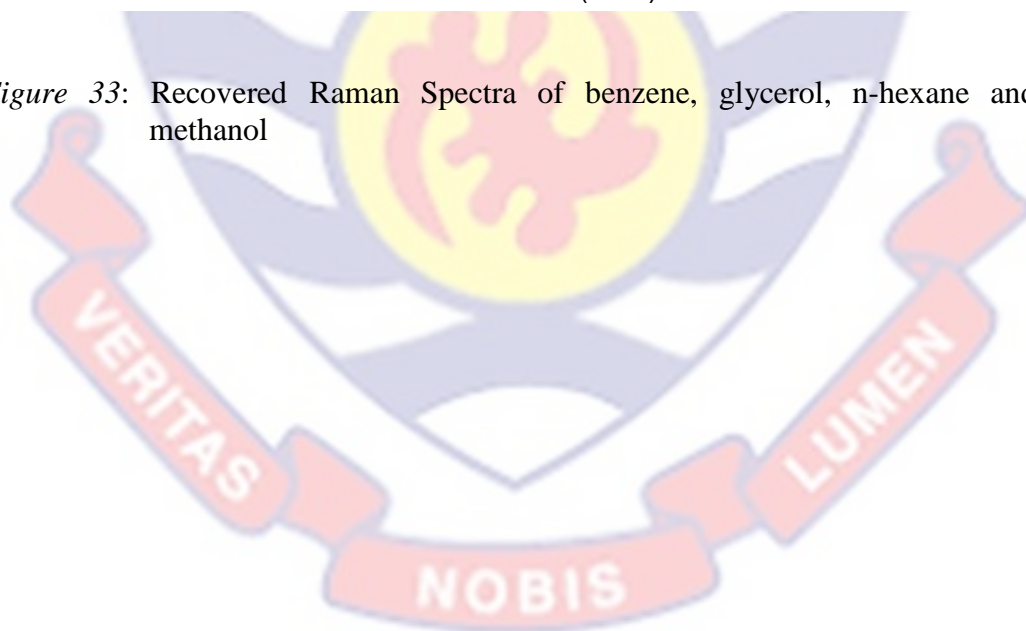


Figure 33: Recovered Raman Spectra of benzene, glycerol, n-hexane and methanol



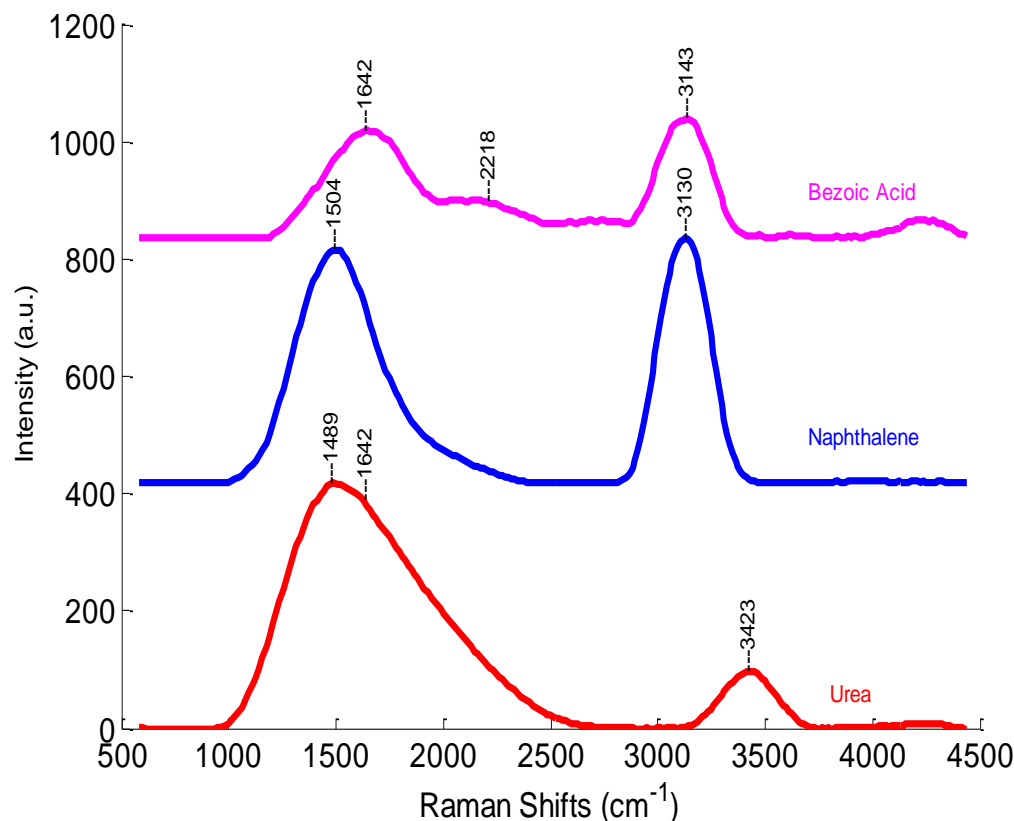


Figure 34: Recovered Raman spectra of benzoic acid, naphthalene and urea

The structure, peak position and possible functional group(s) of the peaks from each sample studied are described in Table 7. All the peaks observed in the Raman spectrum of each sample have been compared with results reported in literature.

In the results shown so far, the spectral peaks that can be identified in the samples studied with the developed Raman system setup occur beyond 1400 cm^{-1} . This region is known as the High Wavenumber Region (HWR) (Mo et al., 2009; Santos et al., 2005). The bonding groups or molecular structures found in the HWR are related to hydroxyl (O-H), alkyl (CH, CH_2 , CH_3) Carbonyl (C=O) and Amino (NH) vibrations. As observed from Table 7, the spectral parameters

measured with the developed Raman system setup corresponds very well with standard results. Even though vibrational peaks such as alicyclic (C–C) chain vibrations (n-hexane), C–O bond vibrations (benzoic acid, methanol, and glycerol) and CH₂ rocking mode (glycerol, Cyclohexane) occur around 1400 cm⁻¹, they were not observed because of the absorptive effect of the long pass edge filter used. The use of a holographic notch filter in place of the long pass edge filter will help to counteract this problem. Also, the resolution of the system was not good enough making the peaks observed appear broad and overlapping to distinguish individual peaks. A very sensitive spectrometer in place of the used USB 2000 spectrometer can help resolve this problem. As emphasized earlier, mathematical methods such as FSD and LOMEPE can equally help resolve the problem of system resolution to avoid extra cost and instrumentation.

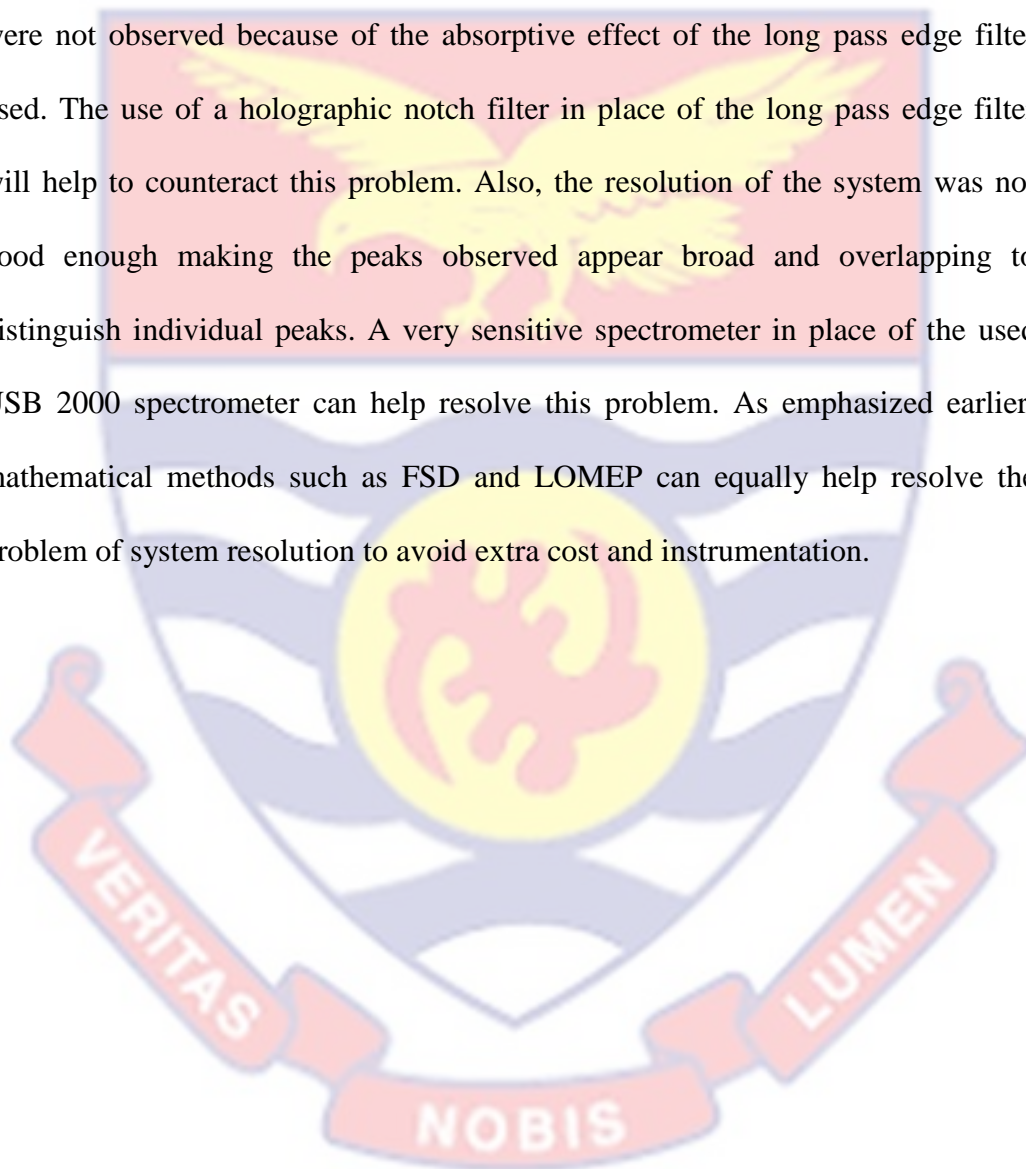
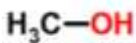
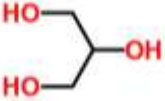


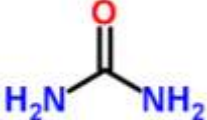
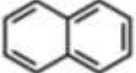
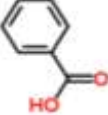


Table 7

Samples described according to their Structure, Peak Position and corresponding Functional Group Assignment. References for assigned values are a (Spectral Database for Organic Compounds, 2015), b (Mc Creery, 2005) and c (Ananthakrishnan, 1937)

SAMPLE	Peak Centre wavenumber(cm^{-1})		Mode Assignment
	Observed	Reported	
Methanol (CH_4O) 	1641.6 2986.3 3547.6	1453 ^a 2835 ^a , 2945 ^a	-CH ₃ asymmetric bend -CH ₃ asymmetric stretch Alcohol, OH
Glycerol ($\text{C}_3\text{H}_8\text{O}_3$) 	1565.4 2986.3 3448.2	1469 ^a 2890 ^a , 2944 ^a	-CH ₂ scissoring mode -CH ₂ asymmetric stretch Alcohol O-H,
Cyclohexane (C_6H_{12}) 	1489 2986.3	1444 ^{bd} 2924 ^{bd} , 2852 ^{bd} , 2938 ^b	-CH ₂ Scissoring mode -CH ₂ asymmetric & symmetric stretch
Benzene (C_6H_6) 	1672.4 2174.3 3143.0	1555 ^d , 1593 ^d , 1628 ^d 3063 ^{a,b}	Aromatic ring vibration Aromatic & Alkene =C-H bond vibration
Urea ($\text{CH}_4\text{N}_2\text{O}$) 	1457.3 1488.6 1641.6 3423.2	1465 ^c 1537 ^c 1576 ^c 3243 ^c , 3324 ^c , 3353 ^c 3467 ^c	Resonance amides C=O group NH group
Naphthalene 	1504.0 3129.9	1460 ^{a,c} , 1460 ^{a,c} , 1460 ^{a,c} 3001 ^c , 3025 ^c , 3050 ^{a,c}	Aromatic Chain vibration =C-H group as found in Aromatic chains & Alkene
Benzoic Acid 	1641.6 2217.5 3143.0	1604 ^a , 1634 ^a - 3064 ^a , 3073 ^a	Aromatic chain vibration, C=O group as found in Organic acids Acid - Acid O-H group

Polarisation Ratio and Polarisation Difference

The recovered Raman spectra of the samples studied to demonstrate polarisation effect in Raman spectroscopy is presented in Figure 35. Equation (11) was used to determine the depolarisation ratio (D) of the recorded spectra from the samples. These are presented in Table 8.

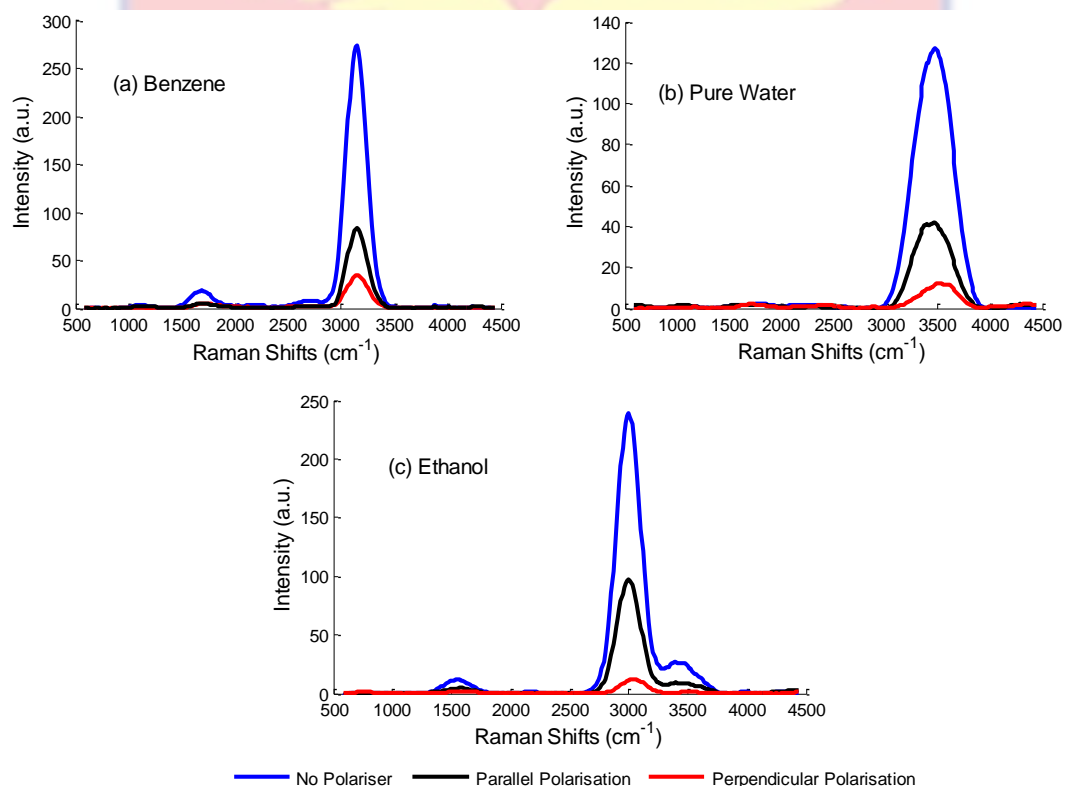


Figure 35: Spectrum of Benzene molecule showing the effect of both vertical and horizontal polarisation states

Table 8

Raman peak polarisation characteristics of Ethanol, Pure Water and Benzene

Sample	Peak position (cm ⁻¹)	Intensity (a.u.)			Depolarisation ratio (D)	
		No polarizer	(P)	(P _⊥)	Experiment	Literature
Water	3473.0	127.0	41.80	11.60	0.28	0.12
Ethanol	1550.0	11.8	4.50	2.00	0.44	-
	3000.0	238.9	97.50	11.30	0.12	-
	3461.0	26.2	8.70	1.30	0.14	-
Benzene	1688.0	18.3	4.70	4.70	1.00	0.75
	3130.0	272.7	83.0	34.7	0.42	0.1

The aromatic ring vibration occurring around 1688 cm⁻¹ for the benzene molecule has a D value greater than 0.75. This is typical of asymmetric molecular vibrations (McCreery, 2000). The peaks occurring at 3050 cm⁻¹ (OH; water, ethanol), 3130 cm⁻¹ (CH; benzene) and 3000 cm⁻¹ (CH₃; ethanol) correspond to symmetric vibrations because they have D values less than 0.5 (long, 1977).

When the parallel polarized Raman spectrum is subtracted from that of the perpendicularly polarized Raman spectrum, a polarisation difference Raman spectrum (PD-RS) is obtained. The aim of the PD-RS measurement is to help retrieve Raman peaks from highly fluorescent backgrounds. Figure 36 shows the parallel and perpendicularly polarized Raman spectrum of the well water sample. In this case the SDM-RPR-RIA has not been applied to recover the Raman peaks. The component of the polarisation difference spectrum (i.e. P_{||} minus P_⊥) is indicated with black dashed lines.

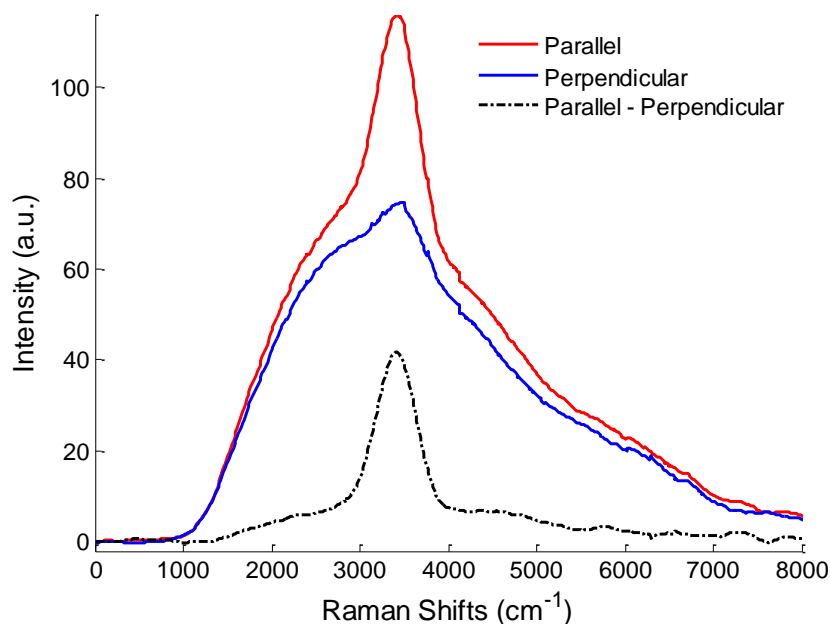


Figure 36: Polarisation difference spectrum (dashed lines) of the two polarisation states of the well water sample

The degree of recovery using equation 12 was found to be 20.14%. This gives evidence of the fact that the PD-RS method is equally a good candidate for Raman peak recovery from fluorescence contaminated spectra (Angel et al., 1984). The limitation to the PD-RS has to do with peaks known to have asymmetric features. These peaks, like the CH_2 vibrations in benzene molecule, show little or no difference in their amplitude for either parallel or perpendicular polarized spectrum. Hence, subtracting the perpendicular from the parallel polarized spectrum will produce either a null spectrum or a very less intense peak.

Chemometric analysis of varying Ethanol concentrations measured with the developed Raman system setup

Figure 37 shows the spectrum of varying concentrations of ethanol corrected from any background (insert) irregularity using the SDM-RPR-RIA.

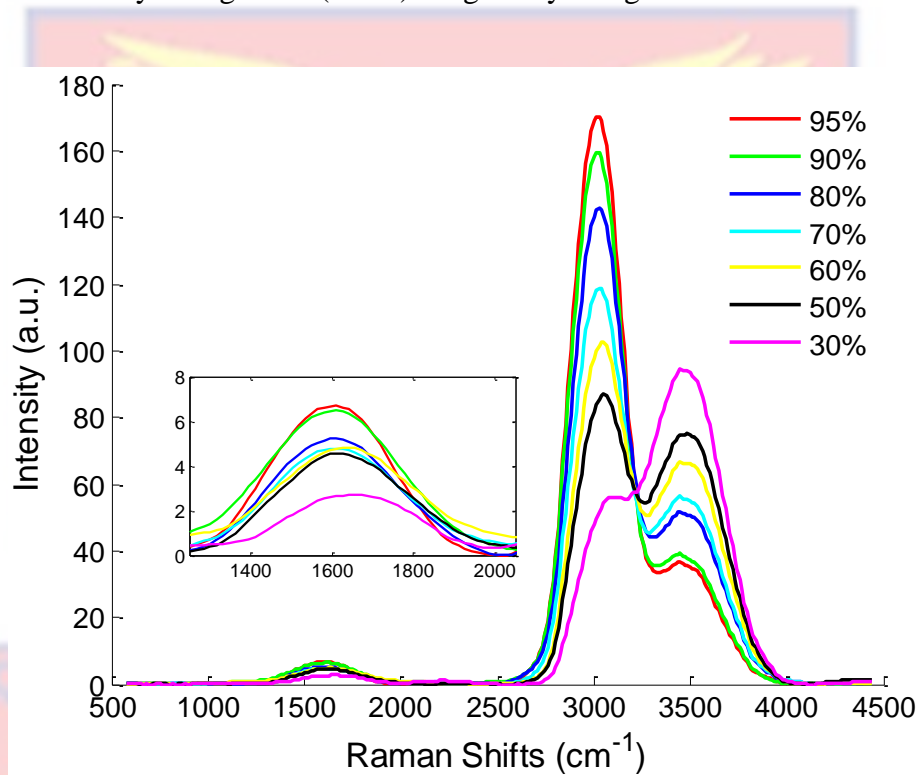


Figure 37: Recovered Raman spectrum of varying concentrations of ethanol

The data plotted in Figure 37 is a training data used to perform Partial Least Square regression (PLSR) analysis. Three PLS components were selected and used in generating a PLS regression vector. The 3 PLS components explain more than 99.95% of the variance in the data (Figure 38).

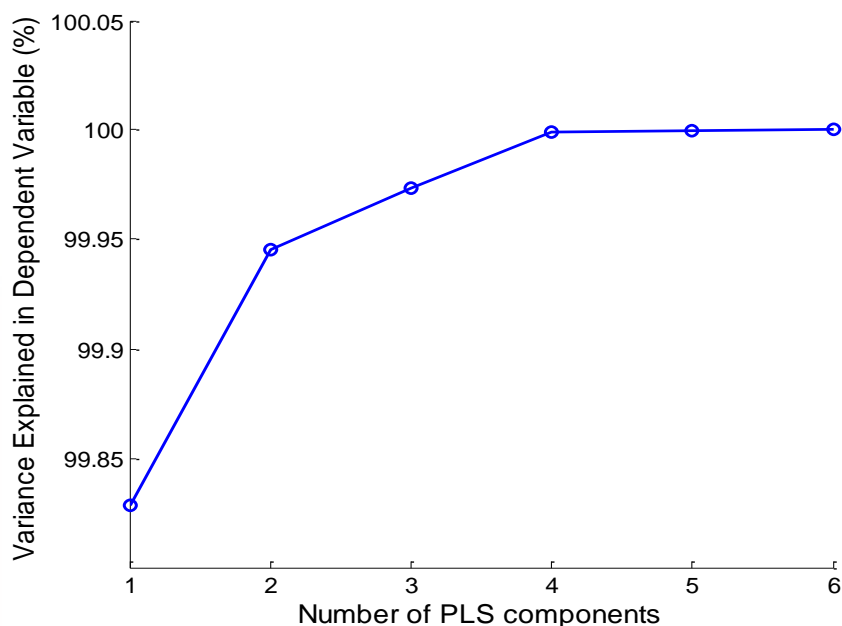


Figure 38: Number of Partial Least Square (PLS) components and their contribution to variation in data set explained percentagewise

The leave one out cross-validation method (Priddy & Keller, 2005) was used to evaluate the predicting ability of the PLS regression vector (Figure 39a). Blind cross-validation (Priddy & Keller, 2005) was also performed using data from repeated measurements of the same samples (Figure 39b). The blind cross-validation method evaluates how well the PLS regression model will predict concentrations from different experiments. In Table 9, the merits of the two validation methods based on the Root Mean Square Error (RMSE), Correlation Coefficient (r^2) and Mean Absolute Prediction Error (MAPE) have been summarized. Lower values of the MAPE and RMSE imply better prediction by the PLS regression vector, whereas, better prediction by the r^2 is indicated by higher values. All the three statistics show excellent prediction with the PLS regression vector.

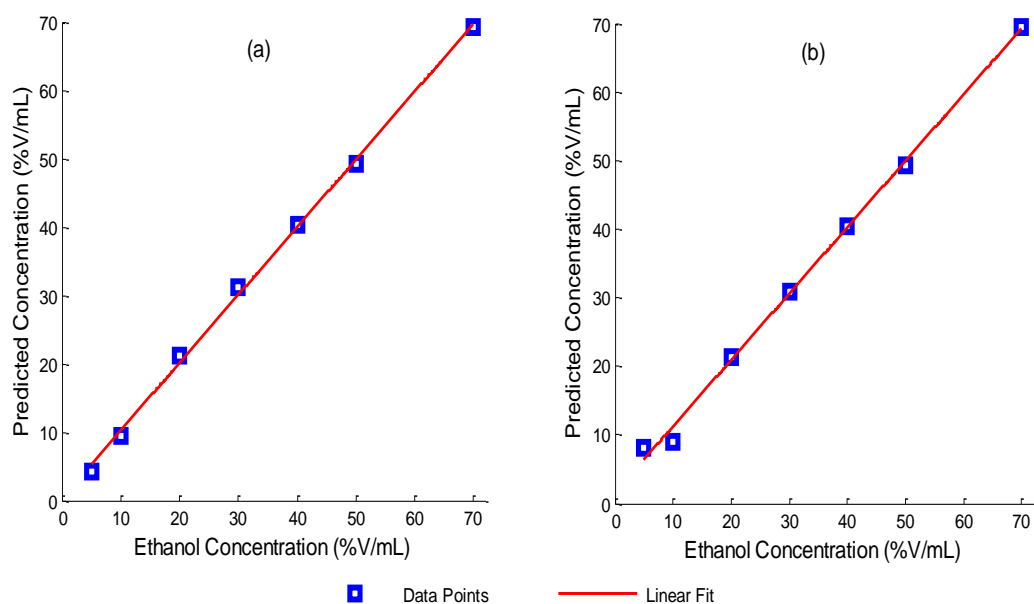


Figure 39: Prediction assessment of the Partial Least Square (PLS) regression model by (a) Leave one out cross-validation method and (b) Blind cross-validation method

Table 9

PLS Regression Model Performance Statistics based on Correlation Coefficient, RMSE and MAPE for the various combinations of the Training and Test Data Set

Cross Validation Method	PLS Regression Model Performance Statistics		
	r^2 (%)	RMSE	MAPE
Leave One Out	99.84	0.90	4.80
Blind	99.57	1.06	11.98

The detection threshold of the PLS calibration vector was determined using the Relative Error (RE) statistic, (Figure 40). In this study, a 20% relative error is

chosen as threshold. Observing from the error bar plots in both validation methods, the developed Raman spectroscopic system can be said to have an excellent detection corresponding to concentrations above 10% by volume. This means that a prediction for samples having concentrations below 10% by volume will be prone to large amounts of error.

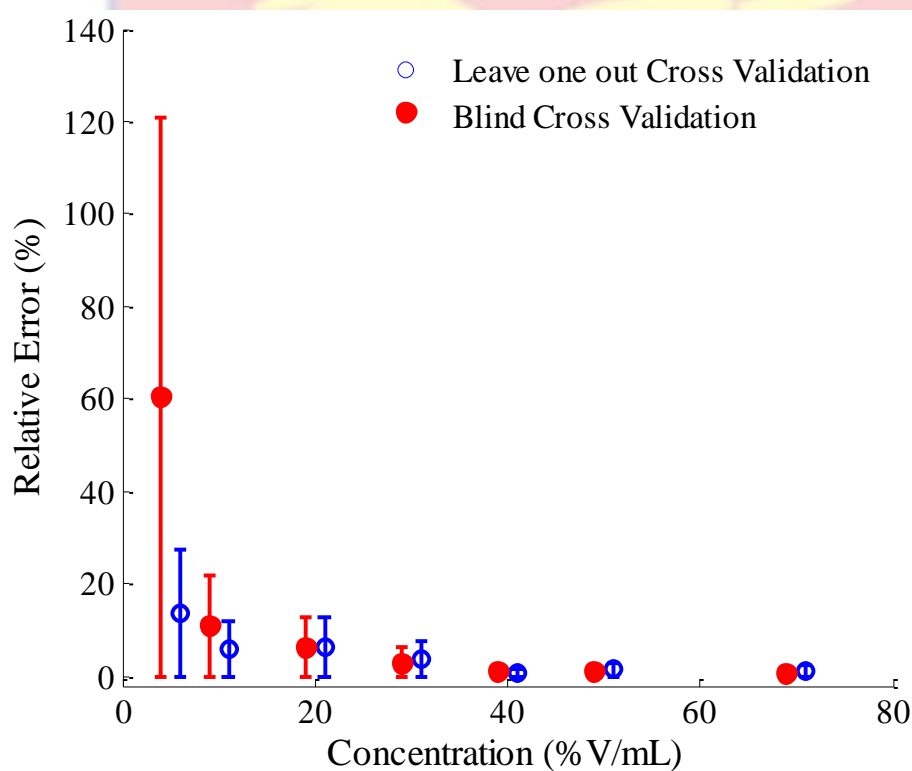


Figure 40: Comparison of the relative error determined for each concentration of ethanol based on Leave one out cross-validation method and Blind cross-validation method

CHAPTER FIVE

CONCLUSIONS AND RECCOMENDATIONS

Conclusions

In this thesis, a low cost Raman system setup has been designed and developed. The developed Raman system setup is a simple, cost effective and non-invasive analytical tool that can help identify, discriminate and quantify molecular species in a sample matrix for research, teaching and industrial uses. The designed system comprises simple and relatively cheap optical components that measure the Raman spectrum of a sample (both solid and liquid). The developed Raman system setup is about 40% less than the cost of existing low cost Raman system setups and 80% less than the cost of commercially available Raman systems.

The functionalities of the developed Raman system setup have been demonstrated by measuring the Raman spectra of several known chemical samples with the functional groups present in the samples identified. The peak parameters of the functional groups determined were all consistent with known results in literature. The functional groups identified include Amide (NH), organic acid (COOH), alcohol (ROH), hydroxyl (OH), methyl (CH₃) and methylene (CH₂). The developed Raman system setup has also been shown to be a suitable tool for polarisation measurement as well as concentration estimation and calibration.

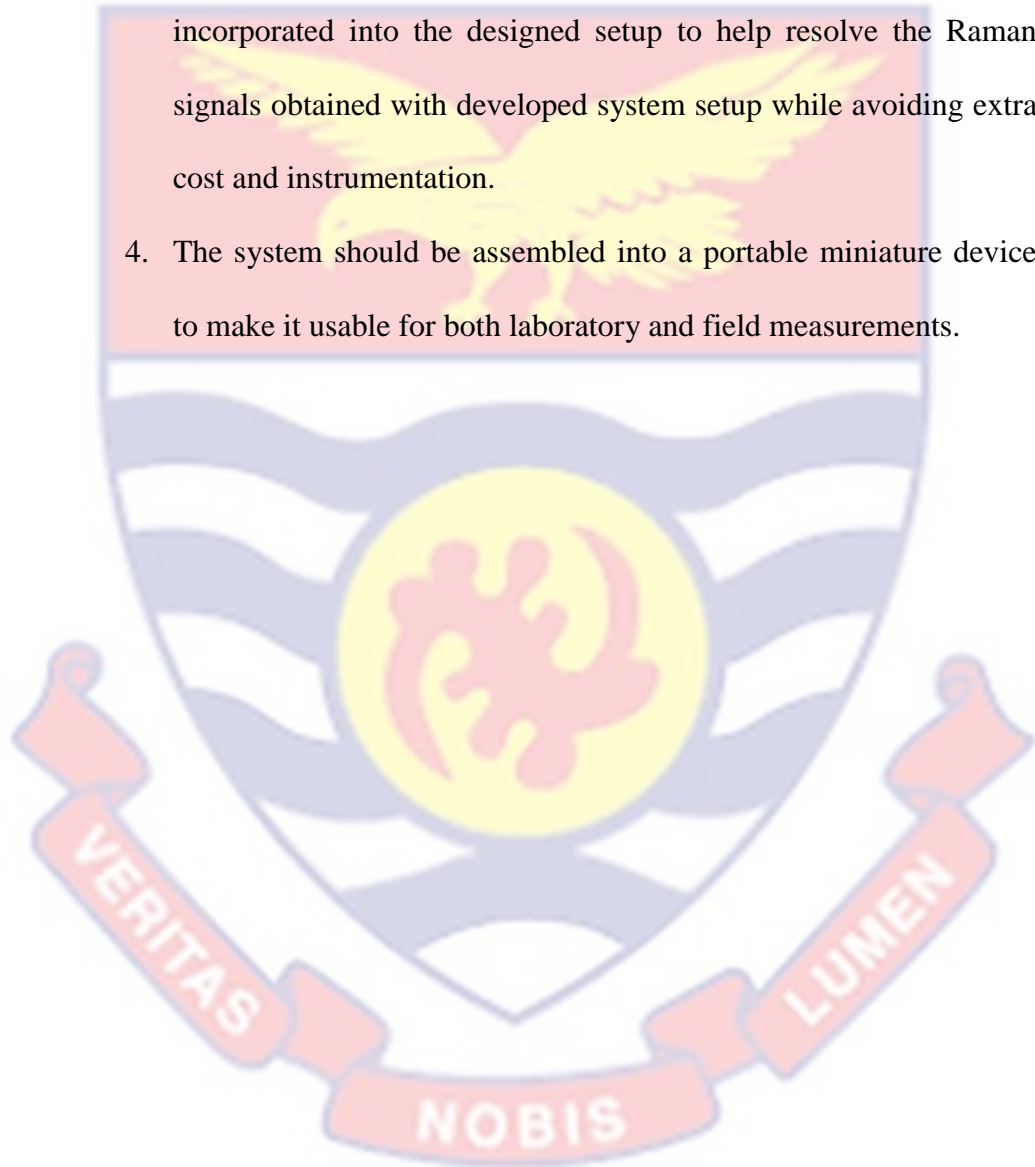
Due to the type of light source and known chemical samples used, fluorescence backgrounds were observed with some hidden Raman peaks. However, a fluorescence background suppression algorithm known as the second derivative method for Raman peak recognition and range independent algorithm (SDM-RPR-RIA) was employed to recover the Raman signals. The SDM-RPR-RIA uses a low pass Savitsky Golay filter to model the slowly varying baseline for the recovery of the Raman peaks in the spectrum. A qualitative and quantitative comparison of the performance of SDM-RPR-RIA with RIA, RIA-SG-SR and SG-RPR-RIA showed that all four methods are roughly comparable, but the SDM-RPR-RIA most often produced the best weighted correlation coefficient (WCC) in Raman peak recovery; especially for baselines of polynomial and Gaussian types. Furthermore, the SDM-RPR-RIA improves on the existing SG-RPR-RIA for full automation implementation since it operates objectively with virtually no need of a user intervention.

Recommendations

This study has brought to light a number of opportunities that can be investigated and studied further. Some recommendations for further studies include;

1. Extra validation and calibration measurements with several other samples should be conducted to make the system much more suitable for advanced studies.

2. The SDM-RPR-RIA method should be improved to use Gauss Seidel iteration to provide faster and better estimation of the fluorescence background.
3. A signal enhancing algorithm in addition to the SDM-RPR-RIA be incorporated into the designed setup to help resolve the Raman signals obtained with developed system setup while avoiding extra cost and instrumentation.
4. The system should be assembled into a portable miniature device to make it usable for both laboratory and field measurements.



REFERENCES

- Abhyankar, S. B., & Subramanian, S. (1995). Raman spectroscopy in undergraduate chemical education. *Spectrochimica Acta Part A: Molecular and Biomolecular Spectroscopy*, 51(12), 2199-2204.
- Adami, R., & Kiefer, J. (2013). Light-emitting diode based shifted-excitation Raman difference spectroscopy (LED-SERDS). *Analyst*, 138 (21), 6258-6261.
- American Society for Testing and Materials [ATSM]. (1993). ATSM Standard E 579-84, Test Method for Limit of Detection of Fluorescence of Quinine Sulfate. *Annual Book of ASTM Standards* (Vol. 14.01). Philadelphia, PA
- Ananthkrishnan, R. (1937). The Raman spectra of crystal powders. In *Proceedings of the Indian Academy of Sciences-Section A* (Vol. 5, No. 1, pp. 76-86). India: Springer.
- Angel, S. M., DeArmond, M. K., Hanck, K. W., & Wertz, D. W. (1984). Computer-controlled instrument for the recovery of a resonance Raman spectrum in the presence of strong luminescence. *Analytical Chemistry*, 56(14), 3000-3001.
- Aparicio, R., & Harwood, J. (2013). *Handbook of olive oil* (pp. 163-395). New York, USA: Springer.

- Ariese, F., Meuzelaar, H., Kerssens, M. M., Buijs, J. B., & Gooijer, C. (2009). Picosecond Raman spectroscopy with a fast intensified CCD camera for depth analysis of diffusely scattering media. *Analyst*, *134* (6), 1192-1197.
- Asher, S. A., & Johnson, C. R. (1984). "Raman spectroscopy of a coal liquid shows that fluorescence interference is minimized with ultraviolet excitation", *Science*, *225*, 311.
- Asher, S. A., Ludwig, M., & Johnson, C. R. (1986). UV resonance Raman excitation profiles of the aromatic amino acids. *Journal of the American Chemical Society*, *108* (12), 3186-3197.
- Atakan, A. K., Blass, W. E., & Jennings, D. E. (1980). Elimination of Baseline Variations from a Recorded Spectrum by Ultra-low Frequency Filtering. *Applied Spectroscopy*, *34* (3), 369-372.
- Auguie, B., Reigue, A., Le Ru, E. C., & Etchegoin, P. G. (2012). Tiny peaks vs mega backgrounds: a general spectroscopic method with applications in resonant Raman scattering and atmospheric absorptions. *Analytical chemistry*, *84* (18), 7938-7945.
- Barron, L. D., Zhu, F., & Hecht, L. (2006). Raman optical activity: An incisive probe of chirality, and of biomolecular structure and behaviour. *Vibrational spectroscopy*, *42* (1), 15-24.
- Bell, S. E. J., Bourguignon, E. S. O., Dennis, A. C., Fields, J. A., McGarvey, J. J., & Seddon, K. R. (2000). Identification of dyes on ancient Chinese

paper samples using the subtracted shifted Raman spectroscopy method.

Analytical chemistry, 72 (1), 234-239.

Bell, S. J., & Bourguignon, E. O. (1998). Analysis of luminescent samples using subtracted shifted Raman spectroscopy. *Analyst*, 123 (8), 1729-1734.

Bhaumik, M. L. (1967). Physics of Raman lasers. *American Journal of Physics*, 35 (4), 330-335.

Bisson, P., Parodi, G., Rigos, D., & Whitten, J. E. (2006). Low-cost Raman spectroscopy using a violet diode laser. *Chemical Educator*, 11 (2), 1-6.

Blackie, E. J., Ru, E. C. L., & Etchegoin, P. G. (2009). Single-molecule surface-enhanced Raman spectroscopy of nonresonant molecules. *Journal of the American Chemical Society*, 131 (40), 14466-14472.

Brandt, N. N., Brovko, O. O., Chikishev, A. Y., & Paraschuk, O. D. (2006). Optimization of the rolling-circle filter for Raman background subtraction. *Applied Spectroscopy*, 60 (3), 288-293.

Bright, F. V., & Hieftje, G. M. (1986). A new technique for the elimination of fluorescence interference in Raman spectroscopy. *Applied spectroscopy*, 40 (5), 583-587.

Brown, C. D., Vega-Montoto, L., & Wentzell, P. D. (2000). Derivative preprocessing and optimal corrections for baseline drift in multivariate calibration. *Applied Spectroscopy*, 54 (7), 1055-1068.

- Cai, W., Wang, L., Pan, Z., Zuo, J., Xu, C., & Shao, X. (2001). Application of the wavelet transform method in quantitative analysis of Raman spectra. *Journal of Raman Spectroscopy*, 32 (3), 207-209.
- Carter III, W. D. (2007). *Raman spectroscopic study of single red blood cells infected by the malaria parasite plasmodium falciparum* (Doctoral dissertation, University of Central Florida Orlando, Florida). Retrieved from http://etd.fcla.edu/CF/CFE0001780/Carter_William_D_200708_MAST.pdf
- Carter, D. A., & Pemberton, J. E. (1995). Frequency/wavelength calibration of multipurpose multichannel Raman spectrometers. Part I: Instrumental factors affecting precision. *Applied Spectroscopy*, 49 (11), 1550-1560.
- Carter, J. C., Angel, S. M., Lawrence-Snyder, M., Scaffidi, J., Whipple, R. E., & Reynolds, J. G. (2005). Standoff detection of high explosive materials at 50 meters in ambient light conditions using a small Raman instrument. *Applied Spectroscopy*, 59 (6), 769-775.
- Chabay, I., Klauminzer, G. K., & Hudson, B. S. (1976). Coherent anti-Stokes Raman spectroscopy (CARS): Improved experimental design and observation of new higher-order processes. *Applied Physics Letters*, 28 (1), 27-29.

- Chalmers, J. M., Edwards, H. G., & Hargreaves, M. D. (2012). *Infrared and Raman Spectroscopy in Forensic Science*. Chichester, United Kingdom: John Wiley & Sons.
- Chen, K., Wei, H., Zhang, H., Wu, T., & Li, Y. (2015). A Raman peak recognition method based automated fluorescence subtraction algorithm for retrieval of Raman spectra of highly fluorescent samples. *Analytical Methods*, 7 (6), 2770-2778.
- Chen, K., Zhang, H., Wei, H., & Li, Y. (2014). Improved Savitzky–Golay-method-based fluorescence subtraction algorithm for rapid recovery of Raman spectra. *Applied Optics*, 53 (24), 5559-5569.
- Church, E., & Takacs P., (1995). Surface scattering. In Bass, M., Stryland, E., Williams, D., & Wolfe, W., (Eds.). *Handbook of Optics: Fundamentals, Techniques, & Design*. (pp. 7.1–7.14). Optical Society of America, New York: McGraw-Hill Inc.
- Colthup, N. (2012). *Introduction to infrared and Raman spectroscopy*. New York: Elsevier Science.
- Craig, D. P., & Thirunamachandran, T. (1984). *Molecular quantum electrodynamics: an introduction to radiation-molecule interactions*. North Chelmsford, United States: Courier Corporation.
- Crawford, A., Silva, E., York, K., & Li, C. (nd). Raman Spectroscopy: A Comprehensive Review. *Department of Textile Engineering, Chemistry*

and Science, North Carolina State University. Retrieved from https://www.academia.edu/1131363/Raman_Spectroscopy_A_Comprehensive_Review

De Luca, A. C., Mazilu, M., Riches, A., Herrington, C. S., & Dholakia, K. (2009). Online fluorescence suppression in modulated Raman spectroscopy. *Analytical Chemistry*, 82 (2), 738-745.

Deckert-Gaudig, T., & Deckert, V. (2009). Ultraflat Transparent Gold Nanoplates—Ideal Substrates for Tip-Enhanced Raman Scattering Experiments. *Small*, 5 (4), 432-436.

DeGraff, B. A., Hennip, M., Jones, J. M., Salter, C., & Schaertel, S. A. (2002). An inexpensive laser Raman spectrometer based on CCD detection. *The Chemical Educator*, 7 (1), 15-18.

Demtröder, W. (2008). *Laser Spectroscopy: Vol. 2 Experimental Techniques*. Berlin, Heidelberg: Springer-Verlag.

Demtröder, W. (2013). *Laser spectroscopy: basic concepts and instrumentation*. Berlin, Heidelberg: Springer-Verlag.

DeNoyer, L. K., & Dodd, J. G. (2002). Smoothing and derivatives in spectroscopy. In J. M. Chalmers & P. R. Griffiths (Eds). *Handbook of vibrational spectroscopy* (pp. 2173). Chichester: John Wiley and Sons.

- Dietrich, W., Rüdel, C. H., & Neumann, M. (1991). Fast and precise automatic baseline correction of one-and two-dimensional NMR spectra. *Journal of Magnetic Resonance*, *91*, 1-11.
- Dirac, P. A. M. (1927). The quantum theory of dispersion. *Proceedings of the Royal Society of London A*. *114*, 710–728.
- Edwards, H. G., & Chalmers, J. M. (2005). *Raman spectroscopy in archaeology and art history* (Vol. 9). Cambridge, UK: Royal Society of Chemistry.
- Efremov, E. V., Buijs, J. B., Gooijer, C., & Ariese, F. (2007). Fluorescence rejection in resonance Raman spectroscopy using a picosecond-gated intensified charge-coupled device camera. *Applied Spectroscopy*, *61* (6), 571-578.
- Ehrentreich, F., & Sümmchen, L. (2001). Spike removal and denoising of Raman spectra by wavelet transform methods. *Analytical chemistry*, *73* (17), 4364-4373.
- Ellis, A. M., Feher, M., & Wright, T. G. (2005). *Electronic and photoelectron spectroscopy: fundamentals and case studies*. New York: Cambridge University Press.
- Ellis, D. I., Brewster, V. L., Dunn, W. B., Allwood, J. W., Golovanov, A. P., & Goodacre, R. (2012). Fingerprinting food: current technologies for the detection of food adulteration and contamination. *Chemical Society Reviews*, *41* (17), 5706-5727.

- Engert, C., Deckert, V., Kiefer, W., Umapathy, S., & Hamaguchi, H. (1994). Design and performance characteristics of a near-infrared scanning multichannel Raman spectrometer. *Applied Spectroscopy*, 48 (8), 933-936.
- Ferraro, J. R., & Nakamoto, K. (2012). *Introductory Raman Spectroscopy*. San Diego: Academic Press.
- Feynman, R. P., & Zee, A. (2006). *QED: The strange theory of light and matter*. New Jersey: Princeton University Press.
- Fibers & probes. (n.d.). Premium reflection probe. [Image] Retrieved from http://oceanoptics.com/wpcontent/uploads/Ocean_Optics_Fibers_Probes.pdf
- Fischer, R., Hanson, K. M., Dose, V., & Von Der Linden, W. (2000). Background estimation in experimental spectra. *Physical Review E*, 61 (2), 1152.
- Friedrichs, M. S. (1995). A model-free algorithm for the removal of baseline artifacts. *Journal of Biomolecular NMR*, 5 (2), 147-153.
- Frontasyeva, M. V. (2011). Neutron activation analysis in the life sciences. *Physics of Particles and Nuclei*, 42 (2), 332-378.
- Gaft, M., & Nagli, L. (2008). UV gated Raman spectroscopy for standoff detection of explosives. *Optical Materials*, 30 (11), 1739-1746.

- Galloway, D. B., Ciolkowski, E. L., & Dallinger, R. F. (1992). Raman spectroscopy for the undergraduate physical and analytical laboratories. *Journal of Chemical Education*, *69*, 79.
- Geladi, P., MacDougall, D., & Martens, H. (1985). Linearization and scatter-correction for near-infrared reflectance spectra of meat. *Applied Spectroscopy*, *39*(3), 491-500.
- Genack, A. Z. (1984). Fluorescence suppression by phase-resolved modulation Raman scattering. *Analytical Chemistry*, *56*(14), 2957-2960.
- Goncharov, A. F., & Crowhurst, J. C. (2005). Raman spectroscopy under extreme conditions. *Journal of low temperature physics*, *139* (5-6), 727-737.
- Grant, W. B. (1991). Differential absorption and Raman lidar for water vapor profile measurements: a review. *Optical Engineering*, *30* (1), 40-48.
- Greenberg, R. R., Bode, P., & Fernandes, E. A. D. N. (2011). Neutron activation analysis: a primary method of measurement. *Spectrochimica Acta Part B: Atomic Spectroscopy*, *66* (3), 193-241.
- Greer, J. S., Petrov, G. I., & Yakovlev, V. V. (2013). Raman spectroscopy with LED excitation source. *Journal of Raman Spectroscopy*, *44* (7), 1058-1059.

Griffiths, P. R., & Shao, L. (2009). Self-weighted correlation coefficients and their application to measure spectral similarity. *Applied Spectroscopy*, 63 (8), 916-919.

Griffiths, T. R., King, K., Hubbard, H. V. S. A., Schwing-Weill, M. J., & Meullemeestre, J. (1982). Some aspects of the scope and limitations of derivative spectroscopy. *Analytica Chimica Acta*, 143, 163-176.

Haka, A. S., Shafer-Peltier, K. E., Fitzmaurice, M., Crowe, J., Dasari, R. R., & Feld, M. S. (2005). Diagnosing breast cancer by using Raman spectroscopy. *Proceedings of the National Academy of Sciences of the United States of America*, 102 (35), 12371-12376.

Harwood, L. M., Moody, C. J., & Harwood, L. M. (1989). *Experimental organic chemistry: principles and practice*. Oxford, United Kingdom: Blackwell Scientific.

Hasegawa, T., Nishijo, J., & Umemura, J. (2000). Separation of Raman spectra from fluorescence emission background by principal component analysis. *Chemical Physics Letters*, 317 (6), 642-646.

Heftmann, E. (Ed.). (2004). *Chromatography: Fundamentals and applications of chromatography and related differential migration methods-Part B: Applications*. Amsterdam: Elsevier.

- Henson, M. J., & Zhang, L. (2006). Drug characterization in low dosage pharmaceutical tablets using Raman microscopic mapping. *Applied Spectroscopy*, 60 (11), 1247-1255.
- Hollas, J. M. (2004). *Modern spectroscopy*. Chichester, United Kingdom: John Wiley & Sons.
- Hu, Y., Jiang, T., Shen, A., Li, W., Wang, X., & Hu, J. (2007). A background elimination method based on wavelet transform for Raman spectra. *Chemometrics and Intelligent Laboratory Systems*, 85 (1), 94-101.
- Huang, Z., McWilliams, A., Lui, H., McLean, D. I., Lam, S., & Zeng, H. (2003). Near-infrared Raman spectroscopy for optical diagnosis of lung cancer. *International journal of cancer*, 107 (6), 1047-1052.
- Jirasek, A., Schulze, G., Yu, M. M. L., Blades, M. W., & Turner, R. F. B. (2004). Accuracy and precision of manual baseline determination. *Applied Spectroscopy*, 58 (12), 1488-1499.
- Joshi, D. D. (2012). *FTIR Spectroscopy: Herbal Drugs and Fingerprints*. In *Herbal Drugs and Fingerprints* (pp. 121-146). New Delhi, India: Springer.
- Kasha, M. (1950). Characterization of electronic transitions in complex molecules. *Discussions of the Faraday society*, 9, 14-19.

- Kiefer, J. (2014). Instantaneous shifted-excitation Raman difference spectroscopy (iSERDS). *Journal of Raman Spectroscopy*, 45 (10), 980-983.
- Kiefer, J. (2015). Recent Advances in the Characterization of Gaseous and Liquid Fuels by Vibrational Spectroscopy. *Energies*, 8 (4), 3165-3197.
- Klinterberg, C., Andreasson, M., Sandström, O., Andersson-Engels, S., & Svanberg, S. (2005). A compact medical fluorosensor for minimally invasive tissue characterization. *Review of scientific instruments*. 76, 034303
- Knee, J. L. (1996). Spectra of Atoms and Molecules by Peter F. Bernath. *American Journal of Physics*, 64, 93-93.
- Kostamovaara, J., Tenhunen, J., Kögler, M., Nissinen, I., Nissinen, J., & Keränen, P. (2013). Fluorescence suppression in Raman spectroscopy using a time-gated CMOS SPAD. *Optics express*, 21 (25), 31632-31645.
- Kramers, H. A. & Heisenberg, W. (1925). On the dispersal of radiation by atoms. *International Journal of Research in Physical Chemistry and Chemical Physics*. 31, 681–708.
- Krishna, H., Majumder, S. K., & Gupta, P. K. (2012). Range-independent background subtraction algorithm for recovery of Raman spectra of biological tissue. *Journal of Raman Spectroscopy*, 43 (12), 1884-1894.

- Lakowicz, J. R. (2006). *Principles of Fluorescence Spectroscopy*. New York: Springer Science & Business Media.
- Laserna, J. (2001). An Introduction to Raman Spectroscopy: Introduction and Basic Principles. *Raman Resource including Vibrational Spectroscopy*. Retrieved from <http://www.spectroscopynow.com/Spy/basehtml/SpyH/1.1181>, 6-1.
- Lawaetz, A. J., & Stedmon, C. A. (2009). Fluorescence intensity calibration using the Raman scatter peak of water. *Applied Spectroscopy*, 63 (8), 936-940.
- Le Ru, E. C., & Etchegoin, P. G. (2008). *Principles of Surface-Enhanced Raman Spectroscopy and related plasmonic effects*. Oxford, UK: Elsevier.
- Le Ru, E. C., Schroeter, L. C., & Etchegoin, P. G. (2012). Direct measurement of resonance Raman spectra and cross sections by a polarisation difference technique. *Analytical chemistry*, 84 (11), 5074-5079.
- Leger, M. N., & Ryder, A. G. (2006). Comparison of derivative preprocessing and automated polynomial baseline correction method for classification and quantification of narcotics in solid mixtures. *Applied Spectroscopy*, 60 (2), 182-193.
- Lewis, I. R., & Edwards, H. (2001). *Handbook of Raman spectroscopy: from the research laboratory to the process line*. New York: Marcel Dekker.

- Li, Z., & Deen, M. J. (2014). Towards a portable Raman spectrometer using a concave grating and a time-gated CMOS SPAD. *Optics express*, 22 (15), 18736-18747.
- Lieber, C. A., & Mahadevan-Jansen, A. (2003). Automated method for subtraction of fluorescence from biological Raman spectra. *Applied Spectroscopy*, 57(11), 1363-1367.
- Liland, K. H., Almøy, T., & Mevik, B. H. (2010). Optimal choice of baseline correction for multivariate calibration of spectra. *Applied Spectroscopy*, 64 (9), 1007-1016.
- Lin, J. F., Santoro, M., Struzhkin, V. V., Mao, H. K., & Hemley, R. J. (2004). In situ high pressure-temperature Raman spectroscopy technique with laser-heated diamond anvil cells. *Review of scientific instruments*, 75 (10), 3302-3306.
- Lin, K., Cheng, D. L. P., & Huang, Z. (2012). Optical diagnosis of laryngeal cancer using high wavenumber Raman spectroscopy. *Biosensors and Bioelectronics*, 35 (1), 213-217.
- Long, D. A. (1988). Early history of the Raman effect. *International Reviews in Physical Chemistry*, 7 (4), 317-349.
- Long, D. A., (1977). *Raman Spectroscopy*. New York: McGraw-Hill.

- López-Díez, E. C., Bianchi, G., & Goodacre, R. (2003). Rapid quantitative assessment of the adulteration of virgin olive oils with hazelnut oils using Raman spectroscopy and chemometrics. *Journal of Agricultural and Food Chemistry*, *51* (21), 6145-6150.
- Lorigan, G. A., Patterson, B. M., Sommer, A. J., & Danielson, N. D. (2002). Cost-Effective Spectroscopic Instrumentation for the Physical Chemistry Laboratory. *Journal of Chemical Education*, *79*, 1264.
- Luypaert, J., Heuerding, S., Massart, D. L., & Vander Heyden, Y. (2007). Direct orthogonal signal correction as data pretreatment in the classification of clinical lots of creams from near infrared spectroscopy data. *Analytica chimica acta*, *582* (1), 181-189.
- Maiman, T. H. (1960). Stimulated Optical Radiation in Ruby. *Nature*, *187*, 493-494.
- Maker, P. D., & Terhune, R. W. (1965). Study of optical effects due to an induced polarisation third order in the electric field strength. *Physical Review*, *137* (3A), A801.
- Mann, C. K., & Vickers, T. J. (1987). Raman measurements in the presence of fluorescence. *Applied Spectroscopy*, *41* (3), 427-430.
- Marquardt, D. W. (1963). An algorithm for least-squares estimation of nonlinear parameters. *Journal of the Society for Industrial & Applied Mathematics*, *11* (2), 431-441.

Martins, M. A. D. S., Ribeiro, D. G., Pereira dos Santos, E. A., Martin, A. A., Fontes, A., & Martinho, H. D. S. (2010). Shifted-excitation Raman difference spectroscopy for in vitro and in vivo biological samples analysis. *Biomedical optics express*, 1 (2), 617-626.

Martyshkin, D. V., Ahuja, R. C., Kudriavtsev, A., & Mirov, S. B. (2004). Effective suppression of fluorescence light in Raman measurements using ultrafast time gated charge coupled device camera. *Review of scientific instruments*, 75 (3), 630-635.

Material and Technical information. (n.d.). *Transmission of empty cells made of different materials*. [Graph]. Retrieved from <http://www.hellmanalytics.com/text/283/en/material-and-technical-information.html>

MatLab (2012b). Computer Software. Natick, Massachusetts, United States: The Mathworks Inc.

Matousek, P., Towrie, M., Stanley, A., & Parker, A. W. (1999). Efficient rejection of fluorescence from Raman spectra using picosecond Kerr gating. *Applied Spectroscopy*, 53 (12), 1485-1489.

McCain, S. T., Gehm, M. E., Wang, Y., Pitsianis, N. P., & Brady, D. J. (2006). Coded aperture Raman spectroscopy for quantitative measurements of ethanol in a tissue phantom. *Applied Spectroscopy*, 60 (6), 663-671.

McCartney, E., (1976). *Optics of the Atmosphere: Scattering by Molecules and Particles*. New York, John Wiley & Sons Inc.

McCreery, R. L. (2000). *Raman Spectroscopy for Chemical Analysis* (Vol. 127).

Toronto, Canada: John Wiley & Sons.

McCreery, R. L. (2005). *Raman spectroscopy for chemical analysis* (Vol. 225).

Toronto, Canada: John Wiley & Sons.

Meier, R. J. (2005). On art and science in curve-fitting vibrational spectra.

Vibrational Spectroscopy, 39 (2), 266-269.

Mo, J., Zheng, W., Low, J. J., Ng, J., Ilancheran, A., & Huang, Z. (2009). High

wavenumber Raman spectroscopy for in vivo detection of cervical dysplasia. *Analytical chemistry*, 81 (21), 8908-8915.

Mosier-Boss, P. A., Lieberman, S. H., & Newbery, R. (1995). Fluorescence

rejection in Raman spectroscopy by shifted-spectra, edge detection, and FFT filtering techniques. *Applied Spectroscopy*, 49 (5), 630-638.

Moskovits, M. (2005). Surface-enhanced Raman spectroscopy: a brief

retrospective. *Journal of Raman Spectroscopy*, 36 (6-7), 485-496.

Movasaghi, Z., Rehman, S., & Rehman, I. U. (2007). Raman spectroscopy of

biological tissues. *Applied Spectroscopy Reviews*, 42 (5), 493-541.

Myers AB (1997) "Time-dependent" resonance Raman theory. *Journal of*

Raman Spectroscopy. 28, 389– 401.

Nakamoto, K. (1977). *Infrared and Raman spectra of inorganic and*

coordination compounds. Hoboken, New Jersey: John Wiley & Sons.

- Nijssen, A., Schut, T. C. B., Heule, F., Caspers, P. J., Hayes, D. P., Neumann, M. H., & Puppels, G. J. (2002). Discriminating basal cell carcinoma from its surrounding tissue by Raman spectroscopy. *Journal of Investigative Dermatology*, *119* (1), 64-69.
- O'Haver, T. (1997). A Pragmatic Introduction to Signal Processing. Retrieved from, <http://terpconnect.umd.edu/~toh/spectrum/SignalsAndNoise.html>
- Osticioli, I., Zoppi, A., & Castellucci, E. M. (2006). Fluorescence and Raman spectra on painting materials: reconstruction of spectra with mathematical methods. *Journal of Raman Spectroscopy*, *37* (10), 974-980.
- Osticioli, I., Zoppi, A., & Castellucci, E. M. (2007). Shift-excitation raman difference spectroscopy–difference deconvolution method for the luminescence background rejection from raman spectra of solid samples. *Applied Spectroscopy*, *61*(8), 839-844.
- Parson, W. W. (2007). *Modern optical spectroscopy*. Berlin: Springer.
- Patil, C. A., Pence, I. J., Lieber, C. A., & Mahadevan-Jansen, A. (2014). 1064 nm dispersive Raman spectroscopy of tissues with strong near-infrared autofluorescence. *Optics letters*, *39* (2), 303-306.
- Pavia, D., Lampman, G., Kriz, G., & Vyvyan, J. (2008). *Introduction to spectroscopy*. Belmont, USA: Cengage Learning.

Phillips, A. J., & Hamilton, P. A. (1996). Improved detection limits in Fourier transform spectroscopy from a maximum entropy approach to baseline estimation. *Analytical Chemistry*, 68 (22), 4020-4025.

Photon Technology International, (2005). The measurement of sensitivity in Fluorescence Spectroscopy. Retrieved from <http://www.pti-nj.com/products/Steady-State-Spectrofluorometer/TechNotes/MeasurementSensitivity.pdf>

Platt, U., & Stutz, J. (Eds).(2008). Differential absorption spectroscopy. In Y. Kim, U. Platt, M. B. Gu, & H. Iwahashi. *Atmospheric and Biological Environmental Monitoring* (pp. 135-174). Heidelberg, Berlin: Springer.

Priddy, K. L. & Keller, P. E., (2005), Artificial Neural Networks: An Introduction. (pp. 101 –105). Washington, USA: SPIE Press

Quarthey, P. (2005). Innovative ways of making aid effective in Ghana: tied aid versus direct budgetary support. *Journal of international development*, 17(8), 1077-1092.

Ralston, R. H., & Wilcox, G. E. (1968). A computer method of peak area determinations from Ge (Li) gamma spectra. *The 1968 International Conference on Modern Trends in Activation Analysis*, 37. 36-41.

Raman, C. V., & Krishnan, K. S. (1928). A new type of secondary radiation. *Nature*, 121 (3048), 501-502.

- Ramos, P. M., & Ruisánchez, I. (2005). Noise and background removal in Raman spectra of ancient pigments using wavelet transform. *Journal of Raman Spectroscopy*, 36 (9), 848-856.
- Renishaw plc, (n.d.). Introduction to Raman spectroscopy. In manualzz. Retrieved from <http://manualzz.com/doc/6481604/tm001---introduction-to-raman-spectroscopy>
- Rosi, F., Paolantoni, M., Clementi, C., Doherty, B., Miliani, C., Brunetti, B. G., & Sgamellotti, A. (2010). Subtracted shifted Raman spectroscopy of organic dyes and lakes. *Journal of Raman Spectroscopy*, 41 (4), 452-458.
- Rusciano, G., De Luca, A. C., Sasso, A., & Pesce, G. (2007). Enhancing Raman Tweezers by phase-sensitive detection. *Analytical chemistry*, 79 (10), 3708-3715.
- Saarinen, P. E., & Kauppinen, J. K. (2002). Resolution enhancement approaches. *Handbook of Vibrational Spectroscopy*. In D. G. Cameron & P. R. Griffiths (Eds). *Handbook of vibrational spectroscopy* (Vol. 3). New York: John Wiley and Sons.
- Santos, L. F., Wolthuis, R., Koljenovic, S., Almeida, R. M., & Puppels, G. J. (2005). Fiber-optic probes for in vivo Raman spectroscopy in the high-wavenumber region. *Analytical chemistry*, 77 (20), 6747-6752.

- Šašić, S. (2007). Raman mapping of low-content API pharmaceutical formulations. I. Mapping of alprazolam in Alprazolam/Xanax tablets. *Pharmaceutical research*, 24 (1), 58-65.
- Sastry, M. I. S., & Singh, S. (1987). Derivative analysis of Raman spectra of liquid water in the O-H (D) stretching region. *Journal of Molecular Structure*, 158, 195-204.
- Sauer, M., Hofkens, J., & Enderlein, J. (2010). *Handbook of Fluorescence Spectroscopy and Imaging: From Ensemble to Single Molecules*. Weinheim, Germany: John Wiley & Sons.
- Schultz, Z. D. (2014). Submolecular Spectroscopy?. *The Journal of Physical Chemistry Letters*, 5 (18), 3279-3280.
- Schulze, G., Jirasek, A., Yu, M. M., Lim, A., Turner, R. F., & Blades, M. W. (2005). Investigation of selected baseline removal techniques as candidates for automated implementation. *Applied Spectroscopy*, 59 (5), 545-574.
- Senior, J. M., & Jamro, M. Y. (2009). *Optical fiber communications: principles and practice*. New Jersey, United States: Prentice Hall.
- Signorell, R. & Reid, J.P. (Eds) (2011). *Fundamentals and Applications in Aerosol Spectroscopy*. Boca Raton, FL: CRC Press.

- Sigrist, M. W. (1994). *Air monitoring by spectroscopic techniques* (Vol. 127). New York: John Wiley & Sons.
- Sinfield, J. V., & Colic, O. (2012). *U.S. Patent No. 8,325,337*. Washington, DC: U.S. Patent and Trademark Office.
- Singh, R. (2011). The Discovery of the Raman Effect and Early Applications of Infrared and Raman Spectroscopy to Chemistry Studies. *Current Physical Chemistry, 1* (2), 152-157.
- Smith, B. C. (2015). IR Spectroscopy Interpretation Workshop, More Theory and Practice: The Thorny Problem of Mixtures and More on Straight-Chain Alkanes. *Spectroscopy, 30* (7), 26 -31.
- Smith, D. W. (1990). *Inorganic substances: a prelude to the study of descriptive inorganic chemistry*. Melbourne, Australia: Cambridge University Press.
- Smith, E., & Dent, G. (2013). *Modern Raman spectroscopy: a practical approach*. Chichester, UK: John Wiley & Sons.
- Somerville, W. R. C., Le Ru, E. C., Northcote, P. T., & Etchegoin, P. G. (2010). High performance Raman spectroscopy with simple optical components. *American Journal of Physics, 78* (7), 671-677.
- Sonntag, M. D., Pozzi, E. A., Jiang, N., Hersam, M. C., & Van Duyne, R. P. (2014). Recent advances in tip-enhanced Raman spectroscopy. *The Journal of Physical Chemistry Letters, 5* (18), 3125-313.

- Sowoidnich, K., & Kronfeldt, H. D. (2012). Shifted excitation Raman difference spectroscopy at multiple wavelengths for in-situ meat species differentiation. *Applied Physics B*, 108 (4), 975-982.
- Spectral Database for Organic Compounds, [SDBS]. (2015, September 10). *National Institute of Advanced Industrial Science and Technology*. Retrieved from <http://sdb.sdb.aist.go.jp>
- Stöckle, R. M., Suh, Y. D., Deckert, V., & Zenobi, R. (2000). Nanoscale chemical analysis by tip-enhanced Raman spectroscopy. *Chemical Physics Letters*, 318 (1), 131-136.
- Strutt, J. W. (1899). On the transmission of light through an atmosphere containing many small particles in suspension, and on the origin of the blue of the sky. *Philosophical Magazine*, 47, 375–384.
- Sun, D. W. (Ed.). (2008). *Modern techniques for food authentication*. Burlington, USA: Academic Press.
- Svanberg, S. (2012). *Atomic and molecular spectroscopy: basic aspects and practical applications* (Vol. 6). Heidelberg, Berlin: Springer Science & Business Media.
- Synovec, R. E., & Yeung, E. S. (1985). Improvement of the limit of detection in chromatography by an integration method. *Analytical Chemistry*, 57 (12), 2162-2167.

- Tahara, T., & Hamaguchi, H. O. (1993). Picosecond Raman spectroscopy using a streak camera. *Applied Spectroscopy*, 47 (4), 391-398.
- Tolles, W. M., Nibler, J. W., McDonald, J. R., & Harvey, A. B. (1977). A review of the theory and application of coherent anti-Stokes Raman spectroscopy (CARS). *Applied Spectroscopy*, 31 (4), 253-271.
- USB Optical Bench. (n.d.). Internal description of the USB 2000 spectrometer with its components. Retrieved from <http://oceanoptics.com/5-great-things-favorite-spectrometers>
- Vandenabeele, P. (2013). *Practical Raman spectroscopy: an introduction*. United Kingdom: John Wiley & Sons.
- Vekemans, B., Janssens, K., Vincze, L., Adams, F., & Van Espen, P. (1995). Comparison of several background compensation methods useful for evaluation of energy-dispersive X-ray fluorescence spectra. *Spectrochimica Acta Part B: Atomic Spectroscopy*, 50 (2), 149-169.
- Vickers, T. J., Wambles, R. E., & Mann, C. K. (2001). Curve fitting and linearity: data processing in Raman spectroscopy. *Applied Spectroscopy*, 55 (4), 389-393.
- Vo-Dinh, T., & Masters, B. R. (2004). Biomedical photonics handbook. *Journal of Biomedical Optics*, 9, 1110.

- Von der Linden, W., Dose, V., & Fischer, R. (1996). How to separate the signal from the background,". In *MAXENT96-Proceedings of the Maximum Entropy Conference* (p. 146).
- Wang, P. G. (Ed.). (2008). *High-throughput analysis in the pharmaceutical industry* (pp 265-270). Boca Raton: CRC Press.
- Wartewig, S., & Neubert, R. H. (2005). Pharmaceutical applications of Mid-IR and Raman spectroscopy. *Advanced drug delivery reviews*, 57 (8), 1144-1170.
- Watanabe, J., Kinoshita, S., & Kushida, T. (1985). Fluorescence rejection in Raman spectroscopy by a gated single-photon counting method. *Review of scientific instruments*, 56 (6), 1195-1198.
- Webster, G. T., Tilley, L., Deed, S., McNaughton, D., & Wood, B. R. (2008). Resonance Raman spectroscopy can detect structural changes in haemozoin (malaria pigment) following incubation with chloroquine in infected erythrocytes. *FEBS letters*, 582 (7), 1087-1092.
- Wei, D., Chen, S., & Liu, Q. (2015). Review of fluorescence suppression techniques in Raman spectroscopy. *Applied Spectroscopy Reviews*, 50 (5), 387-406.
- Wilczak, J. M., Gossard, E. E., Neff, W. D., & Eberhard, W. L. (1996). Ground-based remote sensing of the atmospheric boundary layer: 25 years of

progress. In *Boundary-Layer Meteorology 25th Anniversary Volume, 1970–1995* (pp. 321-349). Netherlands: Springer.

Wirth, M. J., & Chou, S. H. (1988). Comparison of time and frequency domain methods for rejecting fluorescence from Raman spectra. *Analytical Chemistry*, *60* (18), 1882-1886.

Xu, J. L., Riccioli, C., & Sun, D. W. (2015). An Overview on Nondestructive Spectroscopic Techniques for Lipid and Lipid Oxidation Analysis in Fish and Fish Products. *Comprehensive Reviews in Food Science and Food Safety*, *14* (4), 466-477.

Xu, R. (2001). Particle Characterization: Light Scattering Methods. *Particle Technology Series*. Dordrecht: Kluwer Academic Publishers.

Yang, D., & Ying, Y. (2011). Applications of Raman spectroscopy in agricultural products and food analysis: A review. *Applied Spectroscopy Reviews*, *46* (7), 539-560.

Young, M. A., Stuart, D. A., Lyandres, O., Glucksberg, M. R., & Van Duyne, R. P. (2004). Surface-enhanced Raman spectroscopy with a laser pointer light source and miniature spectrometer. *Canadian journal of chemistry*, *82* (10), 1435-1441.

Zhang, Z. M., Chen, S., & Liang, Y. Z. (2010). Baseline correction using adaptive iteratively reweighted penalized least squares. *Analyst*, *135* (5), 1138-1146.

Zhao, J., Carrabba, M. M., & Allen, F. S. (2002). Automated fluorescence rejection using shifted excitation Raman difference spectroscopy. *Applied Spectroscopy*, *56* (7), 834-845.

Zhao, J., Lui, H., McLean, D. I., & Zeng, H. (2007). Automated autofluorescence background subtraction algorithm for biomedical Raman spectroscopy. *Applied Spectroscopy*, *61* (11), 1225-1232.



APPENDICES

Appendix A

MatLab code for the SDM-RPR-RIA

```
%% Programme for the SDM-RPR-RIA
% by Andrew A. Huzortey @ the LAFOC, CANS, UCC
% 10th September, 2015
clear all; close all; clc
aayy= textread('ramanAxis.txt'); aayy= aayy(:,1);
ayi= importdata('aluminium_plate.txt'); x=ayi(:,1);
ay1= importdata('A2.time.00097.Master.scope'); ay1=ay1.data(:,1);
ay= xlsread('KHA_SEM.xls'); ay2=ay(:,1);
F1= interp1(ay1,ay2,x); figure; plot(x,F1)
F1= F1(1300:2100); x= x(1300:2100); figure; plot(x,F1)
aayy=aayy(1300:2100); figure; plot(aayy,F1,'linewidth',2)
ylabel('Intensity (a.u.)','fontsize',10);
xlabel('Raman Shifts (cm-1)','fontsize',10);
df1=derivxy(x,F1);
df2=derivxy(x,df1);
i=0;
for i=1:20
    df2=sgolayfilt(df2,1,5);
    i=i+1;
end
```

```

figure; plot(x,df2)

%% fit data

[pks, locs]=max(-df2); %figure; plot(x(locs),df2(locs),'o', x,df2)

vv=[10 x(locs)];

Ao3=df2./(1/(vv(1).^2)).*(((x-vv(2))./vv(1)).^2)-1)...

.*exp((-0.5).*((x-vv(2))./vv(1)).^2);

v=[ Ao3(locs) 10 x(locs)];

F=@(v,x)(v(1)./(v(2).^2)).*(((x-v(3))./v(2)).^2)-1)...

.*exp((-0.5).*((x-v(3))./v(2)).^2);

lsqOpts = optimoptions('lsqcurvefit', 'MaxFunEvals', 1000000);

r1=lsqcurvefit(F,v,x,df2, [ ], [ ], lsqOpts);

% figure; plot(x, F(r1,x),'r'); hold on; plot(x,df2)

r=lsqcurvefit(F,r1,x,df2, [ ], [ ], lsqOpts);

% figure; plot(x, F(r,x),'r'); hold on; plot(x,df2)

figure; plot(aayy, F(r,x),'--r','linewidth',2.5);hold on; plot(aayy,df2,'linewidth',2)

ylabel('Intensity (a.u.)','fontsize',10);

xlabel('Raman Shifts (cm^-^1)','fontsize',10);

title('Maximum Peak Fitted')

Ro=r(3);% peakcentre

Wo=r(2);% bandwidth

```

```

%% modified iterative fitting using a savitzky golay filter of order zero (lowpass
% filter)

G6=F1; % the original data

CC2=F1(:,locs);

CC3=CC2-r(1);

icount=0;

hi_diff=0;

while hi_diff< r(1)

    G6=sgolayfilt(G6,1,11);

    G6(G6>F1)=F1(F1<G6);

    Q1=G6(:,locs);

    hi_diff=CC2-Q1;

    r(1);

end

SBR=r(1)/max(G6);

figure; plot(aayy,G6,'--r','linewidth',2.5); hold on; plot(aayy,F1,'linewidth',2)

ylabel('Intensity (a.u.)','fontsize',10);

xlabel('Raman Shifts (cm^-1)','fontsize',10);

title('Underlying Baseline')

xlim([0 7000]); ylim([min(F1) max(F1)])

set(gca,'FontSize',10); box off;

G7=F1-G6; figure; plot(aayy,G7,'linewidth',2);

```

```
ylabel('Intensity (a.u.)', 'fontSize', 10);  
xlabel('Raman Shifts (cm-1)', 'fontSize', 10);  
title('Recovered Spectrum')  
xlim([1000 4000]); ylim([min(G7) max(G7)])  
set(gca, 'FontSize', 10); box off;
```



Appendix B

Baselines functions and corresponding parameters

Gaussian Function

$$y = e^{\frac{-(x-c)^2}{2\sigma^2}}$$

$$c = 1300$$

$$\sigma = 600$$

5th Degree Polynomial

$$y = ax^5 + bx^4 + cx^3 + dx^2 + ex + f$$

$$a = -1.6268 \times 10^{-14}$$

$$b = 1.9267 \times 10^{-10}$$

$$c = -7.3381 \times 10^{-7}$$

$$d = 1.1690 \times 10^{-3}$$

$$e = 9.2437 \times 10^{-1}$$

$$f = 6.1716 \times 10^2$$

Sigmoidal Function

$$y = \frac{1}{1 + e^{-\alpha(x-c)}}$$

$$\alpha = 0.005$$

$$c = 1030$$

Note: In all three instances the wavelength axis (x) was selected from 0 to 2500 with intervals of 1.